INTERPRETATION OF AEROMAGNETIC, MAGNETIC, AND GRAVITY DATA FROM THE SAN FRANCISCO MOUNTAINS VICINITY, SOUTHWESTERN UTAH

by

James William Schmoker

Thesis submitted to the Graduate Faculty of the

Virginia Polytechnic Institute

in partial fulfillment for the degree of

DOCTOR OF PHILOSOPHY

in

Geophysics

APPROVED:

Chairman Edwin S. Robinson
Assoc. Prof., Dept. of Geol. Sci.

Byron N. Cooper
Chairman, Dept. of Geol. Sci.
Prof., Dept. of Geol. Sci.

John K. Costain
Assoc. Prof., Dept. of Geol. Sci.

Gilbert A. Bollinger
Asst. Prof., Dept. of Geol. Sci.

Charles E. Sears
Assoc. Prof., Dept. of Geol. Sci.

Theodore E. Leinhardt
Prof., Dept. of Physics

June, 1969

Blacksburg, Virginia

TABLE OF CONTENTS

INTERPRETATION OF AEROMAGNETIC, MAGNETIC AND GRAVITY DATA FROM THE SAN FRANCISCO MOUNTAINS VICINITY, SOUTHWESTERN UTAH

(James William Schmoker)

Abstract

Regional and local geologic structures in the San Francisco Mountains vicinity, southwestern Utah, are investigated using magnetic-field intensity and gravimetric data.

Aeromagnetic data are interpreted to indicate a buried Tertiary pluton whose northern boundary runs from east to west across the 980 square mile study area, and which extends beyond the coverage of the aeromagnetic map to the east, south, and west. Local cupolas, some of which outcrop at the surface, extend upward from the main igneous body. A three-dimensional model which generates a magnetic field similar to that which is observed is developed, using a digital computer, for the distribution of the magnetic intrusive rocks in the area. These model studies indicate that the pluton is distinctly tabular, and about five miles thick, and has a near-vertical and linear northern edge which may have resulted from the structural control exerted by an east-west trending fault zone.

The Bouguer gravity anomalies in the San Francisco Mountains district reflect horst and graben structures typical of the Basin and Range Province, and indicate that an approximate density contrast with the surrounding consolidated sedimentary rocks of +.10 grams

per cc. is associated with the local intrusive cupolas. Three interpretive east-west geologic cross sections reproduce the observed residual gravity anomalies. The cross sections are obtained using a computer program for the evaluation of two-dimensional gravity anomalies on the ground surface.

The regional gravity data are interpreted to show the effect of at least three regional structures which are distinct from the local near-surface structure:

1) An underlying intrusive body.
2) An east-west fault zone bounding the intrusive body on the north.
3) A continuation of Basin and Range structure at depths exceeding two miles.

Vertical-field ground magnetic data were obtained during three and one-half months of field work in selected areas of the Star Range, located in the southeast quadrant of the thesis area. The igneous structure comprising the local Milford Flat intrusive body is found to terminate abruptly to the northwest, presumably as a result of post-intrusive faulting, while to the east the depth of burial increases gradually. The intrusive rock near the Wild Bill mine plunges steeply to the east and more gently to the south. An anomaly in the south-central portion of the Wild Bill magnetic grid is interpreted as representing an upward protrusion of the local quartz monzonite body. The contact zone along the southern edge of the Shauntie intrusive body, southeast of the old townsite of Shauntie, is mapped on the basis of magnetic evidence, and four zones of magnetite mineralization between 8 and 25 feet thick are defined.

I. PREFACE

This thesis was begun at the University of Utah, Salt Lake City, Utah, under the direction of Dr. Edwin S. Robinson. When Dr. Robinson accepted a position at Virginia Polytechnic Institute, the author transferred to VPI and continued work on the same thesis under his direction.

II. ACKNOWLEDGEMENTS

The author is greatly indebted to for his continued interest, advice, and guidance throughout all phases of this work. Financial support for the ground magnetic work was given by the Utah Geological and Mineralogical Survey, and it is a pleasure to thank , , and for their advice and assistance.

, University of Utah, made available the torsion magnetometer used in 1967 and the magnetic susceptibility bridge. During the 1966-67 school year, and a portion of the 1967-68 school year, the author was a recipient of a NASA fellowship. Other financial assistance was given by the Geophysics Department, University of Utah, and the Department of Geological Sciences, Virginia Polytechnic Institute. The computer centers at both the University of Utah and Virginia Polytechnic Institute generously made computer time available.

III. LIST OF TABLES

IV. LIST OF FIGURES

V. INTRODUCTION

General

The San Francisco Mountains district is a 980 square mile rectangle bounded by the north latitudes of 38°15' and 38°45' and the west longitudes of 113°00' and 113°30'. The area covers parts of Beaver and Millard Counties, in southwestern Utah. Figure 5-1 is an index map showing the area's location.

The surface features of the region are typical of the Great Basin, with wide desert valleys and abruptly rising, north-south trending mountains. Elevations range from 4500 feet along the north-central boundary to 9600 feet in the San Francisco Mountains.

There are no perennial streams in the region, and surface water is scarce and generally of poor quality. The climate and vegetation are typical of upland arid regions, with local conditions strongly dependent upon altitude. The region is characterized by high summer daytime temperatures, cool nights, severe thunderstorms, few roads, and except for the easternmost portion, near Milford, an almost complete lack of human habitation.

Mining first became important in the region in the early 1870's, when the San Francisco, Star, North Star, Rocky, and Beaver Lake mining districts were established (Butler, 1913). The discovery of the Horn Silver mine, in the San Francisco district, was singularly responsible for the extension of the Utah Southern Railroad into the area in 1880 (Butler, 1913), an event of importance for the entire southwestern part of the state. By 1910 the production from the

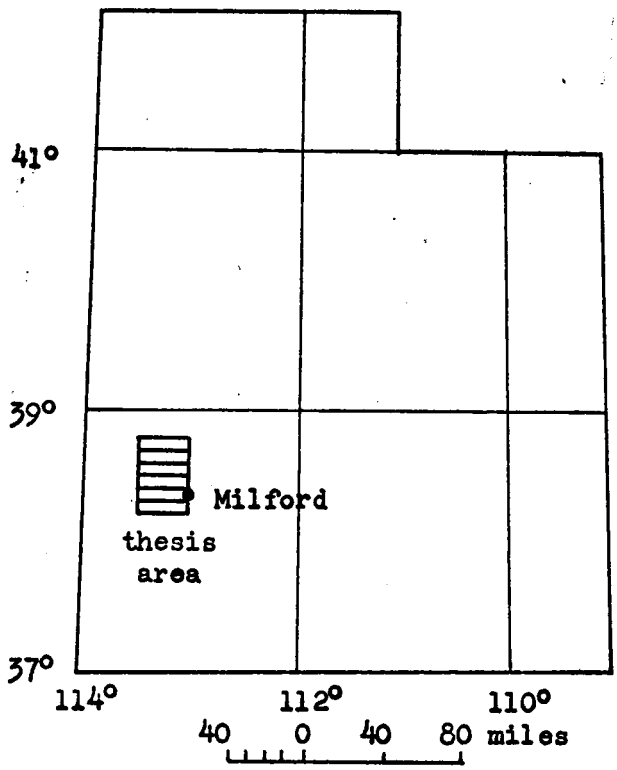

Figure 5-1. Index map of Utah showing the location of the thesis area.

above districts totaled 29 million dollars, with the principal metals being silver, lead, copper, and zinc (Butler, 1913).

The history of mining activity since 1918 has been basically one of decline, although scheelite was discovered in 1940 (Hobbs, 1944), and mined as a strategic mineral during World War II. To the author's knowledge the open pit copper mines and concentrator of the American Mining Company, located in the southern part of the Rocky Range, are currently the only mining operations of appreciable size active in the area.

Geophysical Exploration

The American Mining Company deposit, discovered by geophysical (ground-magnetic) exploration, together with the current demand for copper, has generated considerable interest and exploration activity in the area. The Utah Geological and Mineralogical Survey has sponsored a number of exploration and mapping programs in the region, results of which are available as published reports (see Utah Geol. Survey, 1968). Much of the recent geological and geophysical work has been done by private companies and individuals, and is not available to the public.

The United States Geological Survey has published the "Aeromagnetic Map of the San Francisco Mountains and Vicinity, Southwestern Utah" (U.S.G.S., 1966), and has placed on open file the "Complete Bouguer Gravity Anomaly Map of the San Francisco Mountains Vicinity, Beaver and Millard Counties, Utah" (U.S.G.S., 1966a). These two maps, included in the map pocket on the back cover, provide

the data for a large part of the discussion in this thesis. Both maps cover the same 30 minute rectangle, and have as a base the four U.S. Geological Survey 15 minute topographic quadrangle maps of Frisco Peak (1960), Beaver Lake Mountains (1960), Frisco (1959), and Milford (1958). Plate 1A, in the map pocket, is a topographic map of the area obtained by the juxtapositioning of these four quadrangle maps. The geophysical maps are published with no interpretation.

The author spent three and one-half months in the field under the sponsorship of the Utah Geological and Mineralogical Survey gathering vertical-field, ground-magnetic data in the Star Range, in the southeastern quadrant of the thesis area. Extensive work was done in four areas, and was intended to delineate the configuration of intrusive rocks and contact-zone mineralization in areas of potential economic importance. Section X of the thesis is devoted to the analysis of these data.

VI. GENERAL GEOLOGY

Geologic Setting

The San Francisco Mountains area lies near the eastern margin of the Great Basin, and the physiography of the area is similar to that of other parts of the Basin and Range Geologic Province. From west to east the study area includes the eastern edge of the Wah Wah Mountains, the San Francisco Mountains, and a chain of north-south aligned ranges consisting of the Beaver Lake Mountains to the north, the Rocky Range, and the Star Range. This surface pattern reflects the structural dominance of the Tertiary normal faulting which characterizes the Basin and Range Province.

Structural and Stratigraphic History

The Great Basin in Utah and Nevada lies atop the Cordilleran geosyncline. This geosyncline began to form in Late Precambrian time and continued as a single trough until the Late Devonian, when it was divided into miogeosynclinal (eastern) and eugeosynclinal (western) sections by the Antler Orogenic Belt (Roberts, 1960).

The eastern assemblage (roughly east of 116° west longitude) is typically about 15,000 feet thick, and contains rocks which are approximately 90% carbonates and 10% clastics (Roberts, 1958). Deposition began before the oldest Cambrian fossils appeared, and continued without orogenic interruption through the Triassic (Armstrong, 1968). During the Jurassic, the region of thickest deposition shifted to central and eastern Utah, with the western

part of the miogeosyncline becoming a source area for continental clastic deposits, which spread eastward (Armstrong, 1968).

In Early Cretaceous time the eastern margin of the Cordilleran miogeosyncline became a source area for clastic material (Armstrong, 1968). Armstrong modifies and elaborates upon earlier work by Harris (1959), and describes this source area as the Sevier Orogenic Belt, having a history of deformation - involving folding and thrusting - throughout most of the Cretaceous.

Thrusting in the Sevier Orogenic Belt had virtually ceased by Late Cretaceous time when the Laramide Orogeny began (Armstrong, 1968). In western Utah, the Laramide Rocky Mountains were characterized by folded and thrust-faulted strata of the miogeosyncline (Eardley, 1962). Because of the long history of orogenic activity, the present distribution of miogeosynclinal assemblages does not necessarily represent original stratigraphic positions or sites of deposition. As Eardley notes, the tectonic history of western Utah is complex and obscurred by Quaternary and Late Tertiary orogenic activity, and further study is needed before a final and detailed sequence of events can be presented.

Closely following the end of the Laramide Orogeny, general regional uplift began, together with the block faulting and igneous activity characterizing the present Basin and Range Province (Nolan, 1943). The nature of Basin and Range structure was first properly described by Gilbert (1874), and has been discussed in detail by Davis (1925), Gilbert (1928), Nolan (1943), Moore (1960), and Mackin (1960). Basin and Range block faulting is characterized

by generally north-south trending, high-angle, normal faults, with most fault blocks rotated or tilted. Displacements are commonly greater than 10,000 feet (Armstrong, 1968). Block faulting probably began in post-Oligocene time (Armstrong, 1968), and has been more or less continuous since (Eardley, 1962).

Tertiary igneous activity has resulted in extensive distributions of extrusive and intrusive rocks in the Basin and Range Province. Some 60,000 cubic miles of extrusive rocks (Mackin, 1960a), intermediate to acidic in composition, and composed chiefly of ignimbrites, were erupted in the Late Eocene, Oligocene, and Early Miocene (Armstrong, 1968). The ignimbrites, of which there are at least eleven series in southwestern Utah, spread as density currents and thus form ideal stratigraphic sheets (Mackin, 1960). They confirm that the volcanic activity post-dates the Laramide Orogeny, and that Basin and Range block faulting has been the only regional tectonic activity since the Laramide Orogeny (Mackin, 1960). Basic extrusive rocks are minor in volume and represent the most recent flows (Eardley, 1962).

Intrusive rocks occur throughout the Basin and Range Province, where they post-date Laramide structures (Eardley, 1962). Most absolute lead-alpha age determinations for intrusives in western Utah and eastern Nevada fall between 50 and 20 million years (Jaffe, 1959).

Rock Units in Thesis Area

Plate 1 shows the generalized geology of the thesis area, modified from the geologic map of southwestern Utah published by the

Utah Geological and Mineralogical Survey (Utah Geol. Survey, 1963).

The consolidated sedimentary rocks are mostly carbonate and clastic assemblages from the Cordilleran miogeosyncline. While important to the geologist and miner, their detailed description is of limited importance for this study, because they are non-magnetic and have density contrasts which are of secondary importance in the interpretation of the reconnaissance gravity survey. For further information on the sedimentary geology of the area one could refer to the extensive bibliographies of Armstrong (1968) and Mackin (1960), the Geologic Map Index of Utah (Boardman, 1954), and the publications of the Utah Geological and Mineralogical Survey (1968).

The widely distributed extrusive and intrusive rocks are of considerable importance in geophysical studies. The extrusive rocks originally covered nearly the entire erosional surface of sedimentary rocks, and are mostly quartz latites (Butler, 1913). In the San Francisco district, Butler recognizes two types of intrusive rocks: a granodiorite porphyry, and a quartz monzonite believed to be younger than the granodiorite porphyry. Dikes of quartz monzonite extend from the stocks, and younger, small aplitic and basic dikes have been intruded (Butler, 1913).

Ore Deposits

In western Utah, most ore deposits are closely associated with intrusive rocks, and their origin is directly related to the igneous activity (Butler, 1920). All ore deposits of the San Francisco Mountains vicinity are thought to be of essentially the same age,

and to have closely followed the intrusion of the quartz monzonite (Butler, 1913). Butler describes three types of mineral deposits, classified on the basis of the rock in which they occur:

1) Deposits in quartz monzonite: Characteristically copper deposits resulting from replacement along fissures, also containing minor amounts of lead.

2) Deposits in volcanic rocks: Replacement fissure deposits which contain primarily lead and silver ores. The Horn Silver mine, which produced ore valued at 20 million dollars between 1879 and 1909, was of this type.

3) Deposits in sedimentary rocks: Contact deposits, chiefly copper ores, have resulted from replacement of limestone close to the quartz monzonite, and frequently contain magnetite. Replacement fissure deposits have resulted from the replacement of limestone along fissures, sometimes at some distance from the quartz monzonite. These deposits have their principal values in lead and silver.

Magnetic Susceptibility of Rocks

The magnetic susceptibility of samples representing most of the outcropping rock types in the thesis area was measured using a Model MS-2 Magnetic Susceptibility Bridge, manufactured by the Geophysical Specialties Company, and was done to determine which rock units might generate magnetic anomalies. Table 6-1 summarizes the results of the measurements. The estimated accuracy of each

susceptibility determination was ±.000035 cgs units, based upon repeated measurements.

As expected, the consolidated sedimentary rocks have very low susceptibilities. They are rocks of the Cordilleran miogeosyncline, and contain little ferrous material. The samples of unconsolidated alluvium have significantly higher susceptibilities, although their magnetic effect is still of secondary importance. Magnetite in the alluvium is not easily destroyed by weathering, and appears to have been eroded from the igneous rocks of the area.

Samples from fissure-replacement and contact-zone mineralization were taken from areas which were too small to noticeably influence the aeromagnetic data (obtained 3000 to 4000 feet above the ground surface), but which may be important with respect to ground magnetic surveys. Therefore, the rock samples in these categories were almost entirely from the area of the ground magnetometer surveys in the Star Range. Mineralization of the fissure replacement type, with an average susceptibility of .000160 cgs units, would probably not be detectable by the magnetic methods employed in this study. In contrast, samples from contact zones, selected from areas where copper mineralization was present, contained so much magnetite that susceptibilities exceeded the range of the susceptibility bridge. Four samples were sent to the Hibbing, Minnesota, laboratory of Pickands Mather and Co., which is equipped for the analysis of taconite samples. The average percent by weight of magnetite for the four samples was 27%. With this much magnetite present, individual susceptibility values have little meaning, but it is

Table 6-1. Summary of susceptibility measurements.

	Rock Type	Ave. Susceptibility, cgs units	Number of Samples
1)	Consolidated sedimentary rocks - ls. & quartzite	.000040	5
2)	Alluvium	.000280	3
3)	Fissure-replacement mineralization	.000160	7
4)	Contact-zone mineralization	~ .100000	4
5)	Extrusive igneous rocks - acidic	.000140	4
6)	Intrusive igneous rocks - qtz. monzonite & granodiorite	.003450	14

Individual Intrusive Rock Susceptibility Measurements, cgs units	Sample Location (see Plate 1A)
.003910	Star Range
.002370	"
.003020	"
.004050	"
.003020	"
.004400	"
.002960	"
.003880	"
.004130	San Francisco Mtns.
.003320	"
.003790	Beaver Lake Mtns.
.002580	"
.003110	Rocky Range
.003760	"

obvious that magnetic exploration is a good method to use in the search for contact deposits in this area.

The aeromagnetic map does not appear to be influenced by surface volcanics, and susceptibility measurements confirm that the magnetization of the volcanics is low. Most of the volcanics present are pyroclastic ignimbrites, which in general have minimal magnetization (Mabey, 1964).

Intrusive rocks have significant susceptibilities throughout the area. Fourteen samples, taken from most of the intrusive exposures, have susceptibilities ranging from .002370 to .004400 cgs units, with an average value of .003450 cgs units. Table 6-1 lists the values of these measurements individually. There is no apparent relationship between susceptibility and intrusive location.

The variations in susceptibility among the intrusive samples measured seem characteristic of the intrusive rocks in the area, and occur over intervals as small as a few tens of feet. Figure 6-1 shows a portion of a vertical-field magnetic profile across an intrusive exposure in the Star Range, and demonstrates the irregular magnetization of the quartz monzonite.

There are six areas of intrusive outcrop shown on the geologic map, five of which have definite expression on the aeromagnetic map. The southernmost intrusive outcrop, just southeast of the old mining camp of Shauntie, has no aeromagnetic anomaly. Susceptibility measurements of samples from this outcrop (which were not included in Table 6-1) give an average susceptibility of .000400 cgs units, at least eight times lower than that of the other intrusive outcrops.

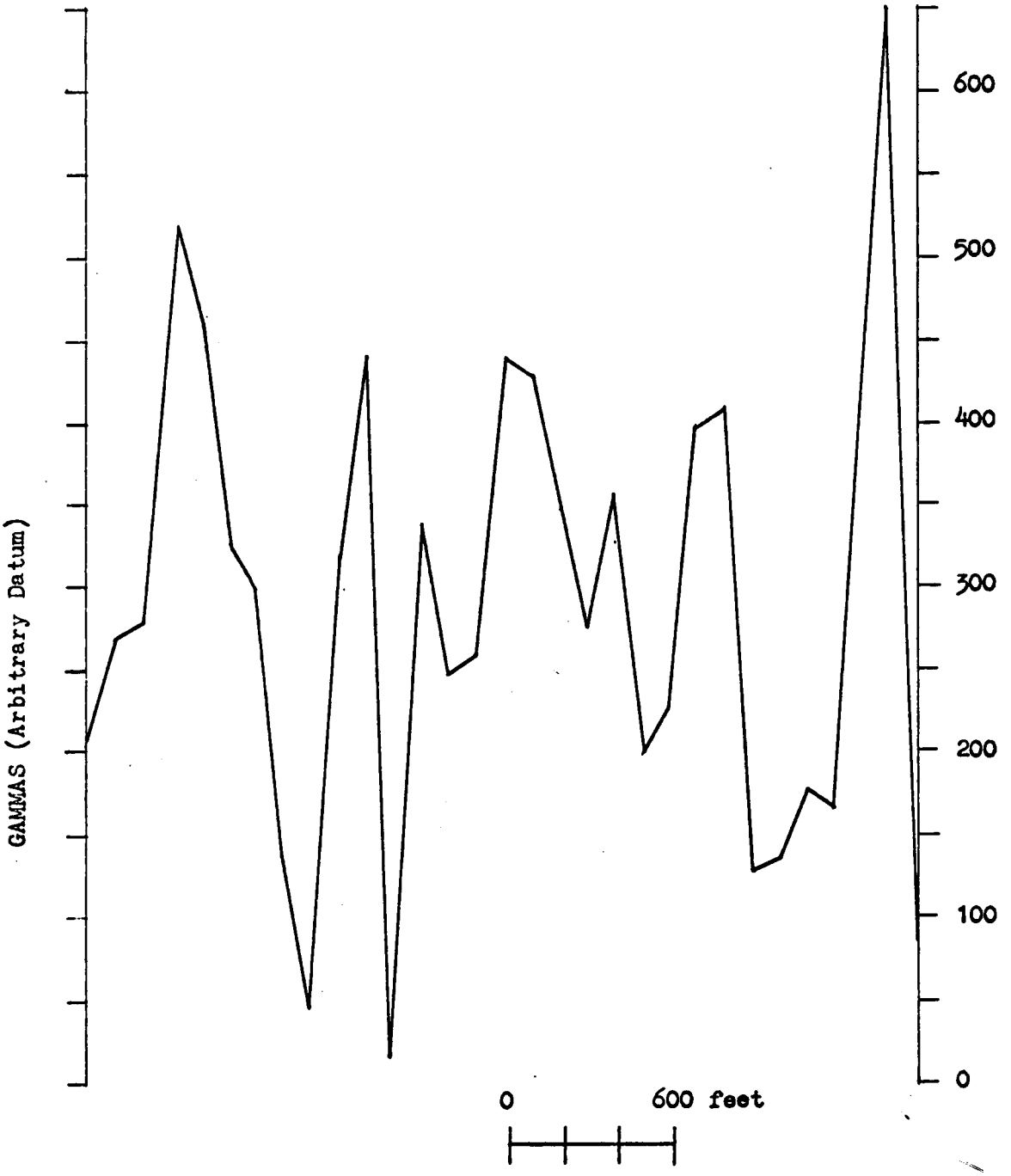

Figure 6-1. Portion of a ground magnetic traverse over a quartz monzonite intrusive exposure showing the irregular nature of the magnetization. Station spacing was 100 feet. Data shown are a portion of profile A, Figures 10-2 and 10-3.

Ground profiles confirm that this igneous body has essentially no magnetic expression, although its contact zone has a high magnetite content, and can be detected by ground-magnetic profiles.

The low susceptibility may have resulted from either the destruction of original iron-bearing minerals by hydrothermal alteration, or an original lack of magnetite. Mabey (1964) notes that an intrusive of similar age, the Bingham stock, southwest of Salt Lake City and associated with the Bingham open pit copper mine, has no appreciable magnetic expression, presumably due to the destruction of magnetite by hydrothermal alteration.

Remanent Magnetization

In the Basin and Range Province the directions of remanent magnetization of rocks of post-Eocene age fall into two groups - a normal group where remanent magnetization parallels the present geomagnetic field, and a reversed group where remanent vectors are directed opposite to the present earth's field (Doell and Cox, 1962). The two directions are presumed to arise from changes in the polarity of the earth's main field - at least 20 polarity changes are suggested since Eocene time (Doell and Cox, 1962).

Allingham and Zietz (1962) found the remanent magnetization to be less than one-eighth the induced magnetization for a granodiorite stock at the Nevada test site. Blank and Mackin (1967) report remanent susceptibilities ranging from .00016 to .005 cgs units for intrusions in the Iron Springs district, Utah, which is about 50 miles south of the San Francisco district.

No measurements of remanent magnetization are available from the thesis area. In all subsequent analysis of magnetic field data, the magnetization vector was assumed to parallel the earth's main field.

Density of Rocks

Densities of 2.70 and 2.25 grams per cc. for consolidated Paleozoic and unconsolidated Cenozoic rocks, respectively, have proven applicable in the Basin and Range Province (Mabey and Morris, 1967). Cenozoic volcanic rocks have average densities of 2.45 grams per cc. (Carlson and Mabey, 1963). The density of Tertiary intrusive rocks ranges from 2.60 to 2.80 grams per cc. (Carlson and Mabey, 1963).

The largest gravity anomalies within the pre-Tertiary rocks are caused by the density contrast between metamorphosed Precambrian rocks and the less dense sedimentary rocks of the Cordilleran miogeosyncline (Cook and Berg, 1961). The metamorphosed Early Precambrian rocks have densities averaging 2.86 grams per cc. (Mabey, 1963), but such rocks are not exposed in the thesis area. The Precambrian rocks exposed in the northern San Francisco Mountains are non-metamorphosed, Late Precambrian rocks, and have little if any density contrast with the Paleozoic rocks (Mabey, 1963; Carlson and Mabey, 1963).

VII. INTERPRETATION OF AEROMAGNETIC MAP - SAN FRANCISCO MTNS. AND VICINITY

Introduction

An aeromagnetic survey of the San Francisco Mountains and adjacent areas has been compiled by the U.S. Geological Survey (U.S.G.S., 1966), and covers an area of about 980 square miles - 28 miles in an east-west direction and 35 miles in a north-south direction. It was flown 9000 feet above sea level, along east-west flight lines with an average separation of one mile. Total-intensity magnetic-field contours are given at 20 gamma intervals.

The original map is included in the map pocket. This map was digitized for subsequent computer analysis by visual interpolation of contoured data to grid points at one-half mile intervals, and the resulting data set was contoured using a printer-plot contouring subroutine (Wendell, 1966).

A plane, regional field corresponding to the gradient of the earth's main magnetic field of 7.6 gammas per mile, increasing in the direction N26°E (U.S. Coast and Geodetic Survey, 1955), was removed from the original data. Plate 1 shows the resulting magnetic field superposed on the geologic map of the area. After removal of this gradient, the northern nine miles of the map showed only an increasing magnetic gradient of about 10 gammas per mile toward the north, corresponding to a slow recovery from the large magnetic low to the south. Because this part of the magnetic map was essentially featureless, subsequent interpretation deals with only the southern 26 miles of

the original map.

Figure 7-1 shows the southern three-fourths of the aeromagnetic data, contoured at 40 gamma intervals, with the gradient of the earth's main field removed. This map was machine-contoured from the digitized data set.

Regional and Residual Maps

The separation of gravity and magnetic maps into regional and residual components has long been an accepted step in the interpretation of potential field data. The basic ambiguity of such separations (see, for example, Skeels, 1947, and Nettleton, 1954) has led to the development of a number of techniques for the extraction of regional fields.

In recent years, efforts have been directed toward digital computer calculations of regional fields. In the course of the effort to assemble an interpretational package of computer programs for use in this study, three such methods were considered and applied to the aeromagnetic data - least-square polynomial fitting, wavelength filtering, and running averaging. A method was sought which economically separated potential field data into two components which corresponded to geologic structures of a regional and local extent, respectively. Since the nature of potential field data at present cannot be defined by a criteria set, the significance of a given computer operation upon a set of data is not yet possible to evaluate rigorously, and the final selection of a method to obtain regional and residual separations must be based upon subjective judgement of the geological significance of

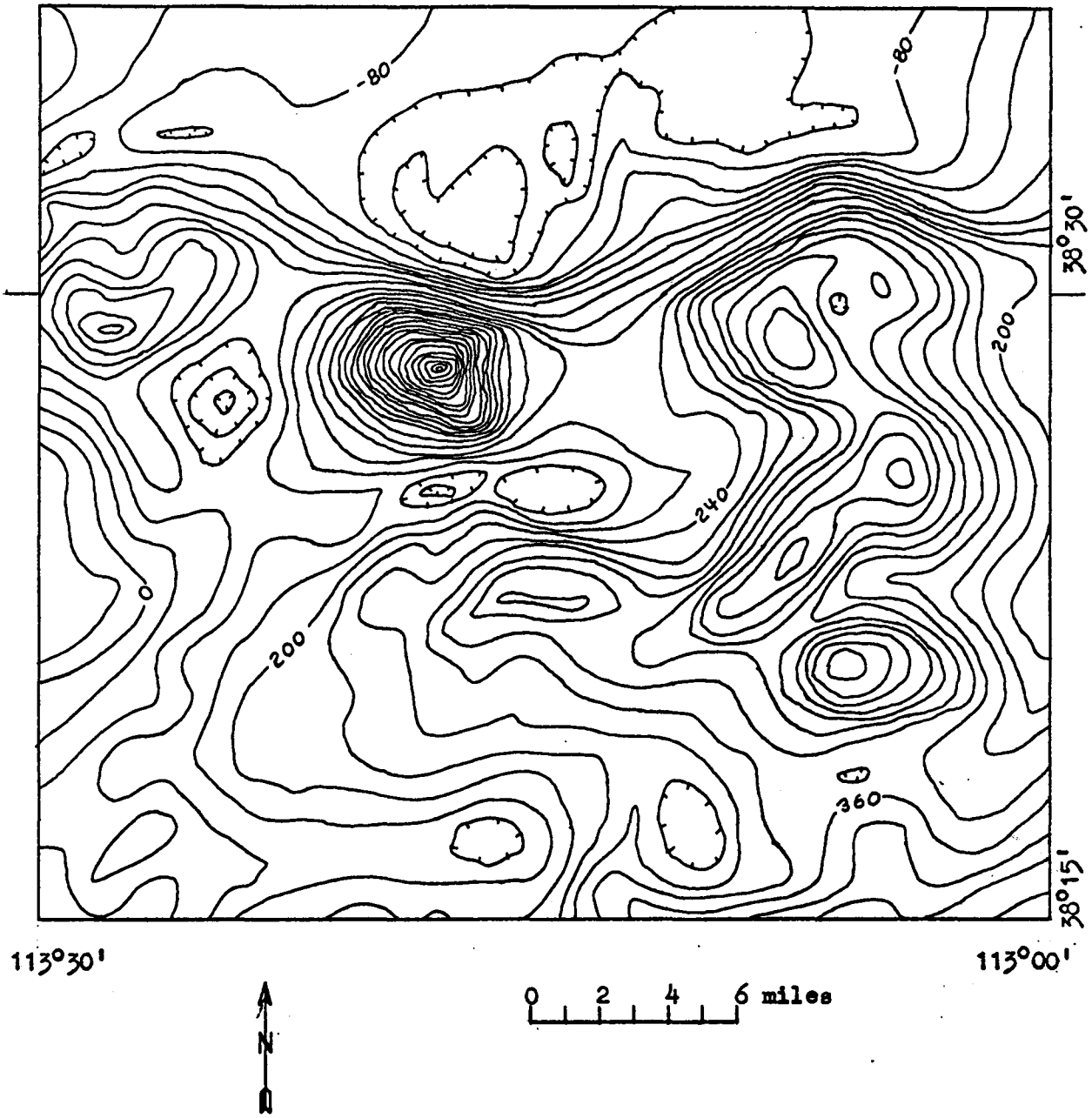

Figure 7-1. Aeromagnetic map of the San Francisco Mountains vicinity, southwestern Utah. Shown is the southern three-fourths of the original aeromagnetic map (U.S.G.S., 1966) of the area, machine-contoured from the digitized data set representing the original map. A plane regional gradient corresponding to the gradient of the earth's main field has been removed. Contour interval = 40 gammas.

the maps produced, and the cost of the method in terms of labor and facilities.

The method used to fit two-dimensional algebraic polynomial surfaces to the aeromagnetic data is described by Mack (1962). A digital computer program, made available by the Gulf Research and Development Corporation, was applied to the digitized aeromagnetic data, and machine-contoured maps of the first, third, fourth, sixth, eighth, tenth, and thirteenth degree polynomial surfaces were computed. Corresponding residual maps were obtained by subtracting each of these polynomial surfaces from the original data.

Two-dimensional wavelength filtering can be done in the space domain by convolving the data with a grid operator (usually designed in the wavenumber domain) intended to pass certain wavelengths and reject others. A low-pass filter emphasizes regional features while a high-pass filter enhances local features. A grid operator designed by Zurflueh (1967) as a low-pass wavelength filter was applied to the aeromagnetic data of Figure 7-1, and regional maps with wavelength cutoffs of 5.3, 10.7, 16.0, and 21.3 units were obtained. One unit, in this case, equaled one-half mile. Corresponding residual maps were obtained by subtracting each of the regional maps from the original data.

The running average method of obtaining regional surfaces involves the determination of mean values for specified overlapping portions of the observed data. For the gridded data of Figure 7-1, the data in a square about a given point of application with sides of N data points were summed and divided by N^2, to obtain regional or

smoothed values. 3*3, 5*5, 7*7, 9*9, 11*11, and 15*15 running average regional maps were computed, and corresponding residual maps were obtained by subtracting each of the regional maps from the original data. The notation N*N running average indicates that data in squares having sides of N data points were averaged.

In this applied geophysical study, concerned primarily with geological interpretation, it was intended to use regional and residual separations as interpretational aids, and not as objects themselves of detailed investigation. Consequently, the evaluation of the three methods described above was based on the applied aspects of geological significance and economy of operation.

It was found that each of the three methods produced regional maps that showed many similarities, and there was, in fact, little difference between them with respect to the geologic implications of the regional and residual maps. An example is shown in Figure 7-2, which compares regional maps, computed from the data of Figure 7-1, of the tenth degree polynomial, the 16.0 unit wavelength filter, and the 11*11 running average.

In terms of economy of operation, the method of least-square polynomial fitting had definite weaknesses. The computer program required considerable computer storage and execution time, and its use was restricted by the capability of the IBM 7040 computer used for most of the thesis work. The data treated in the thesis generally required high degrees of freedom, and on the 7040 computer it would have been necessary to subdivide the maps into smaller, overlapping squares and then compute the polynomial surfaces. The polynomial

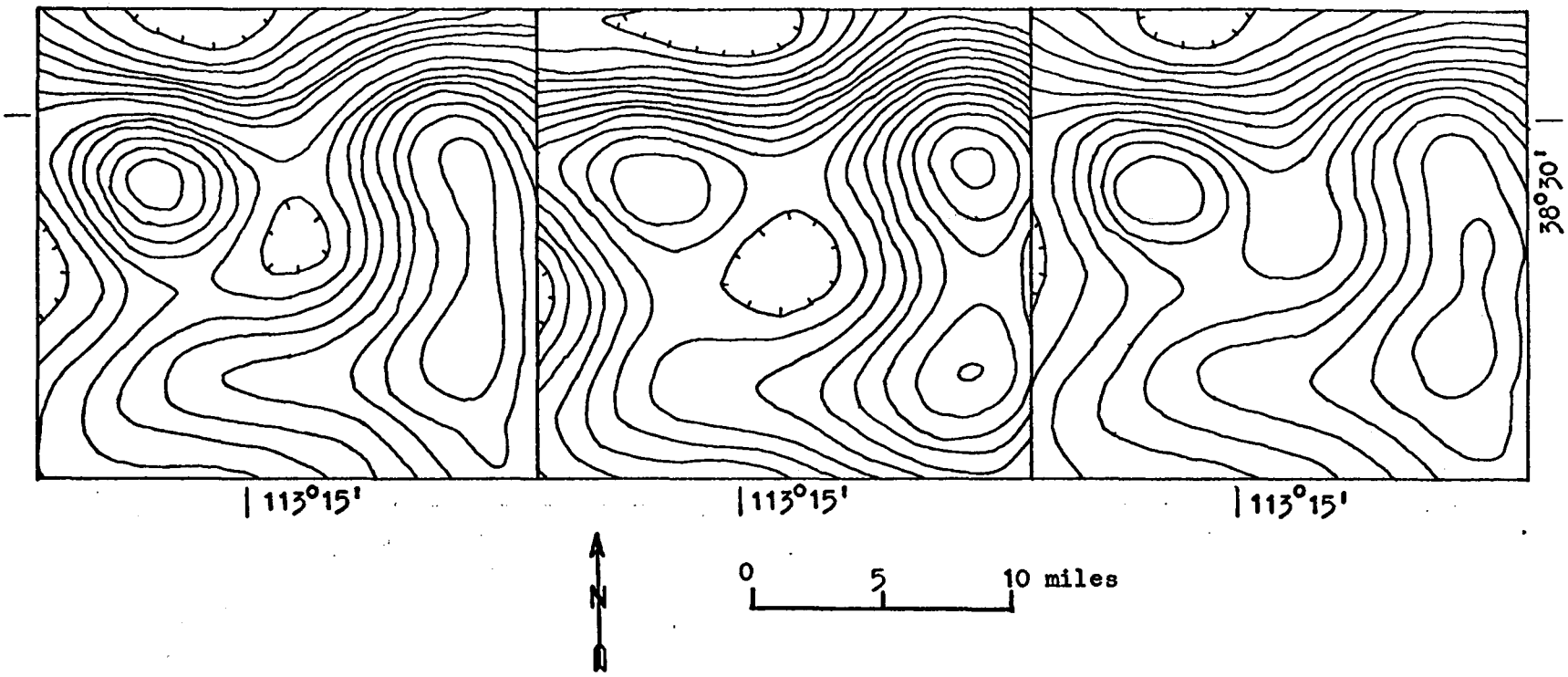

16.0 unit wavelength filter | 10th degree polynomial | 11*11 running average

Figure 7-2. Comparison of regional maps of the data of Figure 7-1, generated by wavelength filtering, least-square polynomial fitting, and running averaging. Contour interval = 40 gammas.

surfaces which were computed were done on a Univac 1108 computer available during early stages of thesis work at the University of Utah. For these reasons polynomial surface fitting was not used for subsequent geological interpretation.

All maps used in the study were limited in areal extent. In the convolution of Zurflueh's coefficient set with the data, as well as the running average method, which can be regarded as a convolution, a strip of data around the map edges equal to half the grid operator width cannot be properly convolved. For a given cutoff wavelength, however, the running average coefficient set was considerably smaller than Zurflueh's coefficient set, and thus, to obtain subjectively similar filtered maps, the running average method resulted in considerably less data lost at the map edges. In addition, as the running average coefficient set began to overlap the edge of the data, the number of data points averaged became fewer, and it was felt that the resulting values tended toward the values of the original data points, and could be retained. Therefore, the running average method for producing regional and residual separations was used most extensively. A FORTRAN subroutine was written which performed the N*N running average convolution upon any rectangular gridded data set. Near a map's edge areas, those data points that were available were used in the averaging, so that data along the edges were not discarded.

The running average method can be thought of as a filtering operation, in that the regional map is obtained by convolving the original data with a coefficient set, each point of which has an

amplitude of $1/N^2$. Referring to the one-dimensional case for simplicity, the running average coefficient set can be regarded as a box-car function, symmetric about the origin, or in terms of electrical engineering, the coefficient set describes a rectangular pulse, although in the present case the abscissa is not time, but distance. The wavenumber representation of the running average coefficient set is the Fourier transform of a rectangular pulse. Figure 7-3 compares the wavenumber representation of the running average coefficient set to Zurflueh's filter, in one dimension.

One notes from Figure 7-3 that the running average method is equivalent to filtering with a low-pass filter. Considered as a low-pass filter, the running average filter does not appear as good as Zurflueh's filter, for it passes more high frequency components. This, in some measure, is the penalty imposed by a smaller coefficient set in the space domain, but it was felt that differences in performance as a filter were, in practice, quite negligible. Both filters introduce relatively small but unknown distortion in filtered anomaly shapes, and there is little objective basis for selecting one method over the other.

Of the various running average operators applied to the aeromagnetic data, the 15*15 operator appears, subjectively, to produce the most meaningful separation of the data. Figures 7-4 and 7-5 present the 15*15 running average regional and residual maps of the aeromagnetic data. In subsequent analysis, geological explanations will be provided for both the regional and residual maps. Consequently, the ambiguity encountered in removing a "regional" field by an arbitrary

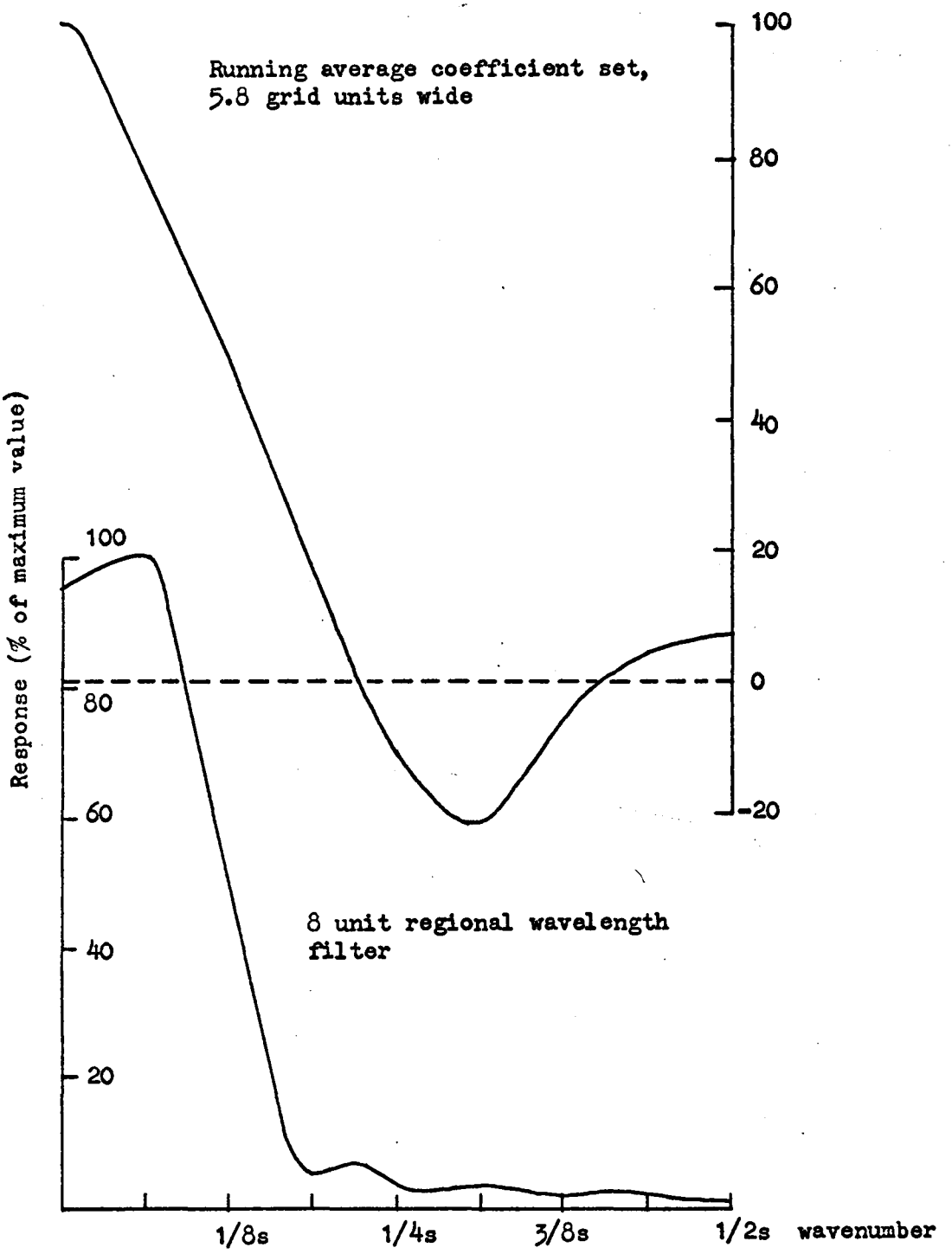

Figure 7-3. Comparison of Zurflueh's wavelength filter to wavenumber response of the running average coefficient set. Phase angle = 0, s = grid interval.

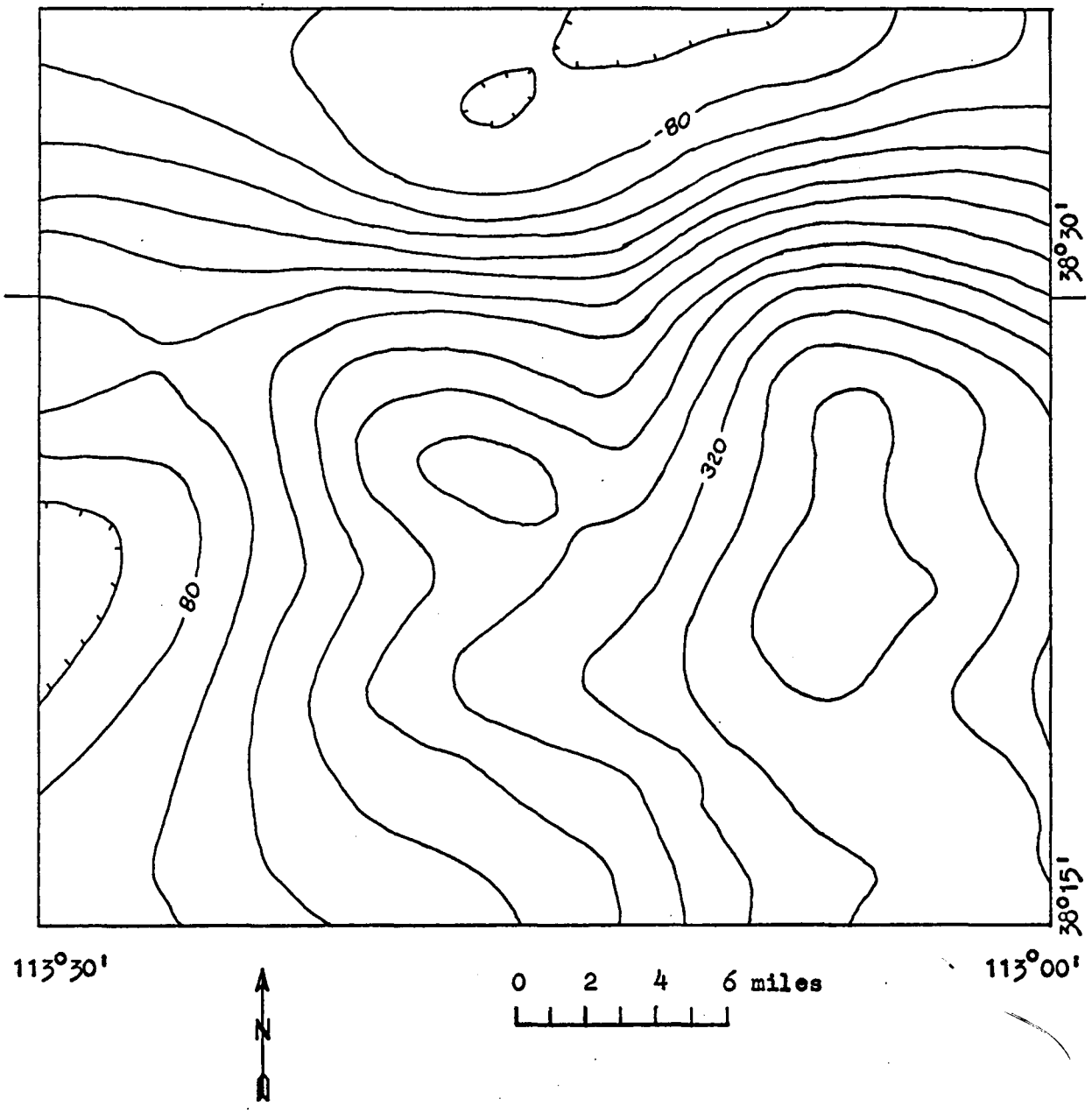

Figure 7-4. 15*15 running average regional map of the aeromagnetic data of Figure 7-1. Contour interval = 40 gammas.

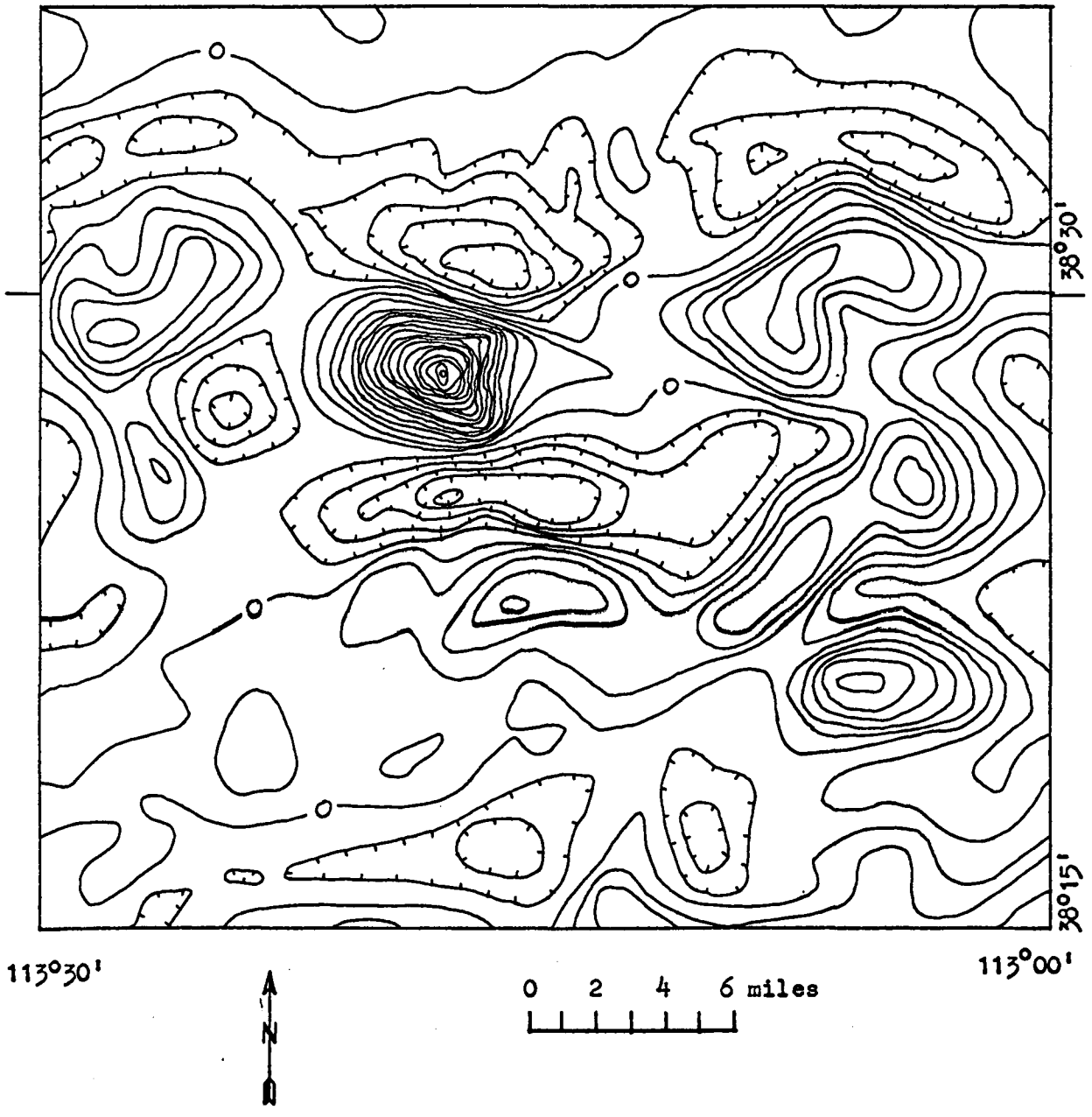

Figure 7-5. 15*15 running average residual map of the aeromagnetic data of Figure 7-1. This map was obtained by subtracting the data of Figure 7-4 from that of Figure 7-1. Contour interval = 40 gammas.

method is avoided.

Observations of the Aeromagnetic Data

It has been noted that the upper nine miles of the original aeromagnetic map are devoid of anomalies and reflect primarily a regional gradient, while the lower three-fourths of the map shows a considerably more disturbed magnetic field. As Affleck (1963) notes, it is common on magnetic surveys to find areas of consistent magnetic character with distinct boundaries - such areas can be referred to as magnetic provinces. On this map, portions of two magnetic provinces appear. Figures 7-1, 7-4, and 7-5 include the southern magnetic province.

Plate 1 shows that unconsolidated sediments comprise most of the surface outcrops in the area. Extrusive igneous rocks rank next in areal extent, but have little if any magnetic expression. The flight line altitude of 9000 feet is high enough to eliminate some of the small scale magnetic fluctuations typically associated with volcanic rocks, but the fact that most of the volcanics are acidic pyroclastics, with low susceptibility, probably is the chief reason for their lack of magnetic expression.

The aeromagnetic map (Figure 7-1) presents two basic features: Local magnetic highs with areal extents of about five miles, and regional gradients covering large areas of the map.

Figure 7-5, the residual aeromagnetic map, clearly shows a group of more or less independent magnetic highs, with closures ranging from 160 gammas to 720 gammas. Each of the intrusive

exposures shown on Plate 1, with the exception of the southernmost intrusive exposure, corresponds to a magnetic high on the residual map. The two remaining magnetic highs - one on the western edge of the map near Wah Wah Springs, and the other south-southeast of the large anomaly just west of the site of Frisco - occur over volcanics and alluvium. They too may be caused by intrusive bodies near the surface, which are covered by relatively thin layers of volcanics and alluvium.

Figure 7-4, the regional aeromagnetic map, shows those magnetic features which are related to larger causative structures. One of the most striking features on the original map (Figure 7-1) is the magnetic gradient, decreasing from south to north, which runs more or less linearly from east to west across the northern part of the map. This feature is transverse to Basin and Range structures. On Figure 7-1, the basic gradient has been intensified by the effect of three more local magnetic features, but Figure 7-4 shows the regional nature of the gradient. Figure 7-4 also shows a regional magnetic gradient, decreasing from east to west, in the southern part of the area. The regional magnetic contours thus tend to strike east-west in the northern one-third of Figure 7-4, and north-south in the southern two-thirds.

Model Studies of Igneous Structure

The aeromagnetic data will be shown to be consistent with the following geological model: The southern magnetic province is the magnetic expression of an intrusive body of batholithic proportions,

with a northern boundary extending from east to west across the northern portion of the area, and otherwise extending beyond the area of aeromagnetic coverage. The depth to the top of the batholithic structure increases from east to west, and local cupolas, some of which outcrop, extend upward from the main intrusive body.

To demonstrate that this model can reproduce the general patterns of the aeromagnetic map, and to investigate the model's physical parameters, computer programs were written for the computation of the magnetic fields over two-dimensional and three-dimensional forms, and models for the distribution of magnetic rocks in the thesis area were developed. The programs are listed in Appendices IV and V.

The program for computing the magnetic field over a two-dimensional model closely followed the approach given by Heirtzler, et.al., (1962). It computed and plotted either the vertical or total magnetic field, on a plane, over a two-dimensional model made up of horizontal laminae individually specified by thickness and edge angle. The program for computing either the vertical or total magnetic field, on a plane, over a three-dimensional model was based on formulas given by Talwani (1965). A three-dimensional model consisted of N horizontal, polygonal plates with vertical sides, each defined by M corner points.

The earth's main field in the area has an approximate declination of 16 degrees (east), an inclination of 64 degrees, and a total field strength of approximately 54,000 gammas (Vestine, 1947). These values were used in the magnetic modeling programs for computing induction effects. A susceptibility of $k = .003450$ cgs units (discussed in Section VI) was used for all igneous models. No remanent magnetization

vectors were introduced.

The approach to the problem of model design for the aeromagnetic data was to develop first a model whose magnetic field resembled that of the regional aeromagnetic map, Figure 7-4, then to develop a model whose magnetic field resembled the residual aeromagnetic data, Figure 7-5, and finally to combine these two models to obtain the complete model representing the distribution of magnetic rocks in the area. Two-dimensional magnetic computations were used to investigate approximately the dependence of the magnetic field upon various physical parameters, as a guide to designing the three-dimensional model required to reproduce the observed aeromagnetic field. Combinations of very simple forms were used for geologic models.

The model developed to fit the regional aeromagnetic data of Figure 7-4 is shown in Figure 7-6 and described in Table 7-1. The northern termination of the model is shown (Figure 7-6), but to the east, south, and west, the aeromagnetic data did not extend to the edge of the magnetic body and the model was assumed to continue to infinity. Figure 7-8 shows the total-intensity magnetic field generated by this model, at an elevation of 9000 feet, and should be compared to Figure 7-4. The model demonstrates that the regional gradients in the observed aeromagnetic field can be generated by a large magnetic body with a steeply inclined or vertical northern edge and a progressively greater depth of burial from east to west. Correlation between Figures 7-4 and 7-8 is poorest in the east-central area, where the model is closest to the flight line. The magnetic response

to geometric detail is more pronounced in this area, making it harder to fit the observed data with an idealized model.

Figure 7-7 and Table 7-2 show and describe the model designed to duplicate the residual aeromagnetic data of Figure 7-5. Figure 7-9 shows the total-intensity magnetic field computed over the residual model, at an elevation of 9000 feet, and should be compared to Figure 7-5, the 15*15 running average residual map. Figure 7-5 has many low amplitude closures and noses, which a model cannot easily duplicate. The model does reproduce the magnetic highs of the residual map both with respect to shape and amplitude. There were severe constraints imposed on the cupolas of the residual model. The lower extent of the cupolas was defined by the top of the regional model, while the upward extent was in most cases controlled by surface topography. A constant susceptibility of k = .003450 cgs units was proscribed. Nevertheless, the residual cupolas generated magnetic anomalies not only with the desired shapes, but with the correct amplitudes.

The magnetic field of the complete model, obtained by adding the regional and residual computed fields, is shown in Figure 7-10 (compare to Figure 7-1). The magnetic field of the final model is a function of the geometric parameters of the eighteen individual plates comprising the final model. Other models, producing a similar magnetic field due wholly or in part to susceptibility variations, could probably be designed. Since only a small fraction of the causative body is exposed, the true susceptibility distribution of the body cannot be determined. It is felt that, lacking additional information, a uniformly magnetized model is more likely to better represent the actual body.

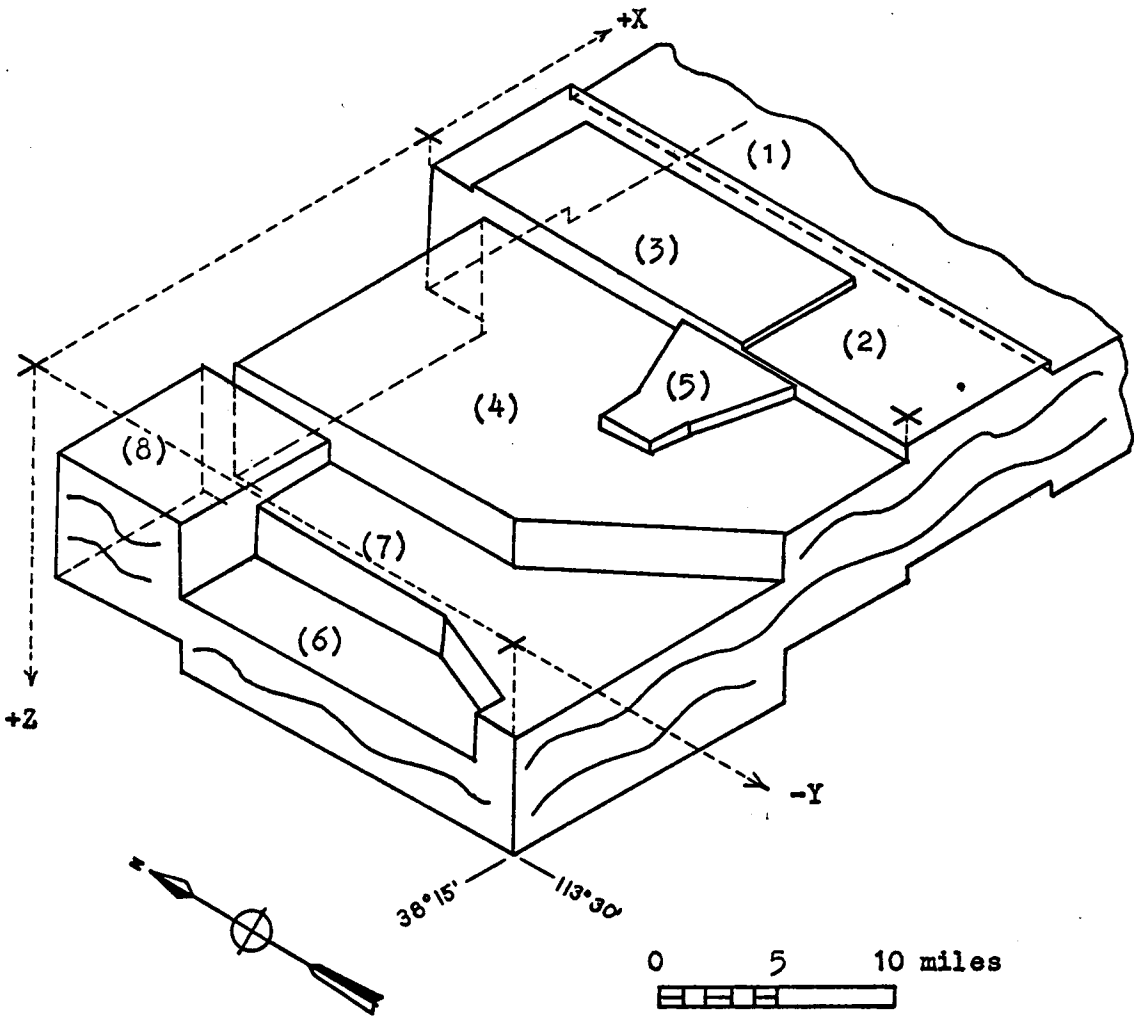

Figure 7-6. Perspective drawing of the regional igneous model. Numbers designate the individual plates comprising the net model. To the east, west, and south, the model continues beyond the area of aeromagnetic coverage. Crosses mark the plane of the flight line.

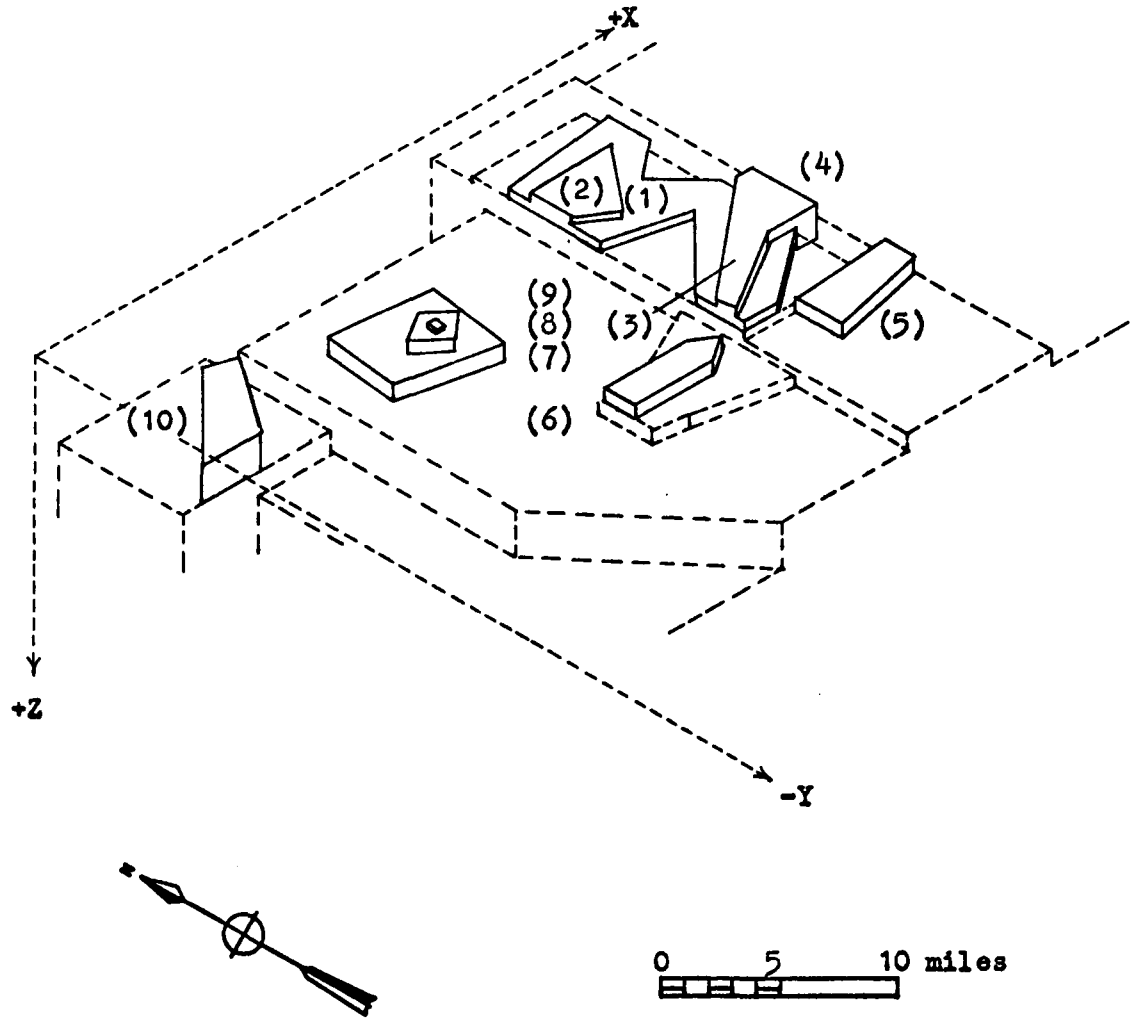

Figure 7-7. Perspective drawing of the residual igneous model. Numbers designate the individual plates comprising the net model. Dotted lines show the top of the regional igneous model, on which the plates of the residual model lie.

Table 7-1. Physical parameters of the regional igneous model. Plate numbers refer to Figure 7-6. Corner coordinates are in miles, measured from the lower, left corner of the original aeromagnetic map. Elevations are relative to sea level.

Plate No.	Elevation of Top	Elevation of Bottom	Corner Coordinates North	East
1	-1,000'	-27,000'	23.0	26.0
			23.0	∞
			-∞	∞
			-∞	26.0
2	2,100'	-24,300'	23.0	19.0
			23.0	26.0
			-∞	26.0
			-∞	19.0
3	3,200'	2,100'	21.0	19.0
			21.0	24.5
			8.0	24.5
			8.0	19.0
4	-1,000'	-27,400'	20.5	7.0
			20.5	19.0
			-∞	19.0
			-∞	13.0
			0.0	13.0
			7.0	7.0
5	1,100'	-1,000'	10.0	12.0
			10.0	15.0
			11.0	19.0
			5.5	19.0
			6.5	15.0
			6.5	12.0
6	-22,200'	-38,000'	16.0	-∞
			16.0	7.0
			7.0	7.0
			0.0	13.0
			-∞	13.0
			-∞	-∞
7	-11,600'	-22,200'	16.0	3.5
			16.0	7.0
			7.0	7.0
			0.0	13.0
			-∞	13.0
			-∞	-∞
			2.0	-∞
			2.0	1.5
			7.0	3.5
8	-6,300'	-32,700'	22.0	-∞
			22.0	7.0
			16.0	7.0
			16.0	-∞

Table 7-2. Physical parameters of the residual igneous model. Plate numbers refer to Figure 7-7. Corner coordinates are in miles, measured from the lower, left corner of the original aeromagnetic map. Elevations are relative to sea level.

Plate No.	Elevation of Top	Elevation of Bottom	Corner Coordinates North	East
1	4,800'	3,200'	19.5	19.0
			20.0	24.5
			18.0	24.5
			16.5	22.5
			14.5	24.5
			11.0	24.5
			8.0	20.5
			8.0	19.0
			10.5	19.0
			14.0	22.5
			15.0	19.0
2	5,800'	4,800'	18.5	19.0
			19.0	23.0
			15.5	21.0
			16.5	19.0
3	5,800'	4,800'	9.5	19.0
			14.0	24.5
			11.0	24.5
			11.0	23.0
			8.5	19.0
4	5,800'	2,100'	14.0	24.5
			14.0	25.5
			11.0	25.5
			11.0	24.5
5	5,300'	2,100'	8.0	21.0
			8.0	26.0
			6.5	26.0
			5.5	21.0
6	4,100'	1,100'	10.0	12.0
			10.0	17.0
			9.0	18.5
			8.0	17.0
			8.0	12.0
7	4,800'	-1,000'	14.5	8.5
			18.0	9.0
			17.5	13.5
			13.5	13.0
8	7,400'	4,800'	15.5	10.0
			16.5	11.5
			15.5	12.5
			14.5	11.5
9	7,900'	7,400'	15.7	11.3
			15.7	11.7
			15.3	11.7
			15.3	11.3
10	1,600'	-6,300'	16.0	1.0
			20.0	5.0
			19.5	6.5
			16.0	4.0

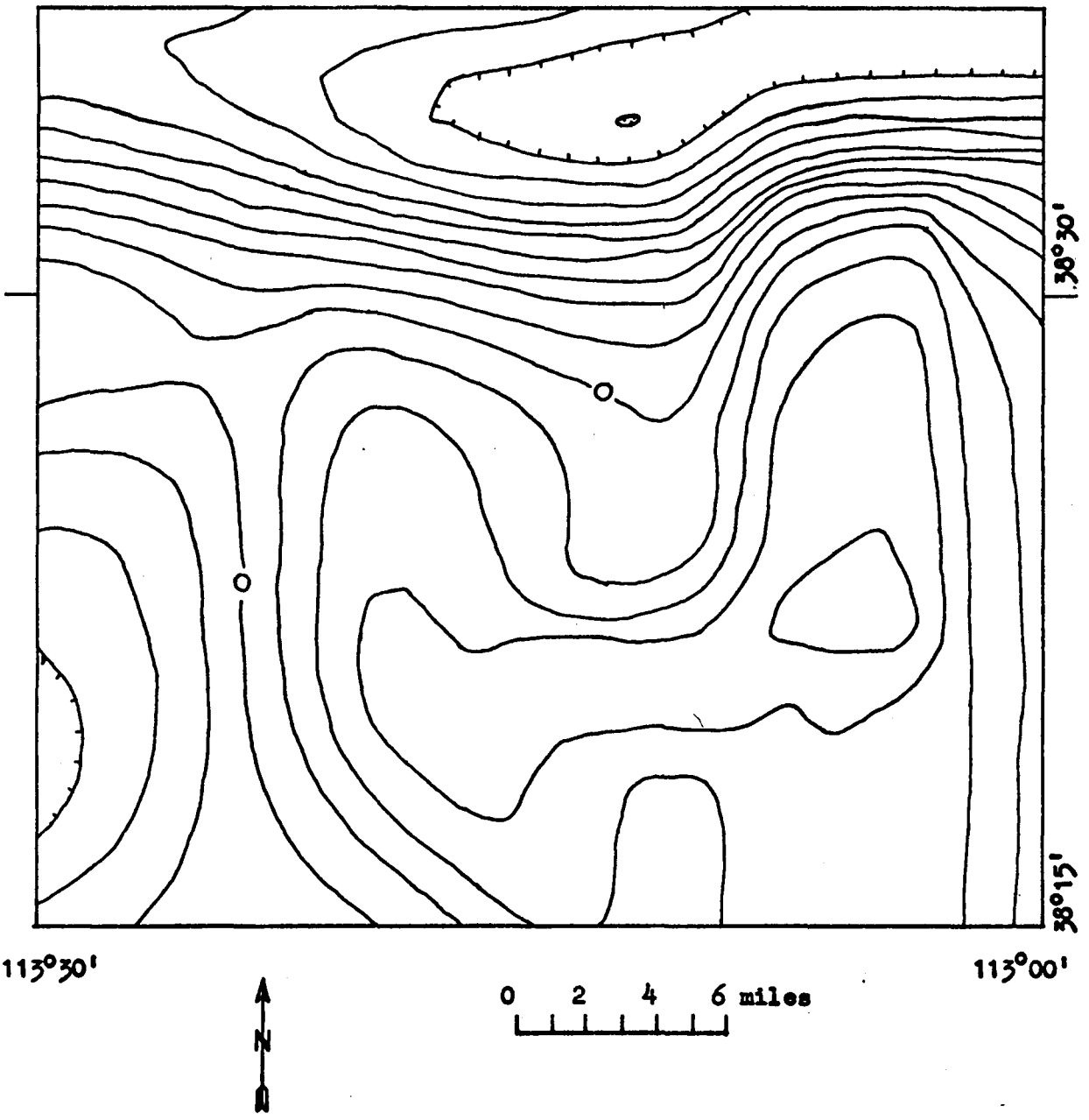

Figure 7-8. Total intensity magnetic field generated by the regional igneous model. Values were computed at an elevation of 9000 feet. This figure should be compared to Figure 7-4. Contour interval = 40 gammas.

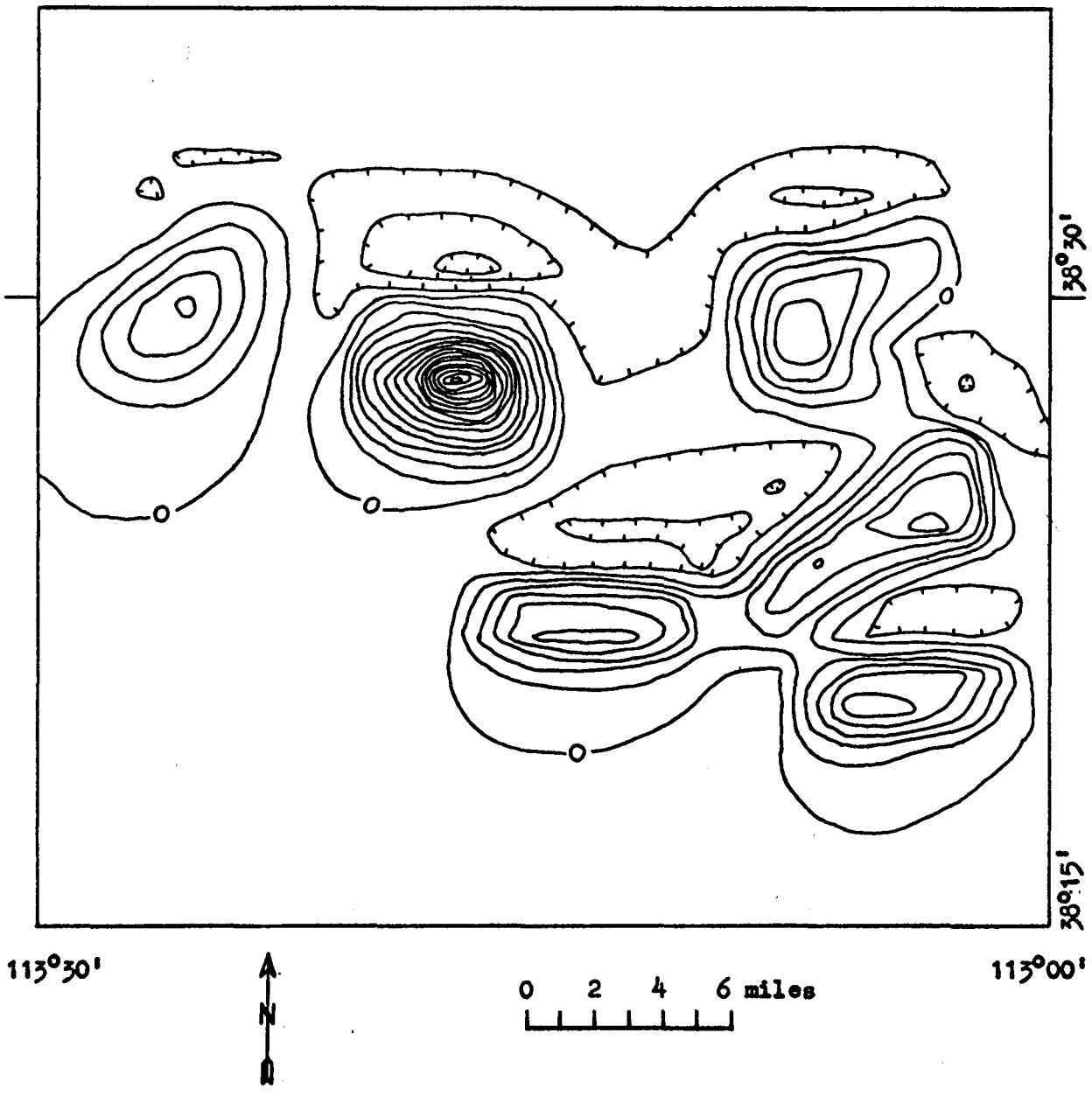

Figure 7-9. Total intensity magnetic field generated by the residual igneous model. Values were computed at an elevation of 9000 feet. This figure should be compared to Figure 7-5. Contour interval = 40 gammas.

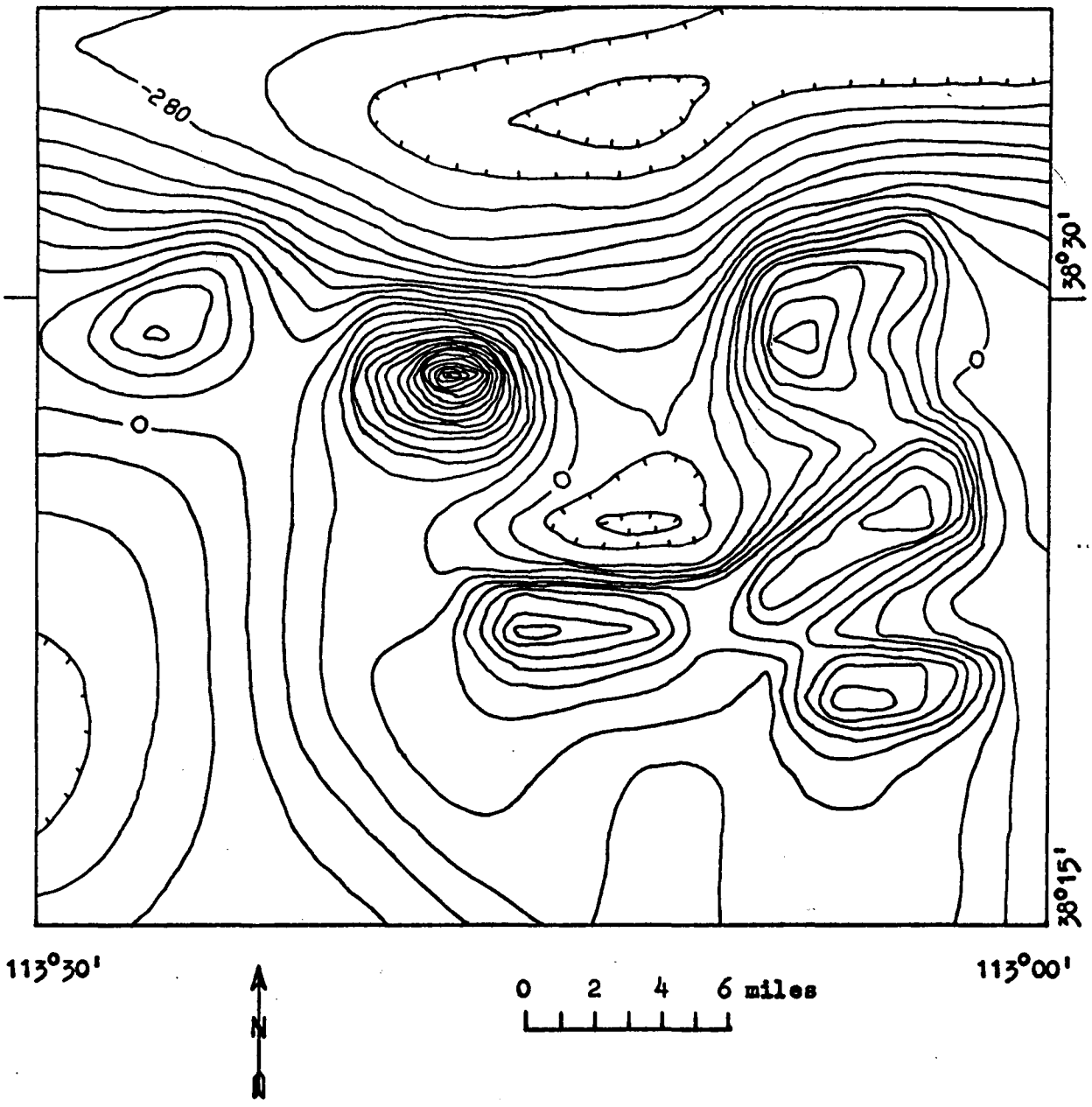

Figure 7-10. Total intensity magnetic field generated by the total igneous model. This figure is the sum of the data of Figures 7-8 and 7-9, and should be compared to Figure 7-1. Contour interval = 40 gammas.

Discussion of Regional Geologic Implications

The following discussion is based on the assumption that the distribution of magnetic material, as shown in Figures 7-6 and 7-7, represents a Tertiary intrusive body of batholithic proportions. On many aeromagnetic surveys, anomalies reflect susceptibility contrasts in crystalline basement rocks. In this case, however, many of the cupolas of the model outcrop as quartz monzonite and granodiorite intrusive bodies of Tertiary age. The finite thickness of the regional model also implies that it does not reflect susceptibility contrasts in older crystalline basement rocks underlying the sedimentary assemblages in the area. Even over the exposure of Precambrian rock in the northern part of the San Francisco Mountains (Plate 1), no magnetic effect of crystalline basement rocks is recognized. Aeromagnetic surveys in the Tintic area to the north (Mabey and Morris, 1967) and the Iron Springs district to the south (Blank and Mackin, 1967) are similarly interpreted in terms of Tertiary igneous rocks only.

The magnetic gradient extending from east to west across the aeromagnetic map, indicating the border of the causative structure, provided an opportunity to investigate the dip of the border and the thickness of the pluton. This gradient, as shown on the original aeromagnetic map (Figure 7-1), was apparently distorted by more localized structure, and it was felt that the regional aeromagnetic map, Figure 7-4, presented the gradient with some of the local perturbations removed.

By assuming a susceptibility of .003450 cgs units, the depth of the top of the pluton was largely determined. The anomaly amplitude was quite insensitive to thickness of the pluton for thicknesses exceeding

about three miles. With the depth to the top of the source known (or assigned), the horizontal separation of the positive and negative peaks of the anomaly, and the amplitude of the negative closure relative to the total anomaly amplitude, provided an indication of the thickness of the intrusive body and the angle of the edge.

Using the two-dimensional magnetic computation program, the relationship between pluton edge angle and thickness, and the magnetic parameters of anomaly width and ratio of negative closure to total anomaly amplitude was investigated. The ratio of negative closure to total anomaly amplitude was sensitive to edge angle, and dictated an edge with a dip of 80 to 90 degrees. For ease of computation, a vertical northern edge was chosen.

With the parameters of depth of burial and edge angle assigned, the separation of the maximum and minimum of the anomaly indicated an approximate thickness of five miles for the pluton. The anomaly computed over a "bottomless" pluton - represented by a model 12 miles thick, the assumed depth of the Curie point isotherm (Vacquier and Affleck, 1941) - clearly did not fit the observed data. Figure 7-11 compares the computed magnetic anomalies over plates 5 and 12 miles thick to the observed data as represented by the regional aeromagnetic map (Figure 7-4).

The question arises as to whether the regional intrusive body should be referred to as a pluton or a batholith. The term batholith is in common usage, and implies that an intrusive body is large (greater than 40 square miles), but a batholith is also defined as enlarging downward, with no visible floor (Billings, 1954). The structure underlying the San Francisco Mountains vicinity is distinctly tabular,

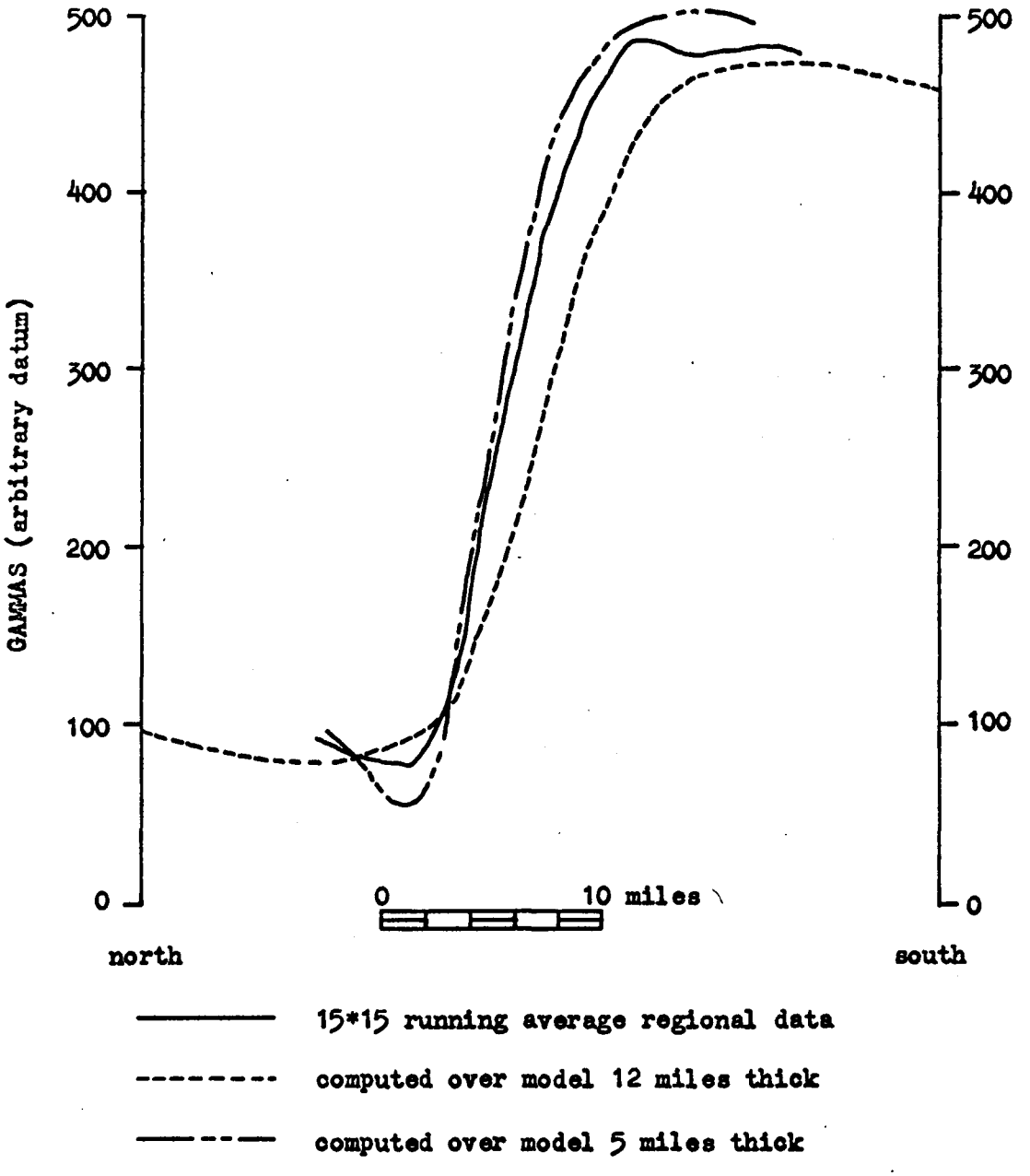

Figure 7-11. Comparison of observed regional aeromagnetic data and the anomalies computed over horizontal plates with thicknesses of 5 and 12 miles. The plates had a susceptibility of .003450 cgs units, a vertical northern edge, and a top elevation of -1000 feet.

with a more or less uniform thickness of five miles, and so does not satisfy the formal definition of a batholith. It has been reported on the basis of geophysical evidence (Hamilton and Meyers, 1967), that the Boulder Batholith, for example, is about 3 miles thick, and the Sierra Nevada Batholith is between 5 and 6 miles thick, and that "batholiths" are generally tabular and thin, having spread out laterally at shallow depth. Perhaps, with the accumulation of more evidence, Billings' definition of a batholith will need revision. The term pluton - a body of igneous rock that has formed below the surface of the earth (Billings, 1954) - is safe to use in all cases, but does not carry the connotation of large size.

The northern edge of the pluton (Figure 7-6) extends east-west, with minor inflections. This trend is not only discordant with Basin and Range structure, which is oriented in a generally north-south direction, but with other structure in the region dating from Late Precambrian time. Mabey and Morris (1967), however, note that in the Tintic Valley and vicinity, some 100 miles north of the San Francisco Mountains area, igneous rocks and related magnetic anomalies occur in a broad west-trending belt. Further north, the Bingham, Alta, and Park City intrusive belt has an east-west alignment (Mabey, 1964). These two areas of igneous activity, together with the Milford area, account for 95 percent of the copper, lead, silver, gold, and zinc produced in Utah (Hilpert and Roberts, 1964).

The full extent of the plutonic body underlying the thesis area is not shown by the aeromagnetic map. The outcrop pattern of intrusive

rocks in southwestern Utah, Figure 7-12, (Cohee, 1962), indicates that the San Francisco Mountains area may be part of an intrusive belt which extends about 85 miles in an east-west direction, and is some 20 miles wide. If so the coverage of the aeromagnetic map may reach nearly to the southern edge of the intrusive body.

The absence of major surface structures coincident or parallel to the belts of abundant igneous rocks in western Utah suggests that the gross configurations of the belts of igneous rocks may be controlled by pre-existing, deep-seated structures only indirectly related to upper crustal structure (Mabey and Morris, 1967). Fuller (1964) has discussed magnetic anomaly patterns in parts of the western United States which appear to be interrupted by east-west features, and considers the interruptions to be an expression of deep fracture patterns, partly decoupled from the upper crust. The possibility of structural control upon the northern edge of the pluton by an east-west trending fault zone is discussed further in Section IX.

Summary of Section VII - Aeromagnetic Data

Least-square polynomial fitting, wavelength filtering, and running averaging, by digital computer, are discussed as means of obtaining regional and residual separations of the aeromagnetic map of the San Francisco Mountains and vicinity (U.S.G.S., 1966). The method of running averages is considered to be as reliable as the others but significantly less costly for the purposes of this thesis. 15*15 running average regional and residual maps of the aeromagnetic

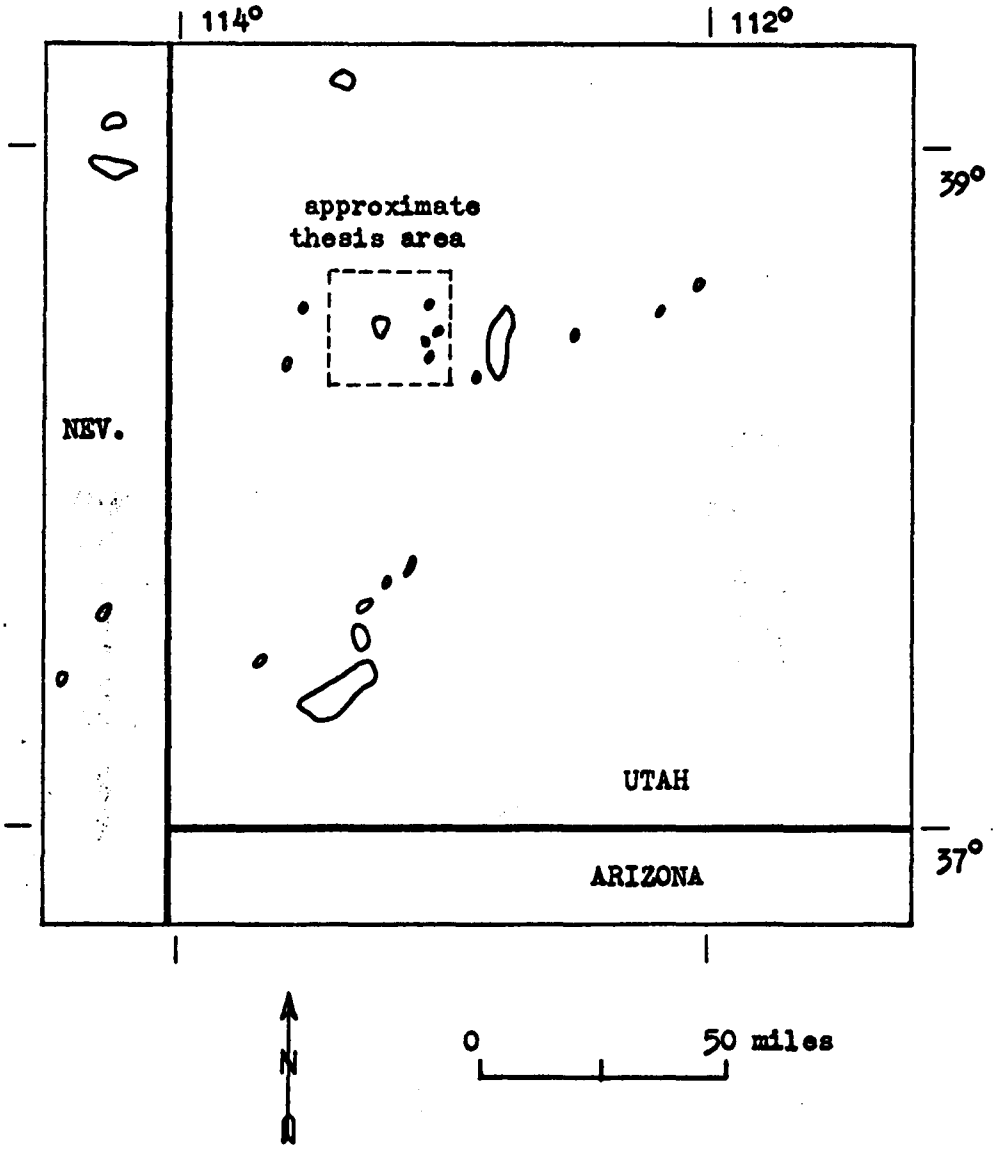

Figure 7-12. Outcrop pattern of intrusive rocks in southwestern Utah.

data are selected for model interpretation.

Magnetic anomalies over three-dimensional bodies are calculated by digital computer, and a model developed to represent the distribution of intrusive rocks in the area.

On the basis of the aeromagnetic data and model studies it is concluded that the area is underlain by a large Tertiary intrusive pluton, whose northern boundary runs from east to west across the northern portion of the map, and which extends beyond the coverage of the aeromagnetic map to the east, south, and west. The elevation of the top of the pluton decreases from about 2000 feet above sea level in the east to about 11,000 feet below sea level in the west, and local intrusive cupolas extend upward from the main igneous body. The pluton is distinctly tabular with a more or less uniform thickness of five miles, and has a vertical or near-vertical northern edge.

VIII. INTERPRETATION OF GRAVITY MAP - SAN FRANCISCO MOUNTAINS AND VICINITY

Introduction

Reconnaissance gravity surveys in the San Francisco Mountains area have been carried out by the U.S. Geological Survey for the purpose of better defining regional geological structure. Gravity data analyzed in this study were obtained from an open-file, complete Bouguer gravity anomaly map (U.S.G.S., 1966a) which covered the area of the aeromagnetic survey. A copy of this map is included in the back-cover map pocket. The map, contoured at a two-milligal interval, was prepared from 390 gravity stations. The Bouguer anomalies were computed by the U.S. Geological Survey for a sea level datum using a density of 2.67 grams per cc., and terrain corrections, using the same density, were made by the method of Hammer (1939). It is estimated that the gravity values have an uncertainty of ±two milligals.

The Bouguer anomaly map was digitized at one-mile intervals to obtain data on a grid for subsequent computer analysis. For most of the area, a one-mile sampling interval was adequate to properly represent the observed anomalies. In a few small areas of the map where the station spacing was more dense, the contoured map contains detail which cannot be properly sampled at a one-mile interval.

Observations of the Gravity Data

Over most of Nevada and western Utah, the dominant Bouguer gravity anomalies are produced by the density contrast between pre-Tertiary rocks and less dense, younger volcanic and sedimentary rocks (Mabey, 1960). The largest anomalies are located over basins underlain by thick accumulations of low-density clastic material. Local inter-montaine anomalies associated with density contrasts in the pre-Tertiary rocks and between Tertiary intrusive and pre-Tertiary rocks are of much smaller amplitude (Mabey, 1960).

In the San Francisco Mountains vicinity, gravity highs and lows correlate well with topography, since Basin and Range orogenic activity has been the controlling influence on the region's present morphology. The gravity map confirms some of the structural features seen on the geologic map (Plate 1), and indicates a continuation of some structural units beneath alluvial or volcanic cover.

On the westernmost edge of the region, the eastern foothills of the Wah Wah Mountains are present. The Wah Wah Range is an uplifted and tilted fault block, dipping gently eastward (Mackin, 1960) into the downfaulted Wah Wah graben. This structural transition is represented on the Bouguer anomaly map by a gradient of about two-three milligals/mile along the western border.

The San Francisco Mountains are part of a north-south trending, uplifted structural block, also dipping to the east (Mackin, 1960). The well-defined structural transition from the Wah Wah graben to the San Francisco Mountains is represented on the gravity map by a gradient of about six milligals/mile. The gravity map indicates that

the basic structural block of the San Francisco Mountains extends southward, under the volcanics shown on the geologic map, to at least the southern map edge. Several small windows in the volcanic rocks in this area reveal Paleozoic rocks. A small gravity low over this block located seven miles from the southern map boundary may represent either an area where the lower-density volcanic rocks thicken considerably or a small downfaulted area which filled with alluvium prior to being covered by volcanics.

Further to the east, the Beaver Lake Mountains, the Rocky Range, and the Star Range represent high points along an uplifted structural block. The geologic map shows alluvium between these ranges, and between the Beaver Lake Mountains and the San Francisco Mountains, but the gravity data indicate that this alluvium does not represent thick accumulations of basin fill.

In the east-central portion of the Bouguer anomaly map there is a gravity low, flanked on the west and east by the gravity highs corresponding to the San Francisco Mountains and the Beaver Lake-Rocky-Star group. This gravity low represents a graben-like structure - herein called the Big Wash graben - but the structure is smaller than a typical Basin and Range graben. It is felt that the basic horst structure in this area is a single, uplifted structure some 15 miles wide, and that the Big Wash graben represents a more local, down-dropped block within the general horst structure.

On the eastern edge of the gravity map a gradient of about five milligals/mile represents the deepening of alluvial fill on the western edge of the Milford Valley graben. This graben is about

12 miles wide and contains 5500 feet of fill at its deepest point (Cook and Mudgett, 1966).

The Wah Wah graben terminates in the northern part of the map, and at about the same latitude - eight miles north of the edge of the underlying pluton - the north-south structural trend of the San Francisco Mountains and the Beaver Lake-Rocky-Star mountains is distorted. On the geologic map of southwestern Utah (Utah Geol. Survey, 1963) it appears that these features are offset about seven miles to the east and continue due north, but there is not enough supporting data to resolve possible structural implications.

Regional and Residual Maps

The Bouguer anomaly gravity data contain the effects of both deep-seated, regional geologic structures and more local, near-surface structures. The running average method for separating regional and local anomalies (described in Section VII) was applied to the gridded Bouguer anomaly map of the San Francisco Mountains area, and 5*5, 9*9, and 13*13 running average regional and residual maps were generated. Because the gravity map was digitized at one mile intervals, a 5*5 running average map, for example, had the same wavelength characteristics as a 10*10 running average of the aeromagnetic map, which was digitized at one-half mile intervals. The 13*13 running average map (Figure 8-2) was arbitrarily selected to represent gravity anomalies related to deep structure and regional features. The residual map obtained by subtracting the data of Figure 8-2 from the digitized Bouguer anomaly gravity map revealed local anomalies

associated with near-surface structure (Figure 8-1).

The regional gravity map, Figure 8-2, is discussed in Section IX - Interdependence of Gravity and Aeromagnetic Data. The remainder of Section VIII is devoted to the residual gravity map, Figure 8-1.

Modeling of Two-Dimensional Structures

The geologic structures represented by the 13*13 running average residual map (Figure 8-1) have pronounced north-south alignments. Two-dimensional models were considered sufficient to explain the gravity data along selected east-west profiles. Consequently, a FORTRAN program was prepared, following the approach of Talwani (1959), for the computation of the vertical gravitational attraction along a profile perpendicular to a two-dimensional structure (see Appendix III). The complete two-dimensional model consisted of M individual models of polygonal cross-section, with each polygon defined by the coordinates of N corners.

Along a typical east-west profile across the thesis area, the topographic relief could exceed 3500 feet. The observed gravity anomalies are dependent in part on the distance of the gravity stations from the causative body and thus are affected by surface terrain. If computed data are to be compared to observed data, the computed gravity effect of a model should be calculated on the actual topographic surface.

As Dampney (1967) notes, there has been little discussion in the literature concerning the application of analytical techniques requiring data on a horizontal plane to the practical situation where

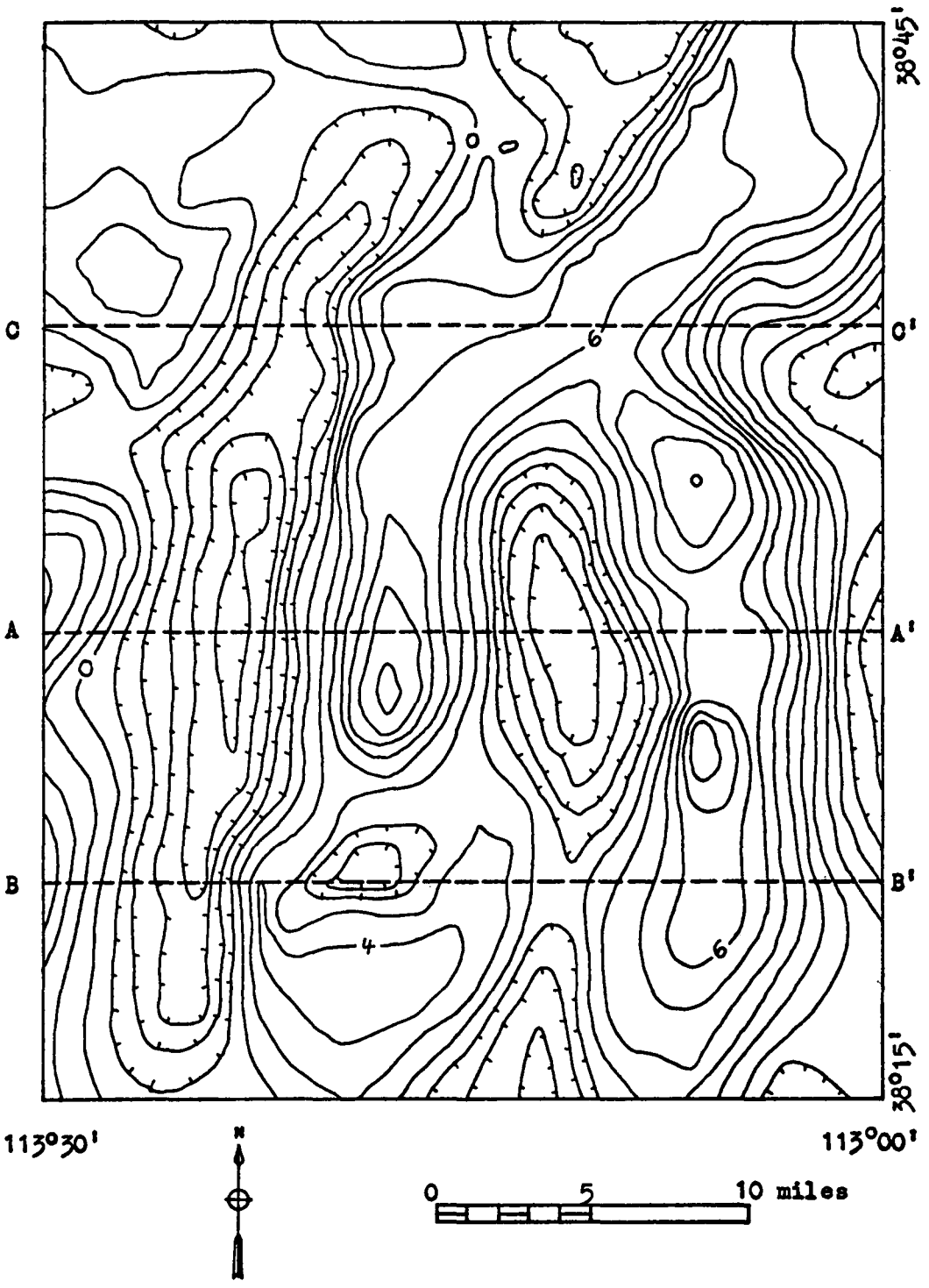

Figure 8-1. 13*13 running average residual map of the Bouguer anomaly gravity data, San Francisco Mountain vicinity. Contour interval = 2 milligals.

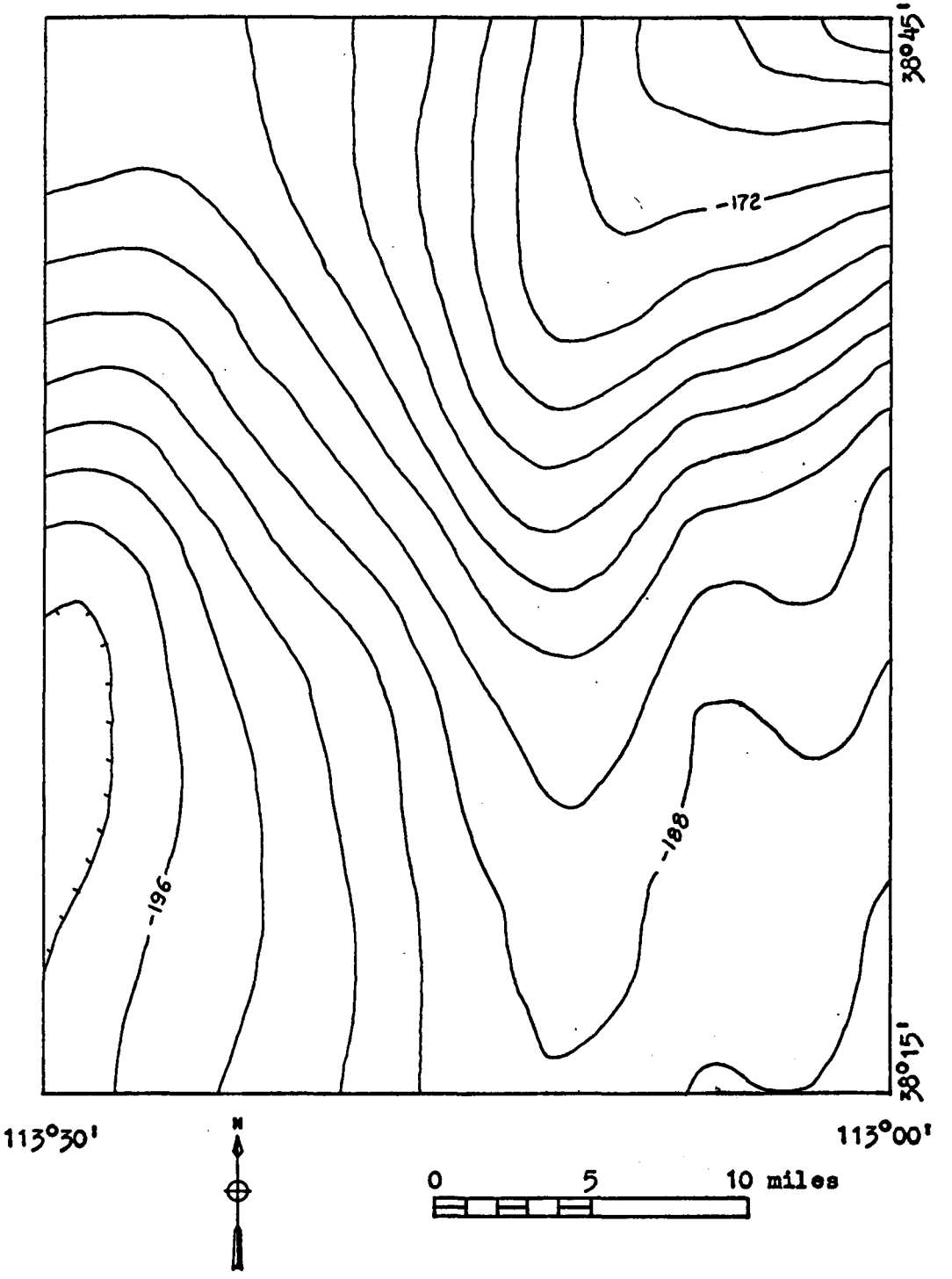

Figure 8-2. 13*13 running average regional map of the Bouguer anomaly gravity data, San Francisco Mountains vicinity. Contour interval = 2 milligals.

points of measurement do not lie on a horizontal plane. Topographic relief in the San Francisco Mountains area is sufficient to introduce significant error in model computations unless relief on the observation surface is considered. Consequently, Talwani's method was modified to compute the gravity effect of a two-dimensional model on the irregular ground surface.

In the case where all causative structures were below the point of computation, the modifications were straightforward, and required only the adjustment of the depth coordinates of each body relative to the elevation of the point of computation. If one or more of the two-dimensional forms included in a model extended above the point of computation, the problem became more difficult, since a portion of the body was then exerting a negative gravitational effect. An approximate method, which required minimal additional programming, was developed to treat this situation.

As shown in Figure 8-3, a two-dimensional model partly above the point of computation can be divided into two parts. If part (1) is formed such that it is symmetrical about a horizontal line through the point of computation (as in Figure 8-3b), it will exert no vertical gravitational force at the point of computation. The gravity effect of the entire model is then equal to the gravity effect of part (2), (Figure 8-3c), which is entirely below the point of computation and fits readily into the format of Talwani's formulas. This method is exact if the sides of the model are vertical or slope outward, and the polygon is sufficiently deep to contain the mirrored portion. In the application of the program to the gravity data of

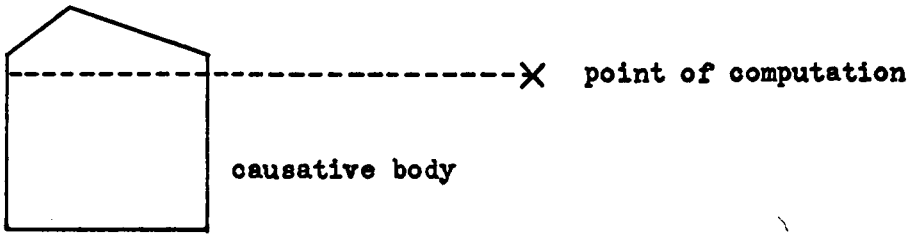

a) Part of causative body lies above point of computation.

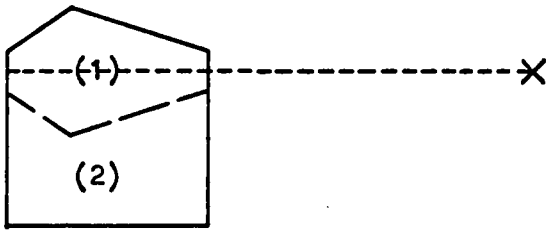

b) The causative body is divided into two parts such that the upper part, part (1), is vertically symmetrical about the point of computation.

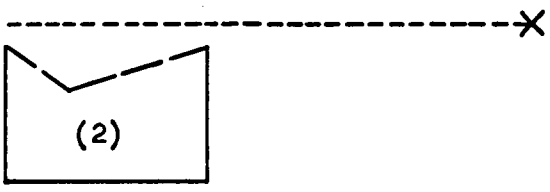

c) The vertical gravitational attraction at the point of computation is due only to part (2).

Figure 8-3. Illustration of the method used to compute gravity over a two-dimensional model when part of the model rises above the point of computation.

Figure 8-1, errors in computation arose from models with sides sloping inward, but in no case exceeded .5 milligals and were generally much smaller.

The sensitivity of gravity anomalies to geologic parameters of interest in the Basin and Range Province was investigated prior to analysis of the structural features represented by the residual gravity data of Figure 8-1. The geometric parameters of the normal faults forming the Basin and Range horst and graben system were of particular interest. Moore (1960) notes evidence, both observed and theoretical, that the master normal faults bounding the ranges are curved, in section, so that they dip less steeply with depth. The usual dips of Basin and Range normal faults are between 50 and 80 degrees (Nolan, 1943), but Longwell (1945) reports some observed dips between 10 and 20 degrees.

Gravity computations over two-dimensional models show that reconnaissance gravity data have little sensitivity to fault detail. At an average station spacing of one mile, for example, the gravity effect of a structural feature such as an en-echelon fault zone is not adequately sampled, nor is an overall accuracy of one-two milligals sufficient to resolve structural detail. Thus, in a typical Basin and Range reconnaissance gravity survey, the dip of individual fault planes cannot be distinguished from the average slope of the graben wall.

Figure 8-4 shows the computed gravity over a normal fault, similar to the wall of a graben structure, having a density contrast

of .45 grams per cc., a vertical displacement of 4000 feet, and a dip of 50 degrees. Gravity values were computed at one-half mile intervals, but profiles were drawn using a one-mile station spacing to illustrate the dependence of apparent anomaly shape upon the sampling interval. The structure is seen to produce a large gravity gradient which is distributed over a horizontal distance of about four miles. If the sampling interval were one mile, which is more representative of the actual gravity survey, the structure could still be located with reasonable accuracy. The dip of the fault, however, could not be determined with confidence, for the apparent anomaly gradient depends on where the points of computation fall with respect to the structure.

Considering an entire graben structure, rather than a single wall, computations over two-dimensional models show that reconnaissance gravity data with a precision of one-two milligals are not sensitive to overall graben shape. Figure 8-5 shows gravity values computed at one-mile intervals over two graben structures of equal density contrast but considerably different shape and implied structural history. The gravity anomalies are not adequately sampled with regard to shape discrimination at one-mile intervals. With no additional geologic control it is questionable whether structural differences as extreme as those shown in Figure 8-5 could be resolved with the available gravity data.

In summary, Figures 8-4 and 8-5 show that only the gross geometry of Basin and Range structures can be determined from the available distribution of gravity data in the San Francisco Mountains area.

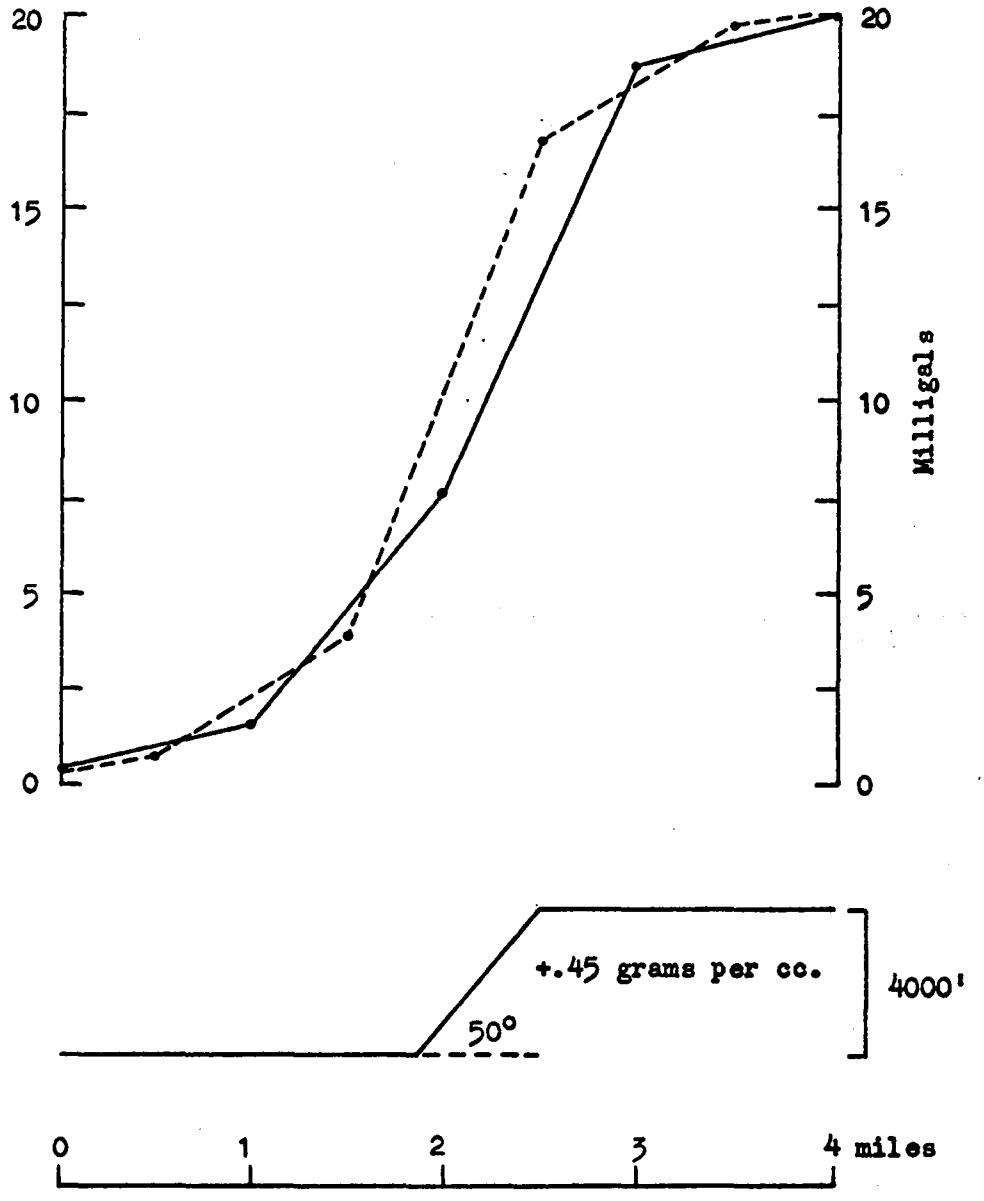

Figure 8-4. Gravity profiles computed at one-mile intervals over a two-dimensional fault, similar to the wall of a graben, illustrating how the shape of the computed profile depends upon the sampling locations. The points of computation of one profile have been shifted one-half mile with respect to the other.

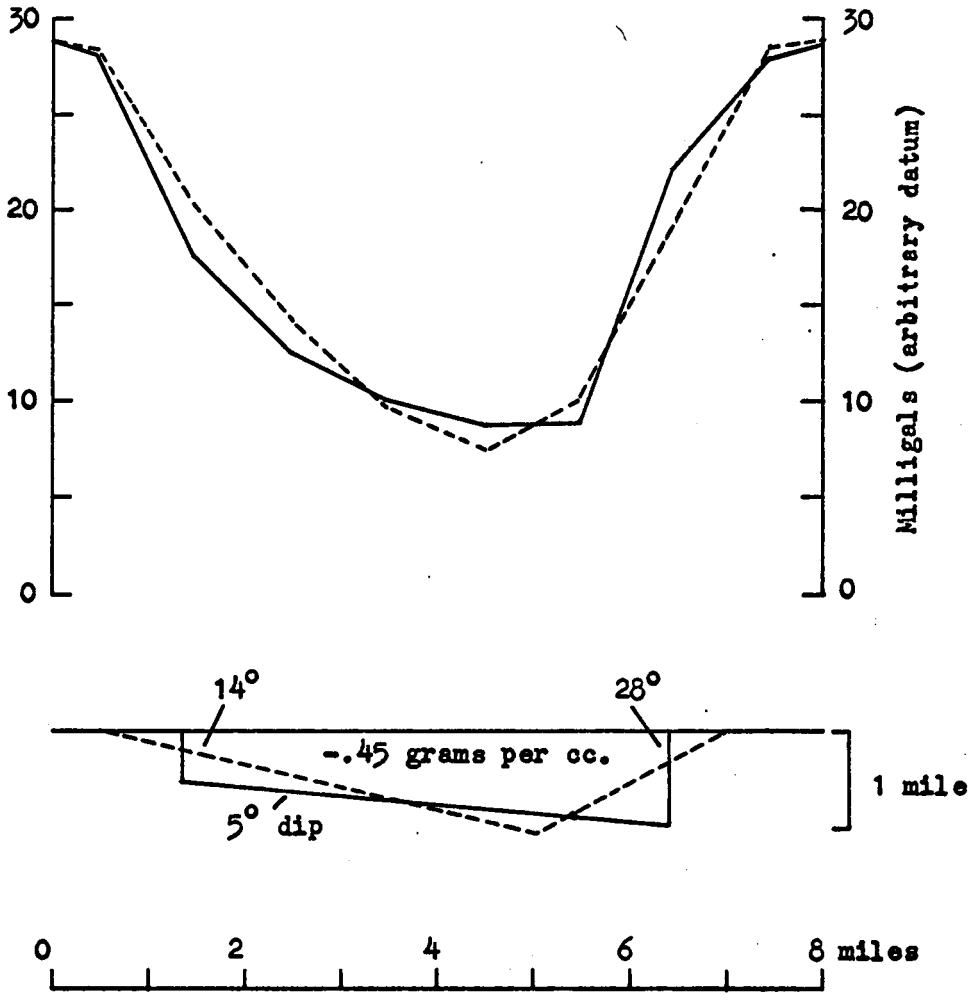

Figure 8-5. Computed gravity profiles over two grabens with equal density contrasts but different shapes, which illustrate the similarity in anomaly forms. Gravity was computed at one-mile intervals.

Interpretation of Residual Gravity Map

Three east-west profiles, extending across the map, were selected as representative of the region. The locations of the profiles - AA', BB', and CC' - are shown on Figure 8-1 and on Plate 1 in the map pocket. Gravity values along the profiles were taken from the residual gravity map, at one-mile intervals. Computed gravity profiles caused by two-dimensional geologic models were compared to the data. In keeping with the findings of the resolution tests, the models used were geometrically simple. All calculated gravity values were computed on the surface of the ground, rather than on a plane. Models were developed to reproduce the residual profiles to within two milligals, the approximate precision of the gravity data.

Figure 8-6 shows the residual gravity profile AA', the surface geology along the profile, and a scale drawing of a two-dimensional model which would explain the residual gravity profile. Also included are the regional gravity profile taken from Figure 8-2, and the residual gravity values (shown by dots) at gravity station locations within ±1.5 miles of profile AA'.

Profile AA' includes the Wah Wah graben, the Big Wash graben and the western part of the Milford Valley graben. An assumed density contrast of -0.45 grams per cc. for these grabens is sufficient to explain their gravity anomalies. This density contrast is consistent with that used in other gravity studies in the Basin and Range Province (Mabey and Morris, 1967).

Profile AA' also crosses the intrusive body which outcrops near the Horn Silver mine in the San Francisco Mountains, and the intrusive outcrop of the Rocky Range. The residual gravity data along

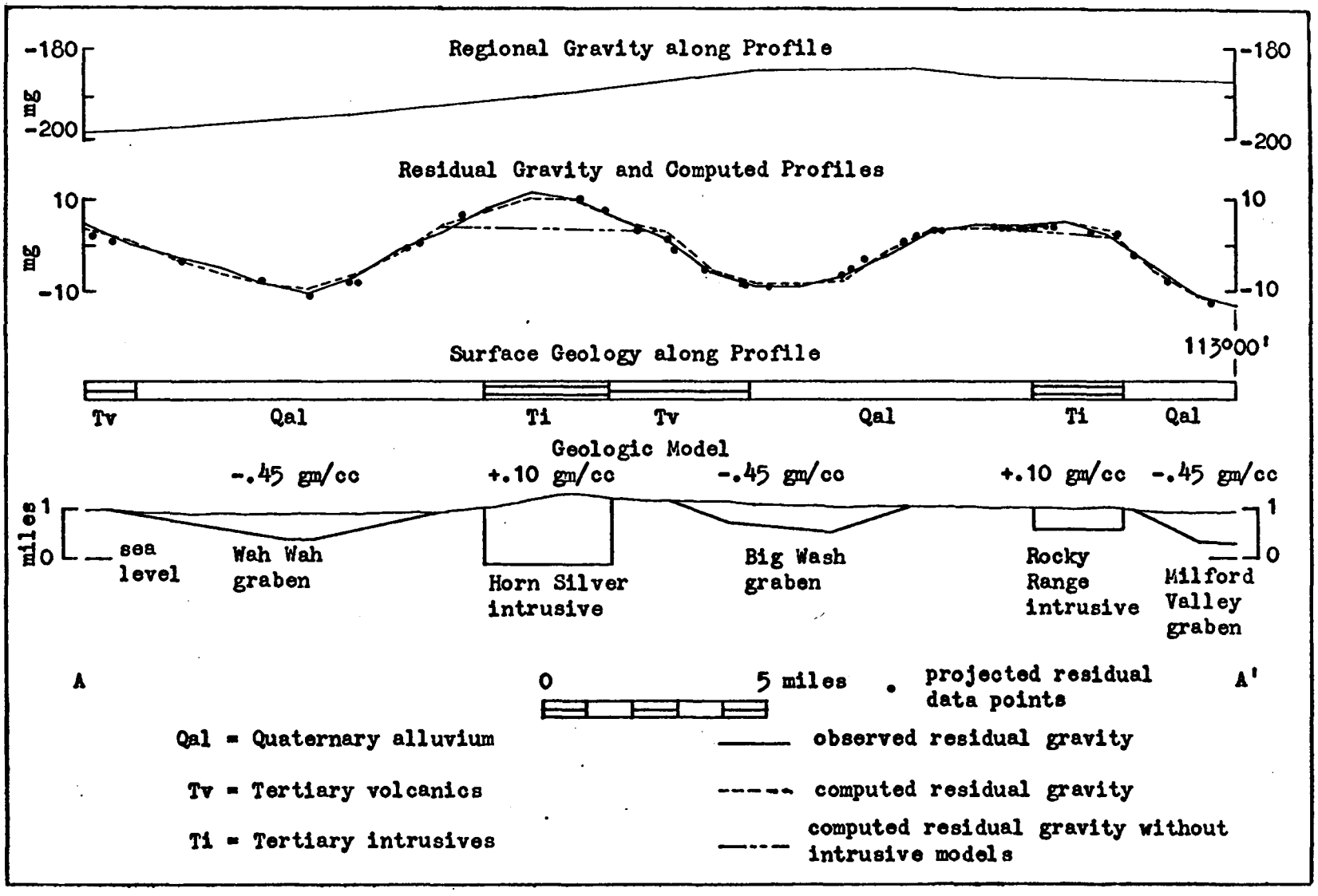

Figure 8-6. Residual gravity profile AA'.

this profile require a positive density contrast of 0.10 grams per cc. between Tertiary intrusive rocks and consolidated Paleozoic sediments. This implies a density of about 2.80 grams per cc. for the Tertiary intrusive rocks, which is at the upper limit of the density range given by Carlson and Mabey (1963). Failure to include such a density contrast for the intrusive rocks results in an inadequate explanation of the residual profile (Figure 8-6). Consequently, the Tertiary intrusive cupolas appear to be of higher density than the pre-Tertiary rocks. The geometry of the models for the intrusive cupolas, as shown in Figure 8-6, is consistent with, and constrained by, the residual igneous models presented in Section VII.

To determine if the computation of gravity on the actual ground surface, rather than on a plane, contributed significantly to the accuracy of the model-fitting procedure, gravity profiles were computed over the geologic model developed to explain profile AA', using the density contrasts shown in Figure 8-6, along horizontal data lines at 5000 and 7000 feet above sea level. Figure 8-7 shows that these profiles differ significantly from the profile computed on the ground surface, indicating the importance of computing gravity effects on the irregular observation surface.

Figure 8-8 shows the data pertinent to residual gravity profile BB'. BB' was a rather complicated profile, requiring six causative bodies in the geologic model. The model for the Milford Flat intrusive was based on the residual igneous model of Figure 7-7 and Table 7-2, and assigned a density contrast of +0.10 grams per cc., which was sufficient to explain the residual gravity data. The Wah Wah and Milford Valley grabens are

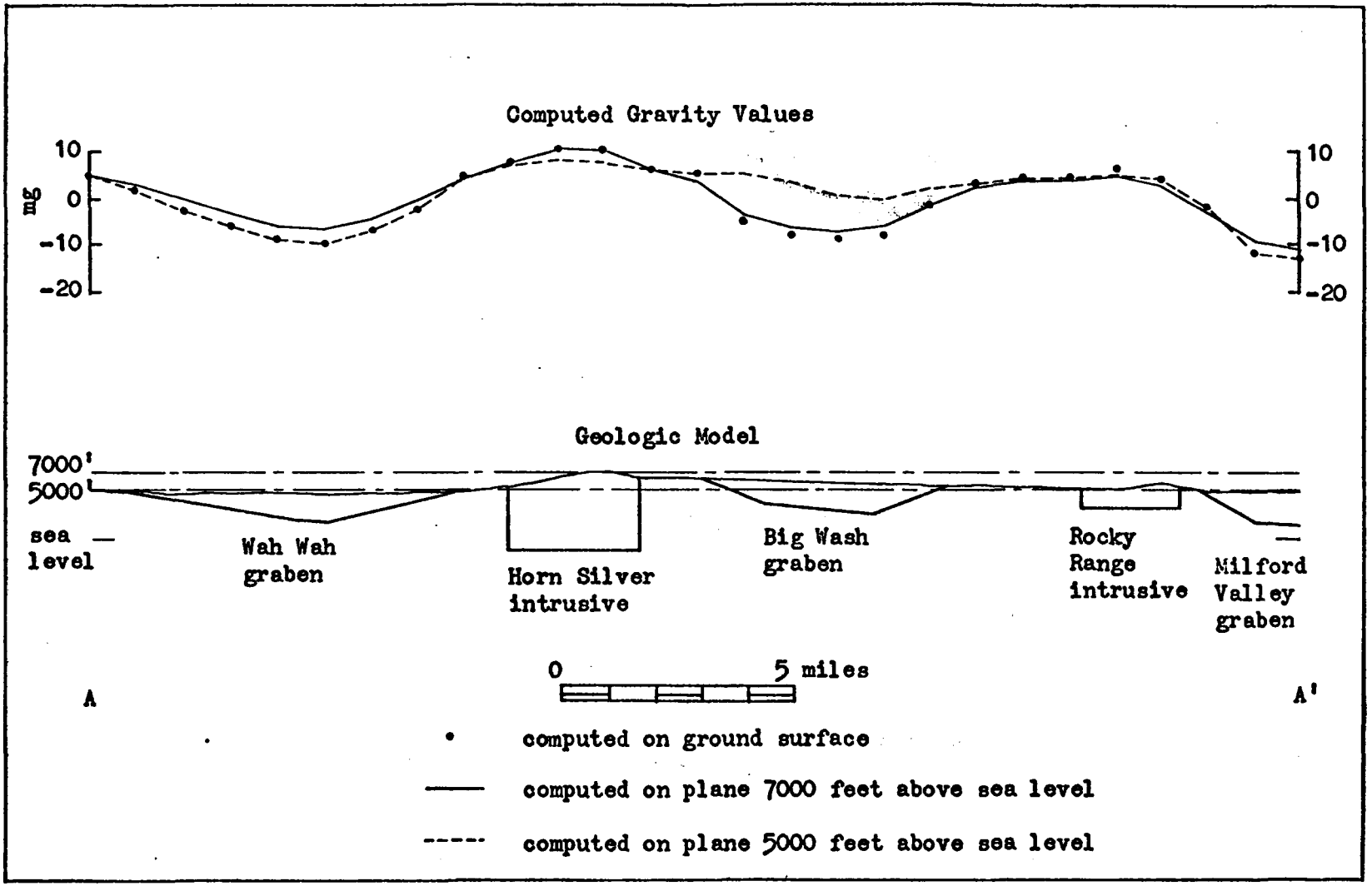

Figure 8-7. Gravity profiles computed on the ground surface and on planes at 7000 and 5000 feet, over the model developed to reproduce the gravity data of profile AA'.

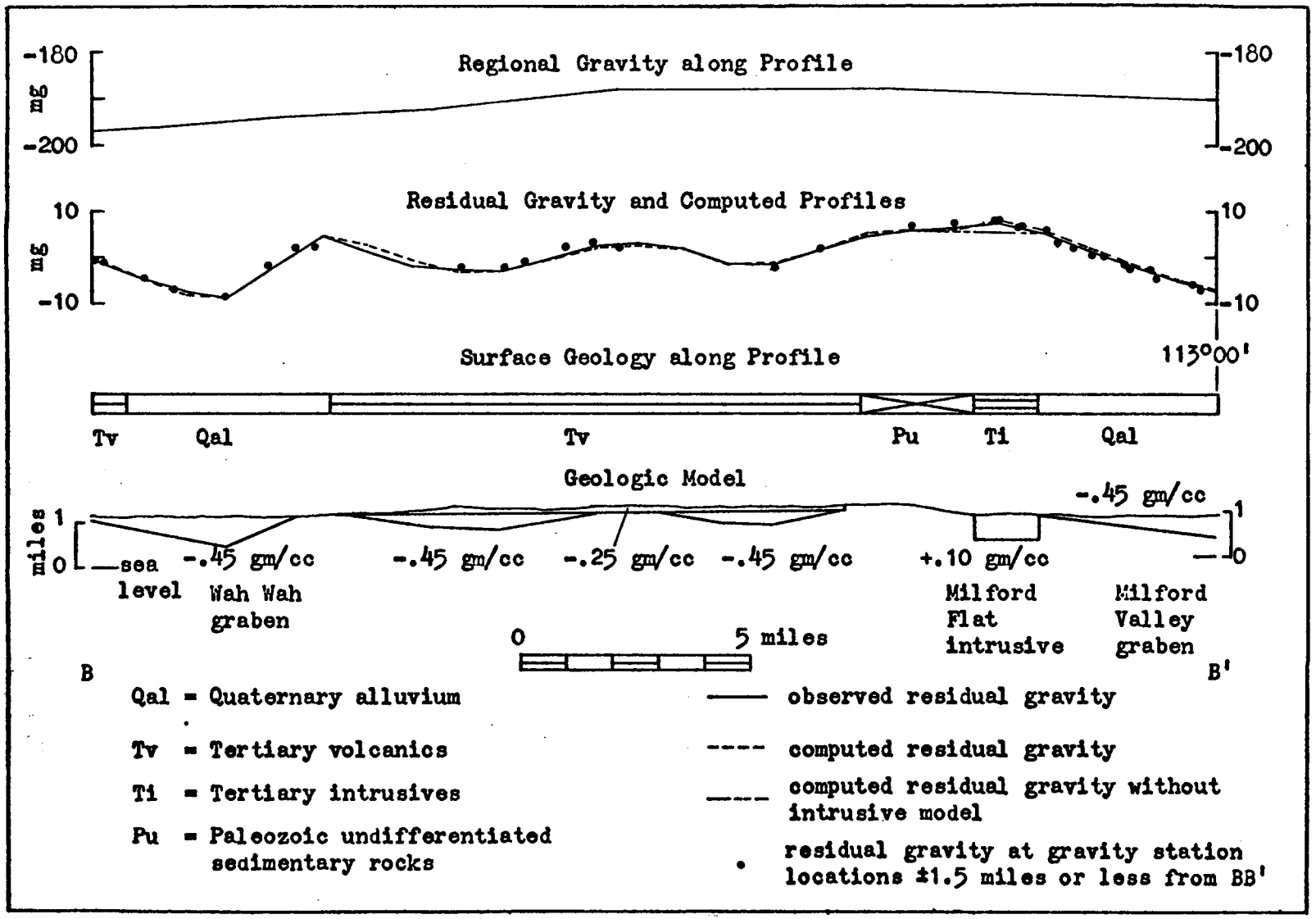

Figure 8-8. Residual gravity profile BB'.

continuations of the structures shown on profile AA', and were represented by models with density contrasts of -0.45 grams per cc.

The central portion of profile BB' traverses a volcanic plateau about 600 feet higher than the surrounding area. This plateau was represented in the model by a layer approximately 600 feet thick, of density contrast -0.25 grams per cc. (Carlson and Mabey, 1963), which represented volcanic material and gave the necessary gravity effect.

A residual gravity minima just east of the Wah Wah graben may correspond to a thickening of the volcanic layer, to a thickness of about 3700 feet. An alluvium-filled graben beneath the volcanic layer could also cause the gravity low. Either interpretation is consistent with normal faulting prior to deposition of the volcanics. Similarly, another residual gravity low over the eastern half of the volcanic layer appears related to the southern part of the Big Wash graben, and could represent either a thickening of volcanic cover or low-density clastic material under the volcanic layer. Both interpretations imply normal faulting which created a structural depression prior to deposition of the volcanics. The models of Figure 8-8 represent clastic-filled grabens under the volcanic layer because it was felt most likely that a structural depression would fill with alluvial material as it was formed.

The data for profile CC' are shown in Figure 8-9. Only two causative bodies comprise the structural model - the northern part of the Wah Wah graben and the Milford Valley graben. The profile

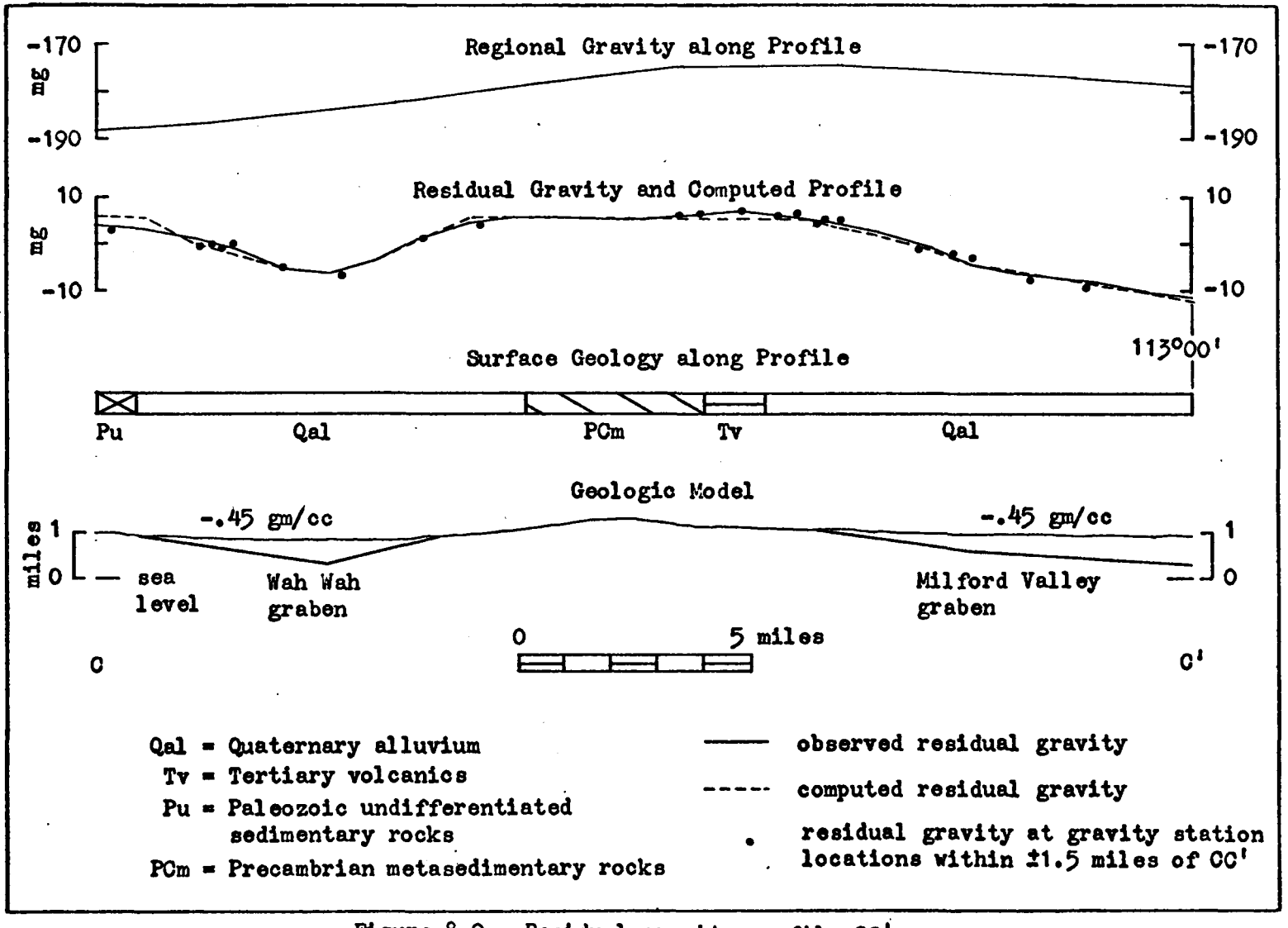

Figure 8-9. Residual gravity profile CC'.

traverses an exposure of Precambrian rock, but it was not necessary to introduce a corresponding model with a positive density contrast. The geologic map (Utah Geol. Survey, 1963) describes these Precambrian rocks as "undifferentiated metasedimentary rocks, chiefly quartzite and argillite, Late Precambrian", and they have no expression on the aeromagnetic map. They apparently are not highly metamorphosed basement rocks. At the western end of the profile, the fit of the computed gravity to the residual data is not good. The difficulty may be that CC' in this area is not perpendicular to geologic structure, as indicated by Figure 8-1 and Plate 1.

Table 8-1 summarizes the maximum depths of fill of the major grabens found along profiles AA', BB', and CC'. The Wah Wah graben has a maximum thickness of fill of about 3600 feet. The displacement on the normal fault zone bounding the eastern edge of this graben must be considerably greater, however. Assuming an initially flat surface, the approximate minimum vertical fault displacement is the distance from the topographic high of the San Francisco Mountains to the bottom of the graben, or about 7600 feet. If one assumes that the horsts and grabens are about equal in volume, and that material eroded from the horsts is deposited in the grabens, one could conclude that the San Francisco Mountains have had 3600 feet of rock removed by erosion, giving an estimated structural relief on the normal fault zone of 11,200 feet. This value is an estimate only, and is open to question, for the material in the graben probably has been mostly eroded from lower elevations and not off the peaks. On the other hand, this area has not had a closed drainage system

Table 8-1. Summary of the maximum depths of fill for the Wah Wah, Big Wash, and Milford Valley grabens.

WAH WAH GRABEN

Profile	Maximum depth of fill
AA'	3200'
BB'	3600'
CC'	2700'

BIG WASH GRABEN

Profile	Maximum depth of fill
AA'	3000'
BB'	1200' (from bottom of volcanics)

MILFORD VALLEY GRABEN

Profile	Depth of fill at east edge of map
AA'	3500'
BB'	2500'
CC'	3400'

throughout its history, and all eroded material has not remained in the graben. The net effect of wind transport is also unknown.

The dip of the walls of the graben models is less than 30 degrees. Since the typical graben is probably bounded by a series of faults rather than a single fault plane, the models represent the gross configuration of the graben walls, and not the dip of individual fault planes.

The geologic map of the region, Plate 1, shows a large area covered by volcanics, and since considerable post-volcanic normal faulting is likely, it is probable that the downfaulted basins contain volcanic rocks. Because of the great uncertainty in the thickness and position of volcanic rocks in the grabens, no volcanic layers were included in the graben models. The volcanic rocks are more dense than the clastic material assumed to fill the grabens, and their actual presence in a graben would cause the computed depth of fill to be too small - an error which could amount to about 400 feet for a volcanic layer 1000 feet thick (Mackin, 1960), and density contrast -0.25 grams per cc. (Carlson and Mabey, 1963).

In separating the original Bouguer anomaly gravity map into regional and residual components, it was assumed that the residual component tended to represent near-surface structures. This assumption is confirmed by the geometry of the models sufficient to explain the residual gravity data along profiles AA', BB', and CC'. None of the models are thicker than 9000 feet, or extend deeper than 1500 feet below sea level.

Summary of Section VIII - Gravity Data

This section treats primarily the 13*13 running average residual gravity map of the San Francisco Mountains vicinity, which represents geologic structures in the upper few miles of the earth's crust. From west to east across the map area, the gravity data delineate the eastern Wah Wah Mountains, Wah Wah graben, San Francisco Mountains, Big Wash graben, Beaver Lake-Rocky-Star ranges, and the western edge of the Milford Valley graben.

Three interpretive east-west cross sections across the area are developed with the aid of a FORTRAN two-dimensional gravity computation program used to compute gravity values on the ground surface. The distribution of the reconnaissance gravity data is sufficient to determine the gross configurations of the Wah Wah and Big Wash grabens. The Wah Wah graben has an interpreted maximum thickness of fill of 3600 feet, and an estimated fault displacement of 7600 to 11,200 feet on its eastern edge. The Big Wash graben has an interpreted maximum depth of fill of 3000 feet, and is thought to represent a down-dropped block within a 15 mile wide horst structure. At the eastern edge of the map area, the Milford Valley graben has an approximate thickness of fill ranging from 2500 to 3500 feet. To adequately explain the residual gravity data, it is necessary to assume a positive density contrast of approximately 0.10 grams per cc. for the near-surface intrusive cupolas. Two small gravity lows along profile BB' occur over volcanic rock, and are interpreted as representing either thickening of the volcanic cover or clastic-filled depressions under the volcanics. Either interpretation is consistent with the premise of pre-volcanic normal faulting.

IX. INTERDEPENDENCE OF GRAVITY AND AEROMAGNETIC DATA

Comparison of Intrusive Models and the Residual Gravity Map

In Section VIII the residual gravity map was interpreted in terms of structures in the upper two miles of the earth's crust. The residual igneous models in Figure 7-7 were originally defined on the basis of the aeromagnetic data, but it was shown in Section VIII that if a positive density contrast was assumed, their computed gravity effects were confirmed by the observed data. Thus the residual aeromagnetic and gravity data, responsive to structures in the upper few miles of the earth's crust, complement one another.

The regional igneous model, Figure 7-6, representing the underlying intrusive body, was also determined from the aeromagnetic data alone. The model appears to reflect in some measure, however, the block faulting inferred from the residual gravity data. Although the residual gravity anomalies are due to near-surface structures, the faults generating the horst and graben structures probably extend to considerable depths. The generally elevated blocks (2) and (3) of Figure 7-6 correspond with the position of the Beaver Lake-Rocky-Star chain of positive structural features, and block (5) of the regional igneous model corresponds in position to a structural saddle indicated by the gravity data at the south end of the Big Wash graben. The termination of block (4) towards the west occurs near the eastern margin of the Wah Wah graben. The relief between blocks (6), (7), and (8) has no close parallel on the residual gravity map (Figure 8-1), and probably reflects initial irregularity of the pluton.

The structural relief between blocks (1) and (2), Figure 7-6, is 3100 feet, which is in reasonable agreement with the depth of fill indicated for the western part of the Milford Valley graben (Table 8-1). The structural relief between blocks (4) and (7) is 10,600 feet, which compares well with the estimated structural relief of 7600 to 11,200 feet on the normal fault zone bounding the east side of the Wah Wah graben. On the basis of this evidence, as well as the fact that none of the cupola-like intrusive bodies of Figure 7-7 occur within grabens, it is postulated that major Basin and Range faulting has occurred after the intrusion of the pluton.

Interpretation of Regional Gravity Anomalies

Figure 8-2 shows the regional gravity map obtained from 13*13 running averages of the gridded Bouguer anomaly data, and tends to represent the approximate gravity effects of deep anomaly sources. The regional gravity map has three dominant features:

1) A gradient in the northern part of the map increasing towards the north.
2) A gradient in the southwestern quadrant of the map decreasing towards the west.
3) A positive nose, coinciding with the position of the main horst structure in the area.

Since analysis of the residual gravity data, Figure 8-1, indicates a positive density contrast between near-surface intrusive rocks and consolidated sedimentary rocks, it is reasonable to examine the regional gravity data for evidence of the large intrusive body

suggested by the aeromagnetic data. This was done using the method of Talwani and Ewing (1960) for computing gravity effects of three-dimensional mass distributions. A FORTRAN program, for computing gravity values on the ground surface rather than on a plane, was developed for this analysis (see Appendix II). The gravity effect of the regional igneous body, Figure 7-6 and Table 7-1, was computed assuming a density contrast of +0.10 grams per cc. with the rocks into which it was intruded, as suggested by the study of near-surface structure.

Another approach to the study of the gravity effects of the pluton defined by magnetic data involves the computation of pseudo-gravity anomalies following the method of Baranov (1957). This approach was pursued in some detail, and is discussed in Appendix I. It became apparent, however, that at least a 20 by 20 coefficient set was required to operate upon the observed magnetic data to obtain the pseudo-gravimetric anomalies. Consequently, this approach to the problem was rejected, because after convolution only 42 percent of the original area of the aeromagnetic map would remain.

The gravitational attraction of the regional intrusive body, computed by the method of Talwani and Ewing, was subtracted from the regional gravity map (Figure 8-2) in an attempt to remove the possible gravity effects of the pluton (Figure 9-1).

Figure 9-1 shows that removal of a positive gravity effect due to the underlying pluton greatly exaggerates the gradient which increases to the north but eliminates the gradient in the southwest quadrant which decreases to the west. The positive nose can still be observed. This implies that the gradient decreasing to the west

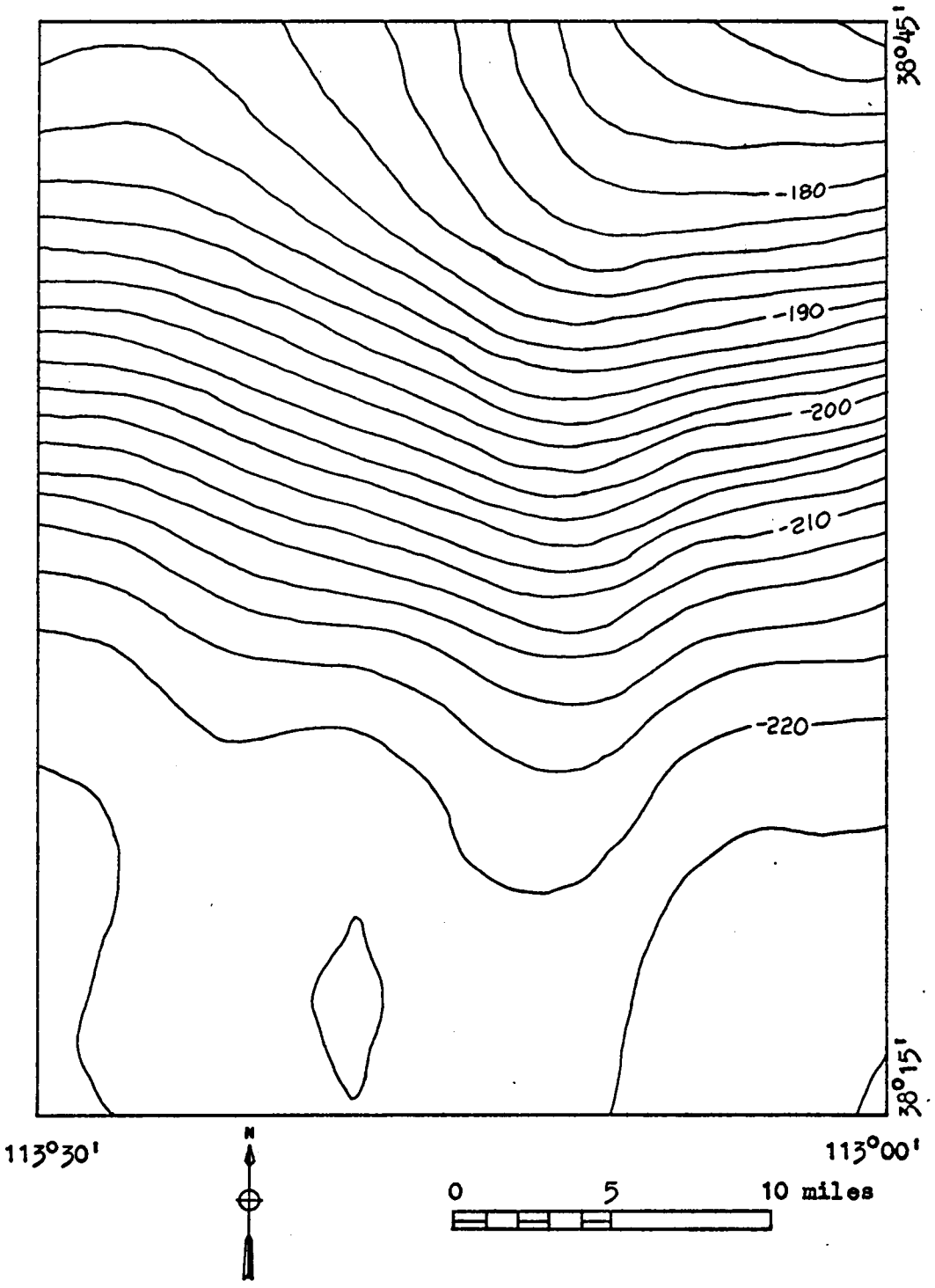

Figure 9-1. The gravitational attraction of the regional intrusive body, computed using a density contrast of +0.10 grams per cc., subtracted from the 13*13 running average regional gravity data, Figure 8-2. Contour interval = 2 milligals.

may be due to the westward-increasing depth of the intrusive body. The distorted northward-increasing gradient shows that the gravity effect of the pluton alone is not sufficient to explain the regional gravity field.

In Section VII, it was pointed out that the near-vertical and generally linear northern edge of the regional igneous model suggests the presence of an east-west fault zone extending across the area. This postulated fault zone permits the introduction of a density contrast between the northern and southern parts of the map area, which could tend to reproduce the strong regional gravity gradient of Figure 9-1.

Consequently, the gravity effect of a single, vertically-sided, horizontal plate was computed using the three-dimensional gravity computation program. The plate extended well beyond the map area to the west, north, and east, and was bounded on the south by the regional intrusive body. The plate was seven miles thick, the elevation of its top was 1560 feet below sea level, and it had a density contrast of +0.10 grams per cc. with the sedimentary rocks on the south side of the postulated fault. Figure 9-2 shows the relationship of this plate to the regional intrusive model. This simple model represents the possibility of differing lithologies on each side of the postulated east-west fault zone. Although the density contrast of the model extends vertically for seven miles, this is not a measure of the displacement along the fault. The extent or nature of the actual displacement cannot be determined from available information.

The gravity effect of this plate was subtracted from the field of Figure 9-1. The resulting map, Figure 9-3, shows the

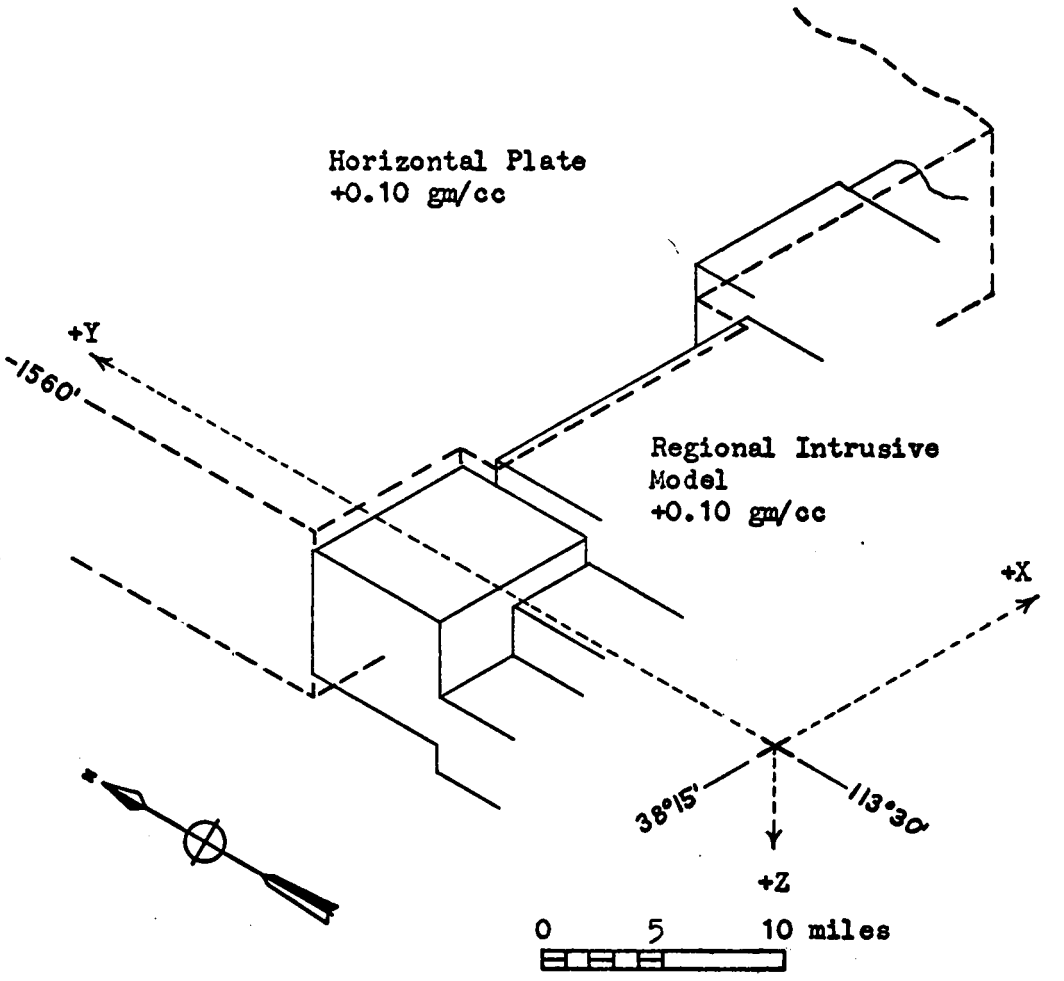

Figure 9-2. Sketch showing the relationship of the regional intrusive model (from Figure 7-6) to the horizontal plate representing the north side of the postulated east-west fault zone. Only the area of contact between the two structures is shown.

regional gravity data with the possible gravity effects of both the regional intrusive body and the postulated fault zone removed. In Figure 9-3, the strong gradient increasing to the north is no longer present. The gravity contours remaining are largely those which define a positive nose, coinciding with the position of the main horst structure. It is thus demonstrated that a major east-west discontinuity extending across the northern part of the thesis area, as first postulated on the basis of aeromagnetic data, is also compatible with the gravity data.

The plate model of Figure 9-2 was designed on the (arbitrary) assumption of no density contrast between the plate and the intrusive pluton, and is presented only as one possible example. More generally, the regional gravity data (Figure 8-2) show an east-west gradient with a total relief of about 14 milligals. Assuming this gradient to be caused by a mass excess on the north side of the postulated fault zone, whose actual distribution is unknown, the mass excess can be described in terms of a surface density. The net amplitude of the gravity anomaly, presumably due to a differing lithology on the north side of the postulated fault zone, can be approximated by the expression for the gravity effect of an infinite horizontal slab:

$$\Delta g = .01277\, \rho L$$

where ρ is the density or density contrast of the slab in grams per cc., L the thickness of the slab in feet, and Δg the gravity effect in milligals. Setting Δg equal to 14 milligals, $\rho L \cong 1100$ gm·ft/cc., the surface density over the north side of the fault zone.

The plate model (Figure 9-2) used above in computing the possible

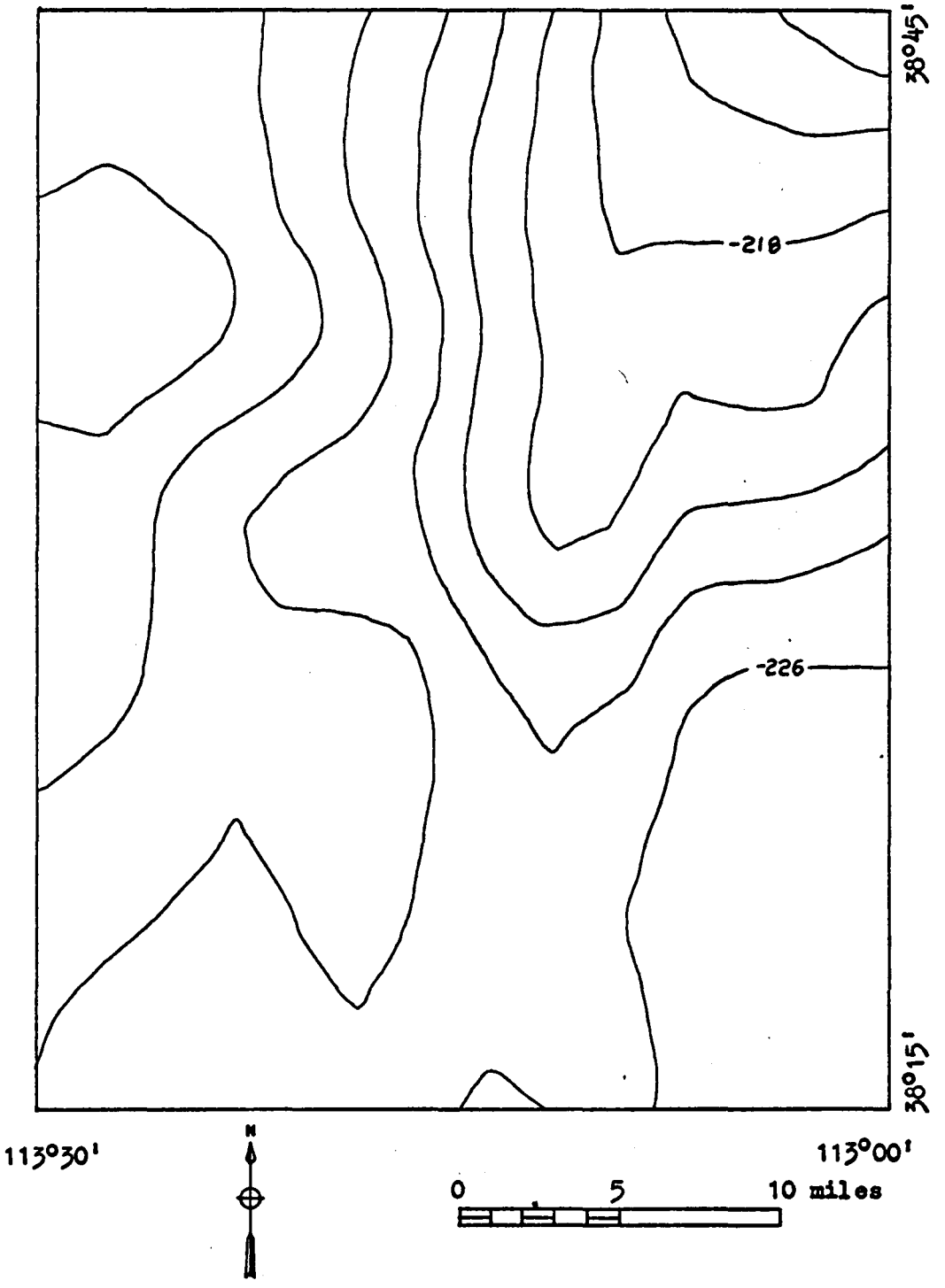

Figure 9-3. The regional gravity data minus the gravity effect of both the regional intrusive body and the postulated high-density plate. Contour interval = 2 milligals.

gravity effect of the fault zone was of the same density contrast as the pluton (+.10 grams per cc.), but about two miles thicker, resulting in a mass excess described by a surface density of (+.10 grams per cc.) x (10,600 feet), or about 1100 gm·ft/cc. as derived above. Assuming that the mass excess was distributed as a plate five miles thick and approximating the vertical configuration of the pluton to the south, the required density contrast of the plate with the pluton would be about 1100/(5 x 5280), or +.04 grams per cc.

If the supposed fault pre-dates the emplacement of the intrusive body, the positive density contrast across the fault zone could have acted as a barrier preventing the intruding magma from migrating northward and thus could have controlled the configuration of the northern edge of the pluton. If the fault post-dates the intrusive body and the pluton is terminated by displacement along the fault, the time of displacement would have to fall between the time of pluton emplacement and the start of major Basin and Range faulting, since the horst and graben structures appear unaffected by displacement on the supposed fault zone. Termination of the five-mile thick pluton by faulting would seem to require a strike-slip fault of at least 30 miles displacement. Such a fault might be confirmed by extended regional aeromagnetic coverage if the magnetic expression of the northern part of the intrusive body was indicated in an area beyond the present limits of the data. Such an anomaly is not apparent on the recently published U.S. Geological Survey's Transcontinental Geophysical Survey (Zietz and Kirby, 1968), which includes the thesis area. The spacing of aeromagnetic flight lines in

the area of interest, however, is about 50 miles, and the Transcontinental Survey thus does not offer conclusive evidence with respect to either of the possible interpretations.

The regional gravity high remaining on Figure 9-3 extends across the postulated east-west fault zone and coincides with a major horst structure. Basin and Range normal faulting appears to post-date the supposed fault zone, and it appears most likely that this gravity high is in large part a reflection of the deeper density contrasts associated with Basin and Range structure.

Cook and Mudgett (1966) observed a regional gravity high in this general area corresponding in position to the Sevier Arch (Harris, 1959), later referred to as the Sevier Orogenic Belt of pre-Laramide age (Armstrong, 1968). The regional gravity high of Figure 9-3 does coincide with the general location of the rather poorly defined Sevier Orogenic Belt as described by Armstrong, and could possibly be caused, in some measure, by the deep-seated structure of the Sevier Belt.

The Bouguer anomaly gravity map was separated into residual and regional components by a more or less arbitrary method, but the basic ambiguity of such a separation was avoided by interpreting both components of the map, which together comprise the initial data. The anomalies of the residual gravity map were attributed to near-surface Basin and Range structure and intrusive rocks, while the anomalies of the regional gravity map were attributed to the effects of the underlying intrusive body, the east-west fault zone, deep-seated Basin and Range structure, and perhaps the Sevier Orogenic Belt. The interpretations of the gravity and aeromagnetic data confirm and

complement one another, and together lead to a reasonable picture of the general geologic structure of the San Francisco Mountains vicinity.

Summary of Section IX -

Interdependence of Gravity and Aeromagnetic Data

The 13*13 running average regional gravity map is interpreted, with the help of a three-dimensional gravity computation program, as reflecting the gravity effect of three and possibly four regional structures:

1) An underlying intrusive body.
2) An east-west fault zone bounding the intrusive body on the north.
3) Deep-seated Basin and Range horst and graben structure.
4) Possibly, the Sevier Orogenic Belt.

The interpretations of the gravity and aeromagnetic data are shown to confirm one another.

X. GROUND MAGNETIC INVESTIGATION

Introduction

As part of a geological exploration and mapping program organized by the Utah Geological and Mineralogical Survey, the author spent three and one-half months in the field conducting ground magnetic surveys in the Star Range, Beaver County, Utah. The Star Range is in the southeastern part of the area covered by the aeromagnetic and gravity maps treated in Sections VII, VIII, and IX. Figure 10-1 is a topographic map of the Star Range and vicinity (taken from the U.S.G.S. 15 minute Milford quadrangle map), and Plate 1 shows the generalized geology of the area.

Local magnetic surveys were carried out in three areas of the Star Range. In the Milford Flat vicinity, eight magnetic profiles with data spacing of 100-200 feet were obtained to define the surface of the intrusive cupola underlying the area. The profile locations are shown in Figure 10-1. Gridded magnetic data with 100 foot station spacing were obtained in the vicinity of the Wild Bill mine (Figure 10-1) to investigate an area of irregular intrusive outcrop and possible contact-zone mineralization. Both gridded data and profiles were taken along the southeastern contact zone of the non-magnetic Shauntie intrusive body to determine the location of the contact zone where buried by alluvium and to define the thickness and dip of the contact zone in areas of heavy magnetite mineralization. This survey was located in the southern half of Section 35, Figure 10-1, on which the location of the station used as a regional base is

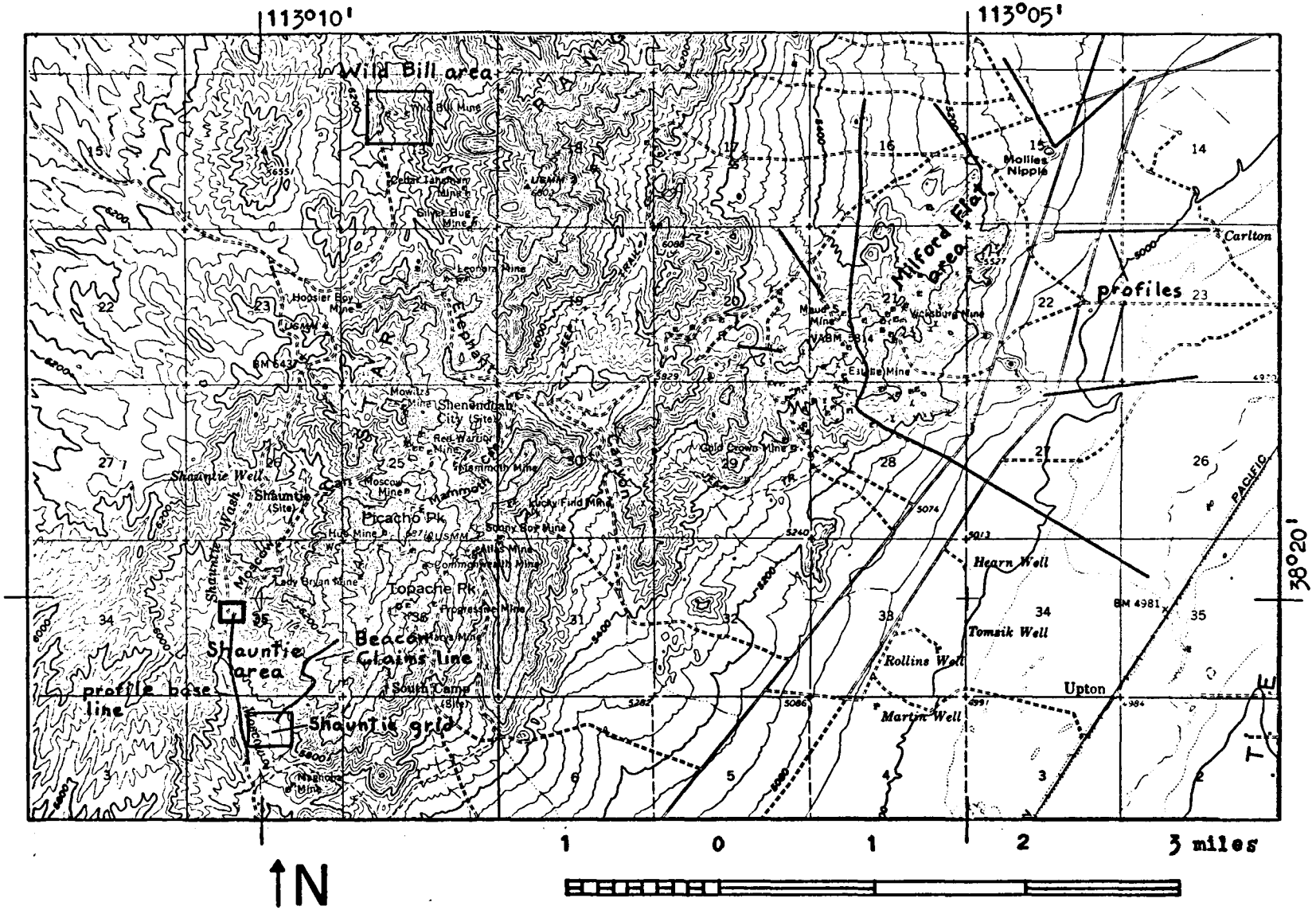

Figure 10-1. Base map of the Star Range vicinity.

indicated by a heavy square, for correlation with Figure 10-12.

Geology of the Star Range

The general structure of the Star Range is that of an uplifted block, bounded by north-south normal faults. There are many smaller faults and fissures in the area, some of which have exerted an important control upon ore deposits. There apparently was little pre-intrusion folding in the immediate Star Range vicinity, and much of the local structure now present is due to the emplacement of intrusive plutons, as evidenced by the accommodation of sedimentary bedding to the igneous contacts (Hobbs, 1944).

The Star Range exposes north-striking, east-dipping sedimentary rocks, mostly limestones and quartzites, ranging in age from Devonian to Jurassic. Table 10-1 shows a preliminary geologic section measured in the Star Range by Dr. James A. Whelan (private communication).

The only exposure of intrusive granodiorite porphyry in the area is a small body of dark, highly altered, porphyritic rock outcropping one-fourth mile east of the Harrington-Hickory mine (Butler, 1913). The remainder of the intrusive rocks exposed in the Star Range are of the younger quartz monzonite. Butler notes that although there are slight differences in the composition of the quartz monzonite throughout the Star Range, there is "little doubt that the rocks of the several masses are derived from the same parent magma." This includes the intrusive exposure southeast of Shauntie, which was noted in Section VI as having a distinctly lower magnetic susceptibility.

Table 10-1. Preliminary geologic section of the Star Range. The table is based on preliminary data supplied by Dr. James A. Whelan of the University of Utah and Utah Geological and Mineralogical Survey.

Formation	Age	Thickness, feet
Navajo Sandstone	Jurassic	?
Chinle Formation	Triassic	300'
Moenkopi Formation	Triassic	2500'
Kaibab Limestone	Permian	600'
Toroweap Formation	Permian	475'
Talisman Quartzite	Carboniferous	1100'
Callville Limestone	Carboniferous	1200'
Monte Cristo Limestone	Carboniferous	975'
Mowitza Formation	Devonian	370'
Guilmette Formation	Devonian	1000'
		8520'

Ore deposits in the Star Range occur chiefly as contact-replacement or fissure-replacement types. To the author's knowledge, there are no deposits of importance in the intrusive or volcanic rocks, such as occur in the San Francisco mining district to the northwest.

The contact-replacement bodies occur as tabular deposits in the alteration zone of quartz monzonite-limestone contacts. Typical contact minerals include quartz, garnet, pyroxene, tremolite, mica, magnetite, and sulphide minerals (Butler, 1913). Fissure-replacement deposits often occur as ore chimneys, following the intersection line of a fissure with a favorable bed (Heyl, 1963). Such ores are highly altered, and contain little or no magnetite.

The Star and North Star mining districts were organized in 1870 and 1871, respectively, and the years 1872 through 1875 were prosperous for these districts (Butler, 1913). After 1880 there was little activity until 1904, when production revived somewhat, but after 1918, mining activity again decreased (Heyl, 1963). For the geology and ore occurrences of some of the mines in the area, see Butler (1913), Butler (1920), Hobbs (1944), Townsend (1950), Townsend (1955), and Heyl (1963).

Magnetometer Characteristics

An Askania Torsion Magnetometer, Model Gfz, was used during the 1966 field season, and an Askania Torsion Magnetometer, Model Gfz-M, provided by the Geophysics Department, University of Utah, was used during the 1967 season. Both instruments measured the vertical magnetic field intensity. The Model Gfz had a reading accuracy of

three gammas, while the Gfz-M, with a more precise reading system, had a reading accuracy of one gamma. The torsion magnetometer is described in detail by Haalck (1956).

The drift of the instrument and diurnal variations in the earth's magnetic field made it necessary to take all data in closed loops, with the initial station usually reoccupied within two hours. The difference between the initial and final readings was distributed linearly over the time interval involved, and the magnetic values corrected according to the time at which they were taken. Depending on terrain and station spacing, a closed loop of 30 to 60 data points could be run in two hours. For both magnetometers the net change in the instrument reading over this time interval, due to instrument drift and diurnal variations, was typically 10 to 20 gammas.

The attainment of data accuracy equal to the reading accuracy of the instrument required extremely careful and time-consuming field procedures. This study, in an igneous area, did not require such accuracy. Field procedures were such that the error associated with a given data point was about ±6 gammas, as determined by frequent reoccupation of stations.

Structure of Milford Flat Area

The western part of the Milford Flat quadrangle, which comprises the southwest quadrant of the 15 minute Milford quadrangle, is mountainous and contains many mines and prospects. Some of the larger mines, such as the Maud S., Vicksburg, and Estelle, are shown on Figure 10-1. Figure 10-2 is a generalized geologic map of the

western part of the Milford Flat quadrangle. As shown by this map, the mountains in the area of magnetic coverage expose consolidated sedimentary rocks, Paleozoic and Triassic in age, and Tertiary quartz monzonite intrusive rocks. The area is bordered on three sides by the alluvium of Milford Valley.

The outcrop pattern of Figure 10-2 suggests that the area is underlain by a Tertiary intrusive body of quartz monzonite, covered in places by a veneer of Paleozoic and Triassic sedimentary rocks. The aeromagnetic data support the presence of an intrusive cupola, projecting upward from the main igneous body. Such a cupola was included in Figure 7-7 and represented by a single rectangular plate (block (5)). Since the measured susceptibilities of quartz monzonite outcrops in the area averaged about .0034 cgs units, it was felt that magnetic profiles of a reconnaissance nature could confirm the presence of the intrusive cupola and determine the configuration of its surface under the alluvium.

Consequently, vertical field intensity observations were made along the profiles whose locations are shown in Figures 10-1 and 10-2. Data were taken at 100 foot intervals for most of profile A, and 200 foot intervals for the other profiles. Profile A traversed the range; profiles B through H began on or near an intrusive exposure and were directed radially outward.

The two-dimensional magnetic computation program was used to develop models for the anomaly source configuration whose computed magnetic fields resembled the observed profiles. Models were developed for profiles B through H, as well as the northern and southern

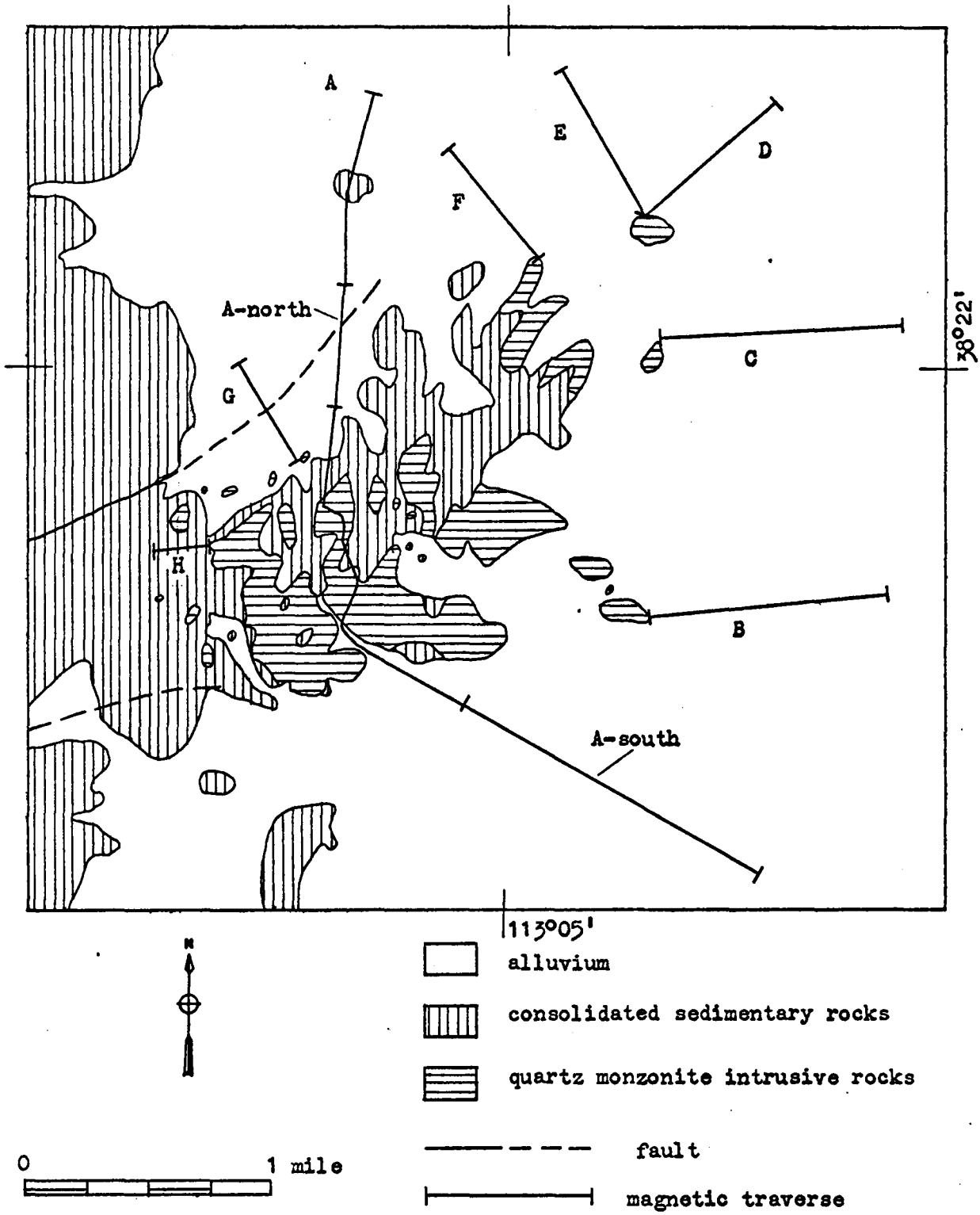

Figure 10-2. Generalized geologic map of the Milford Flat area. Also shown are the locations of the magnetic traverses made in the area.

segements of profile A (A-north and A-south on Figure 10-2). The profiles and profile segements (with the exception of profile H) were over alluvium where the actual surface topography could be accurately represented by an inclined line. The magnetic fields caused by the models were computed on the ground surface, as represented by an inclined straight line. Some error was probably introduced into the model fitting process for profile H because the surface topography in this case was not well represented by a straight line.

Figure 10-3 shows the vertical magnetic field measured along profile A, as well as the surface configuration of the models developed to reproduce the profile segements A-south and A-north and the magnetic values computed over these models. Figure 10-4 shows the observed data for profiles B through H, the corresponding computed magnetic profiles, and the surface configuration of the models over which the computed profiles were calculated. The left side of each profile of Figure 10-4 begins on an intrusive exposure.

A susceptibility of k=.003450 cgs units was assumed for the models. The complete model for each profile consisted of one or more two-dimensional, horizontal plates perpendicular to the profile. The uppermost plate of each model began at the ground surface. The basic geological assumptions used in developing the models were that the anomaly source had a constant magnetization parallel to the present earth's field, and that the observed decreasing magnetic amplitudes were due to increasing depth of burial of the source.

Profile A, Figure 10-3, has magnetic relief of about 1100 gammas, corresponding to the structural relief of the anomaly

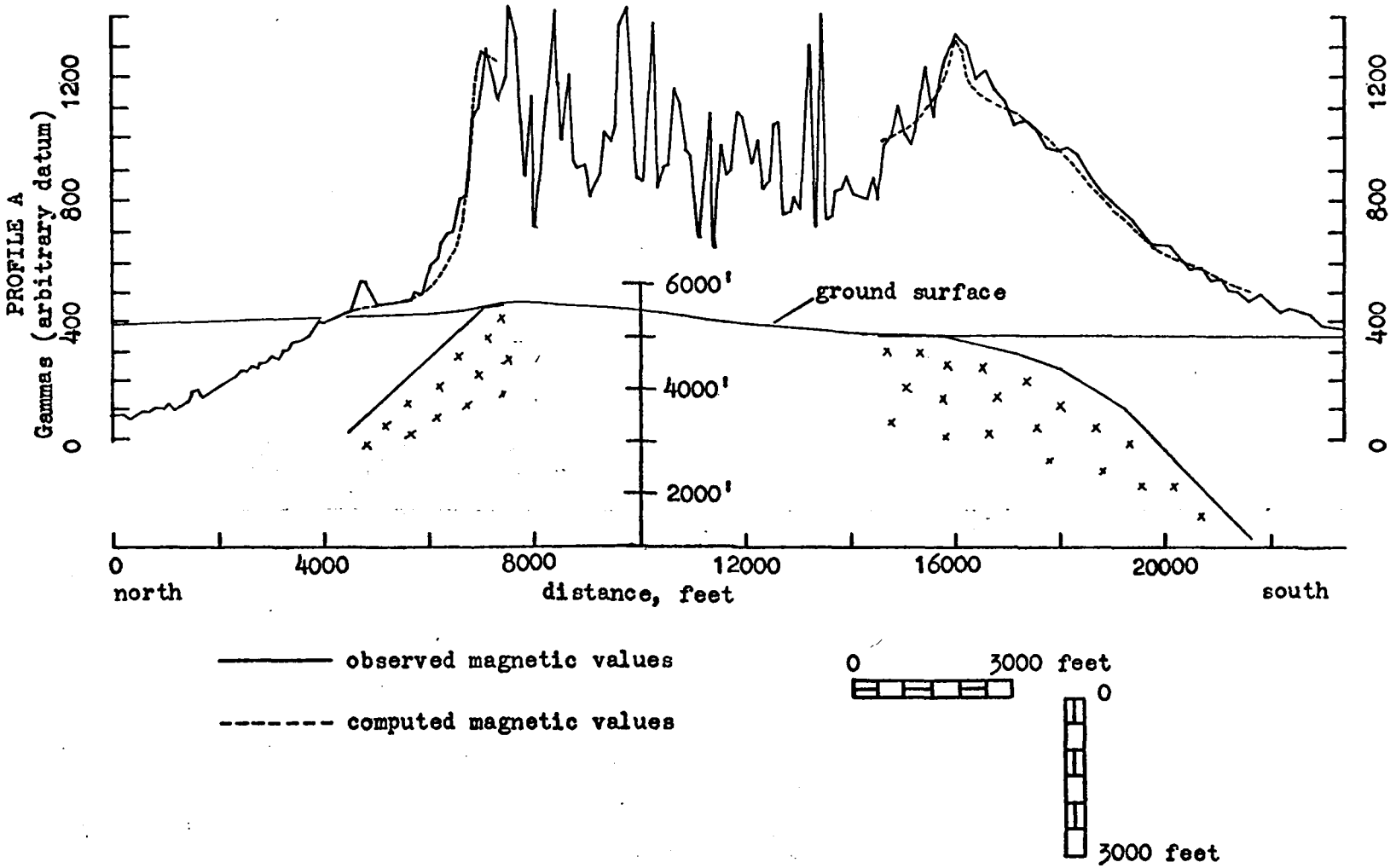

Figure 10-3. Observed magnetic data along profile A. Also shown are the models developed to reproduce portions of the observed data, and the computed profiles over these models.

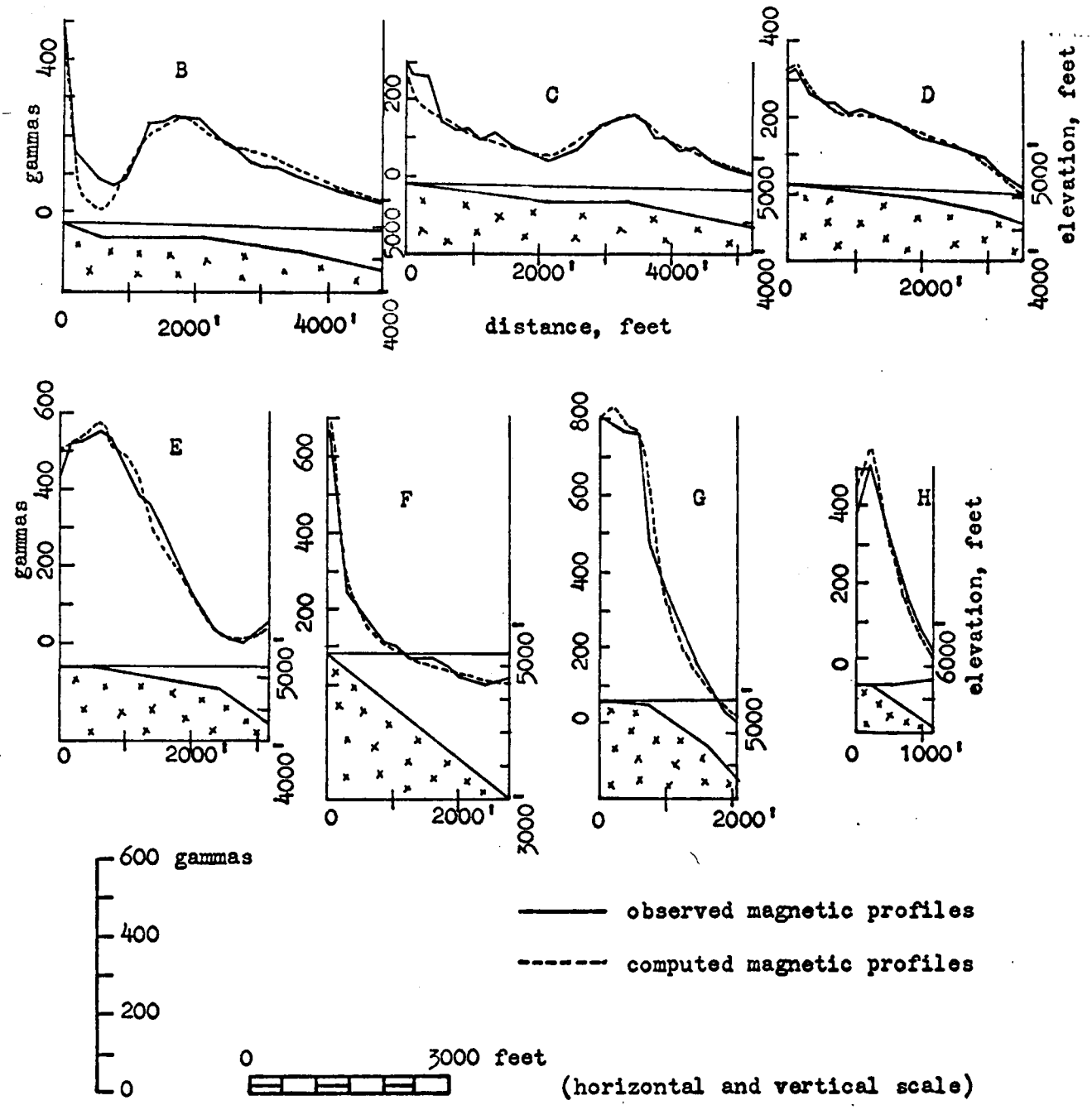

Figure 10-4. Observed magnetic data for profiles B through H, and the corresponding magnetic profile computed over the two-dimensional model representing the intrusive structure. The model surface, and the ground surface is shown below each profile. Observed data has been corrected for instrument and diurnal drift and adjusted to an arbitrary datum.

source. Over the exposed quartz monzonite, the magnetic data are very irregular, with local magnetic fluctuations amounting to 500 gammas and more. The overall anomaly, although irregular, tends to be larger near its northern and southern edges. This is due mainly to the characteristic magnetic anomaly shape over an edge, as shown by the causative models, although some part of the effect could be due to a different mineralogy in the exterior portions of the causative structure.

The computed profiles of Figures 10-3 and 10-4 closely resemble the observed data. Each profile begins on or near an intrusive outcrop. There are exposures of magnetic intrusive rock throughout the elevated portions of the area, and the aeromagnetic data over the Milford Flat area are shown to be consistent with the computed anomaly of an intrusive cupola underlying the profile locations. These facts imply that the model surfaces shown in Figures 10-3 and 10-4 represent the surface of an intrusive body underlying the study area.

Figure 10-5 is a structural contour map on the surface of this intrusive body. Where the body is covered by alluvium, the structural contours are drawn from the two-dimensional models developed to reproduce the magnetic profiles. In elevated areas, the (dashed) structural contours are lines of constant elevation taken from the topographic map.

The entire eastern portion of the intrusive structure mapped in Figure 10-5 is within 700 feet of the ground surface. The low dip of the intrusive surface to the east is also qualitatively apparent on the aeromagnetic map, where the magnetic closures over Milford Flat extend well out into Milford Valley.

The gently dipping intrusive surface shown in the eastern

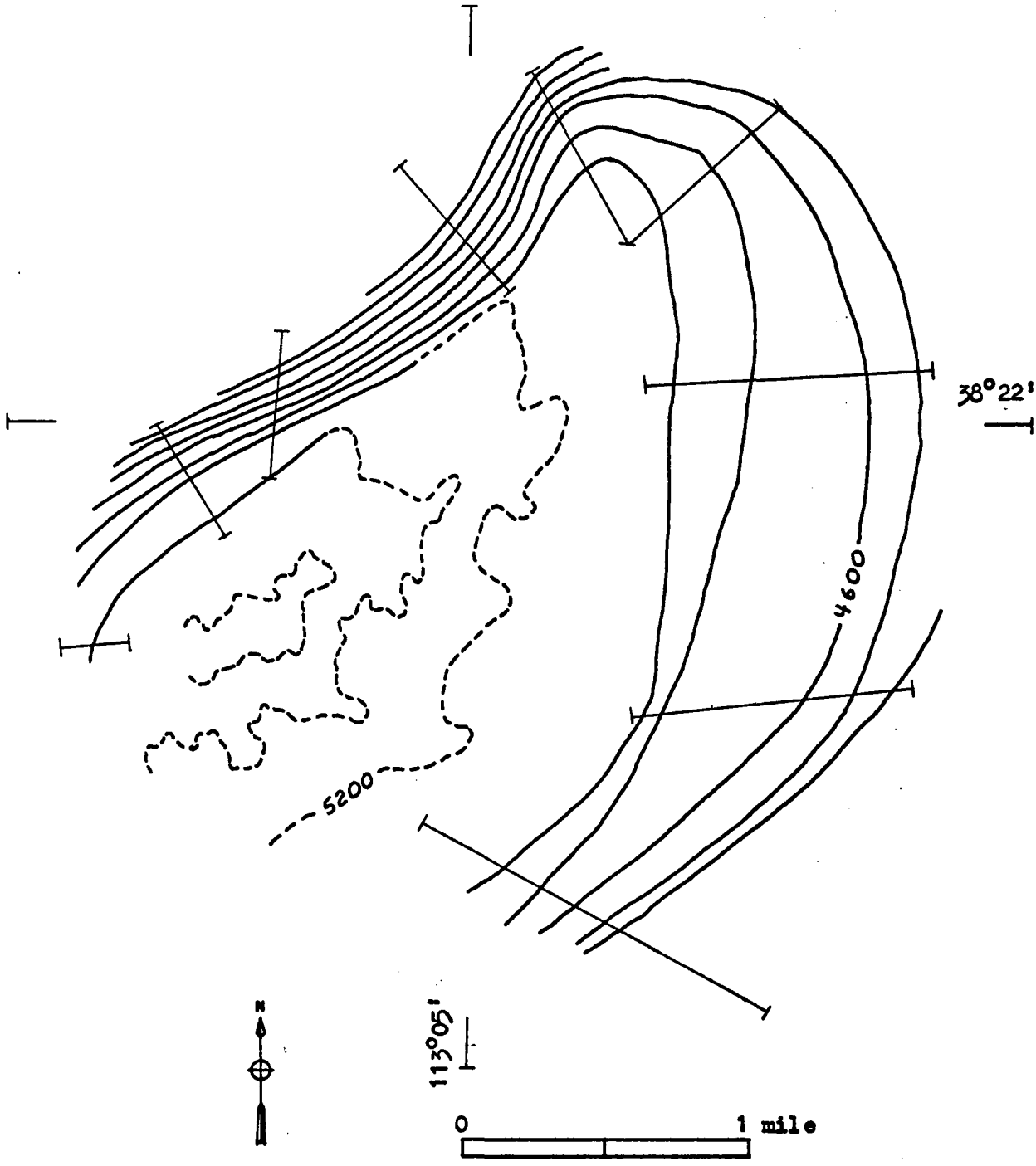

Figure 10-5. Structural contour map on the top of the Milford Flat intrusive body. Elevations are relative to sea level. Contour interval = 200 feet.

portion of Figure 10-5 could represent the original intrusive configuration, or an erosional surface now covered by alluvium. It could also represent an intermediate stage, with an erosional surface grading into the non-eroded original intrusive surface. If the contours represent chiefly the original configuration of the intrusive, it is apparent that there is no structural relief such as would be caused by appreciable post-intrusive normal faulting. The intrusive body in such a case could be overlain by consolidated sedimentary rocks, forming a situation favorable for mineralization.

If the structural contours represent an erosional surface of considerable areal extent, the pediment-like surface must have developed when the intrusive stood higher with respect to the level of alluvial fill. The present burial of the surface need not reflect a lowering of the Milford Flat structure, but rather a filling of the Milford Valley graben with sediments. If erosion of the intrusive is assumed, it is likely that alluvium rests directly on the quartz monzonite, and evidence for post-intrusive faulting in the form of surface relief would have been removed.

To the northwest, the surface of the intrusive body dips sharply, at an angle of about 45 degrees. This could reflect the natural dip of the intrusive surface or its termination by faulting. Whelan (private communication) has independently mapped a fault in the rocks to the west, which when projected under the alluvium closely parallels the dipping intrusive surface (see Figure 10-2). On the basis of this evidence, the hypothesis of termination by post-intrusive faulting is favored. Note that the northern part of profile A (Figure 10-3)

includes a small, positive anomaly which could not be reproduced by the model representing the dipping intrusive surface. The intrusive surface is about 1500 feet deep at this point, and the local anomaly must originate from a source nearer the surface. The position of the anomaly coincides with the zone of postulated faulting, but it is not sufficiently defined by the available magnetic data, however, to speculate on its nature.

Magnetic Exploration Near the Wild Bill Mine

The Wild Bill mine (shown in the northwest part of Figure 10-1) was one of the early mines in the Star Range, and is described by Butler (1913). Its ore body was of the contact-replacement type, grading into fissure-replacement deposits, and contained some magnetite. Figure 10-6 is a generalized geologic map of the area surrounding the Wild Bill mine, prepared by the author from observations made in the field.

The mine is located immediately east of an outcropping of magnetic quartz monzonite which appears to be a local positive element on the cupola designated as block (3) of the residual igneous model (Figure 7-7). The intrusive-limestone contact zone is irregular and covered in places by alluvium and Tertiary volcanics. A clearly-visible bleached zone occurs in the limestone and is probably associated with the intrusive emplacement. Small aplitic dikes, partially obscurred by slope wash,

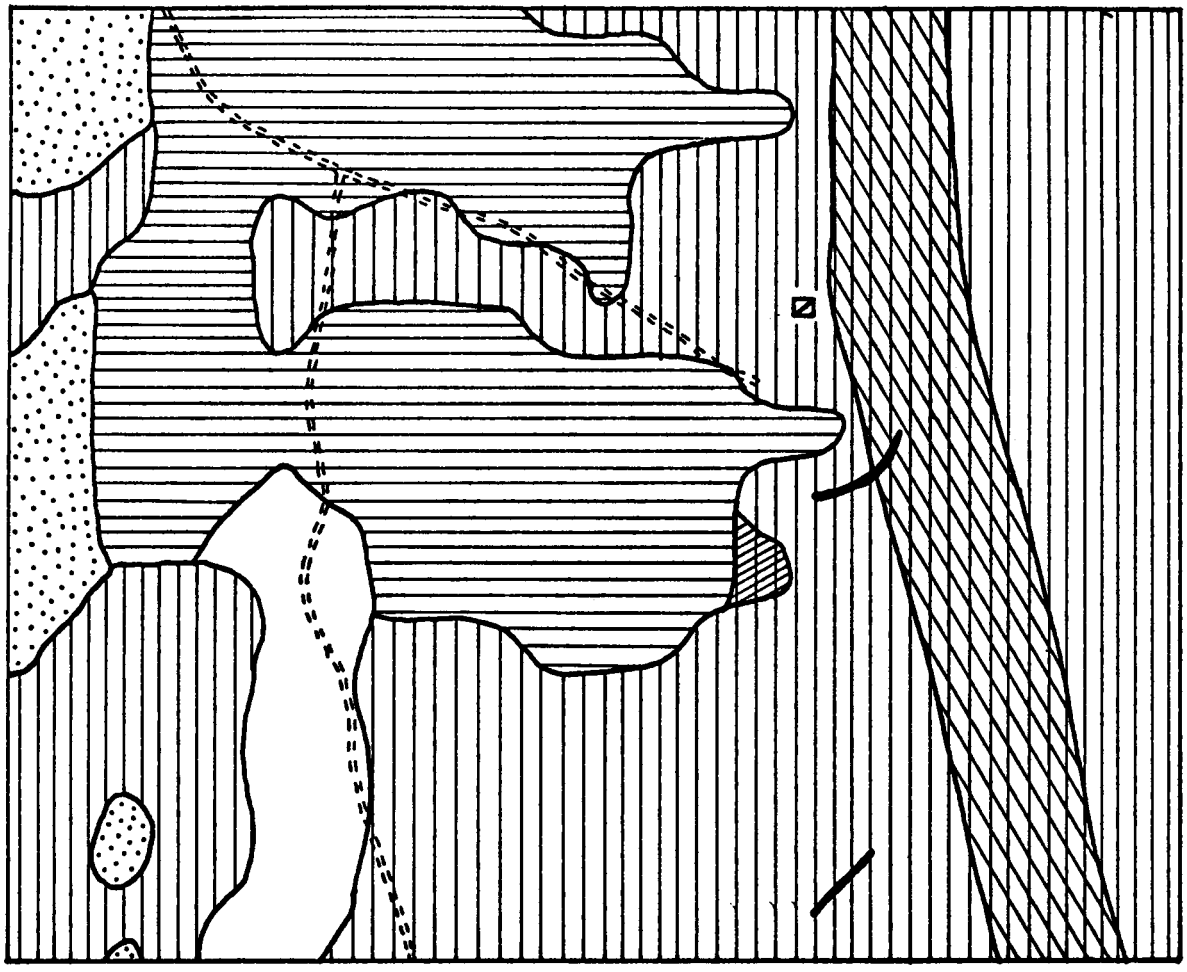

Figure 10-6. Generalized geologic map of the Wild Bill area. The area covered by this map is indicated, by a rectangle, on Figure 10-1.

also occur in the limestone. There are many prospects (not shown on Figure 10-6) scattered throughout the area.

In view of the magnetite reported in the Wild Bill ore body (Butler, 1913), the extensive contact zone, and widespread alteration of the limestone, it was felt that a detailed magnetic survey in the area might locate zones of magnetite mineralization and define the configuration of the intrusive body under the sedimentary cover. Consequently, a vertical-intensity magnetic field survey over the area of the geologic map (Figure 10-6) was carried out.

Magnetic data were taken at the intersection points of a square grid with 100 foot line spacing. The rectangular area of coverage measures 2200 feet (east-west) by 1800 feet (north-south). Grid points were located by Brunton compass and tape. Field work was complicated by steep terrain and a heavy growth of cedar and juniper.

Figure 10-7 shows the resulting vertical magnetic field intensity map. Magnetic values have been corrected for diurnal variation and instrument drift, and adjusted to an arbitrary regional base. 3*3 running average regional and residual maps were obtained from the original data to separate approximately the magnetic effects of the smaller and larger causative structures underlying the map area. Figure 10-8 is the 3*3 running average residual map obtained by subtracting the smoothed field (Figure 10-9) from the original data.

The eastern one-third of the Wild Bill magnetic grid contains a magnetic gradient of about 20 gammas per 100 feet decreasing to the east (Figure 10-7). The smoothed data show this gradient with many local irregularities removed (Figure 10-9). The gradient does not

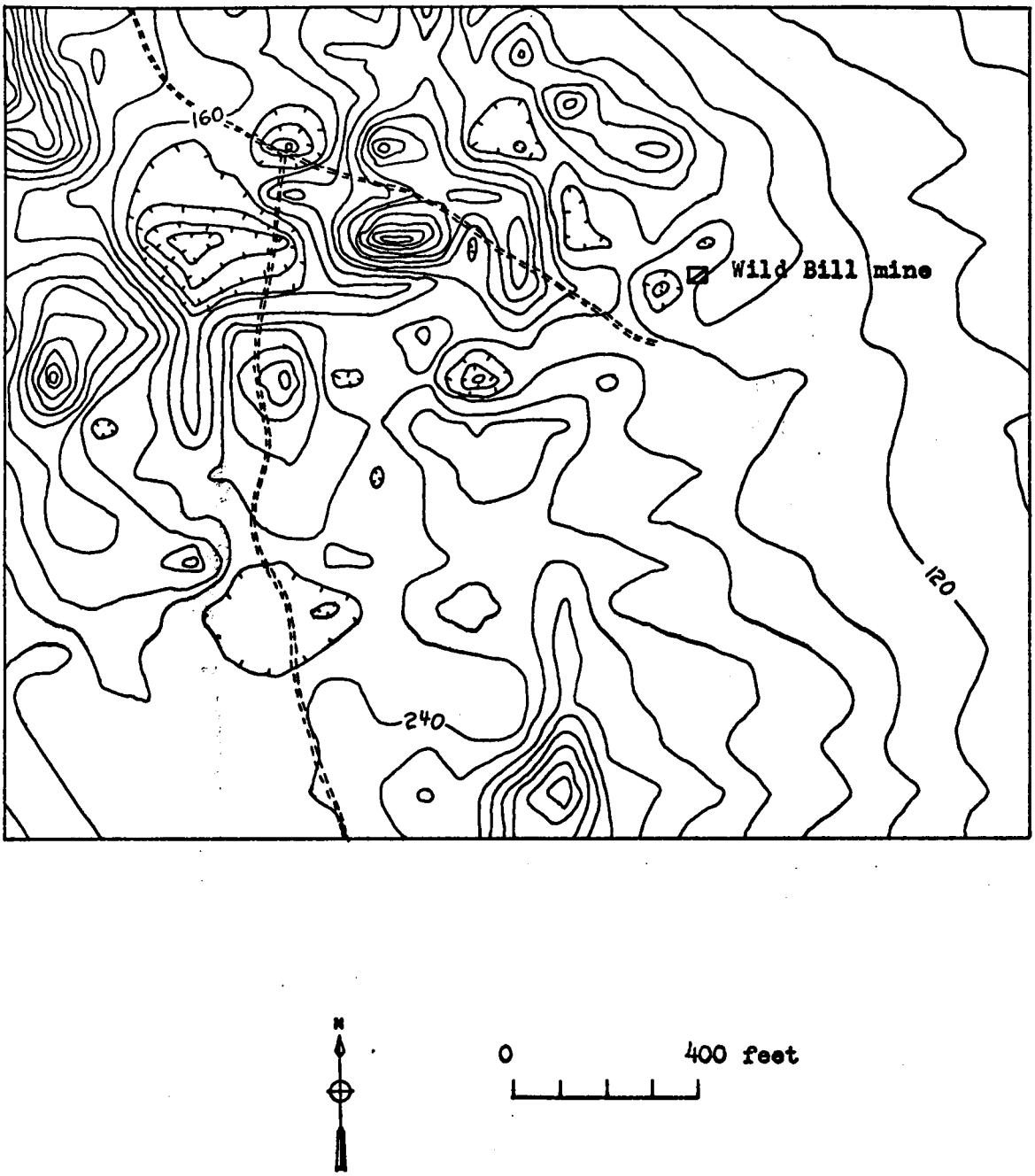

Figure 10-7. The Wild Bill magnetic grid. Data has been corrected for instrument drift and adjusted to an arbitrary datum. Contour interval = 40 gammas. Area of coverage is the same as Figure 10-6.

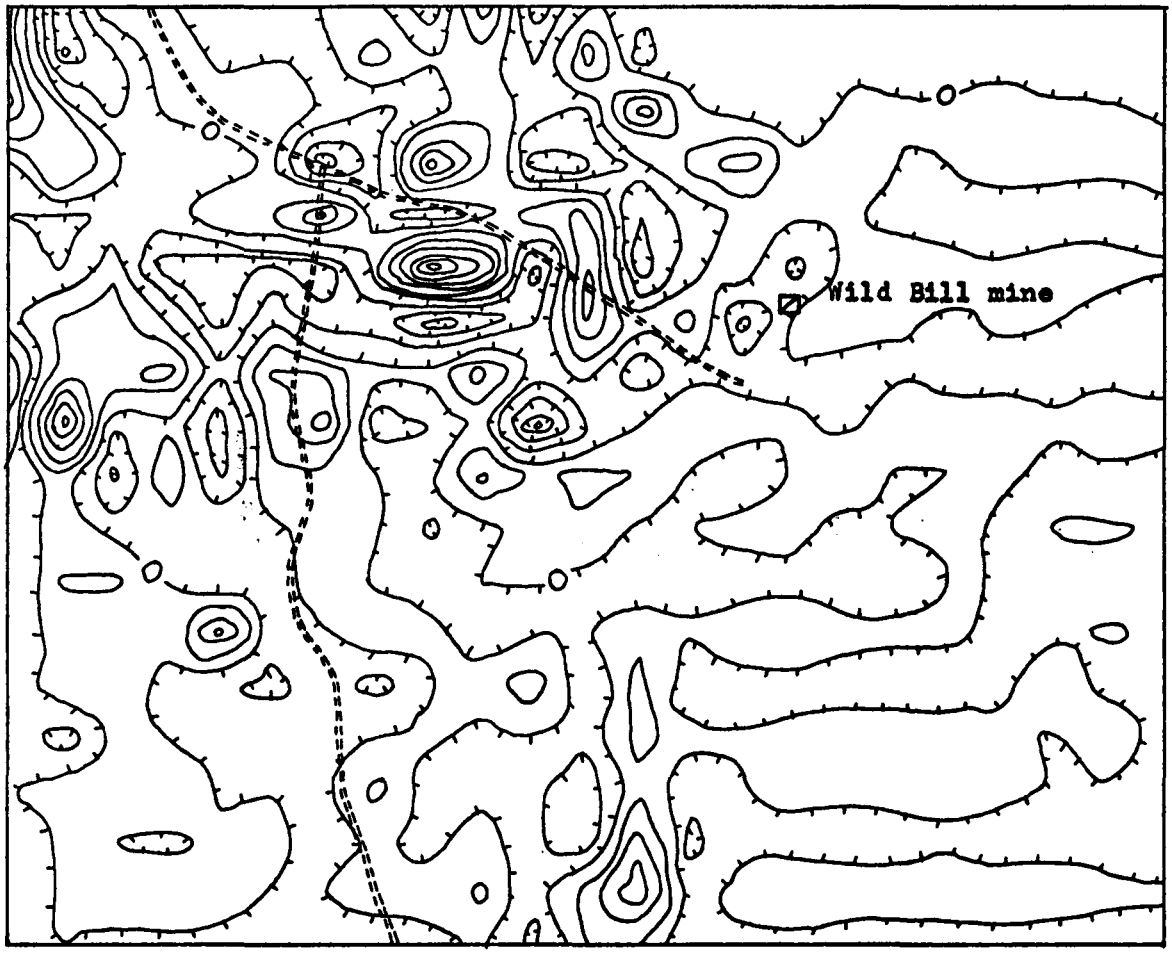

Figure 10-8. 3*3 running average residual map of the Wild Bill magnetic grid. Contour interval = 40 gammas. Area of coverage is the same as Figure 10-6.

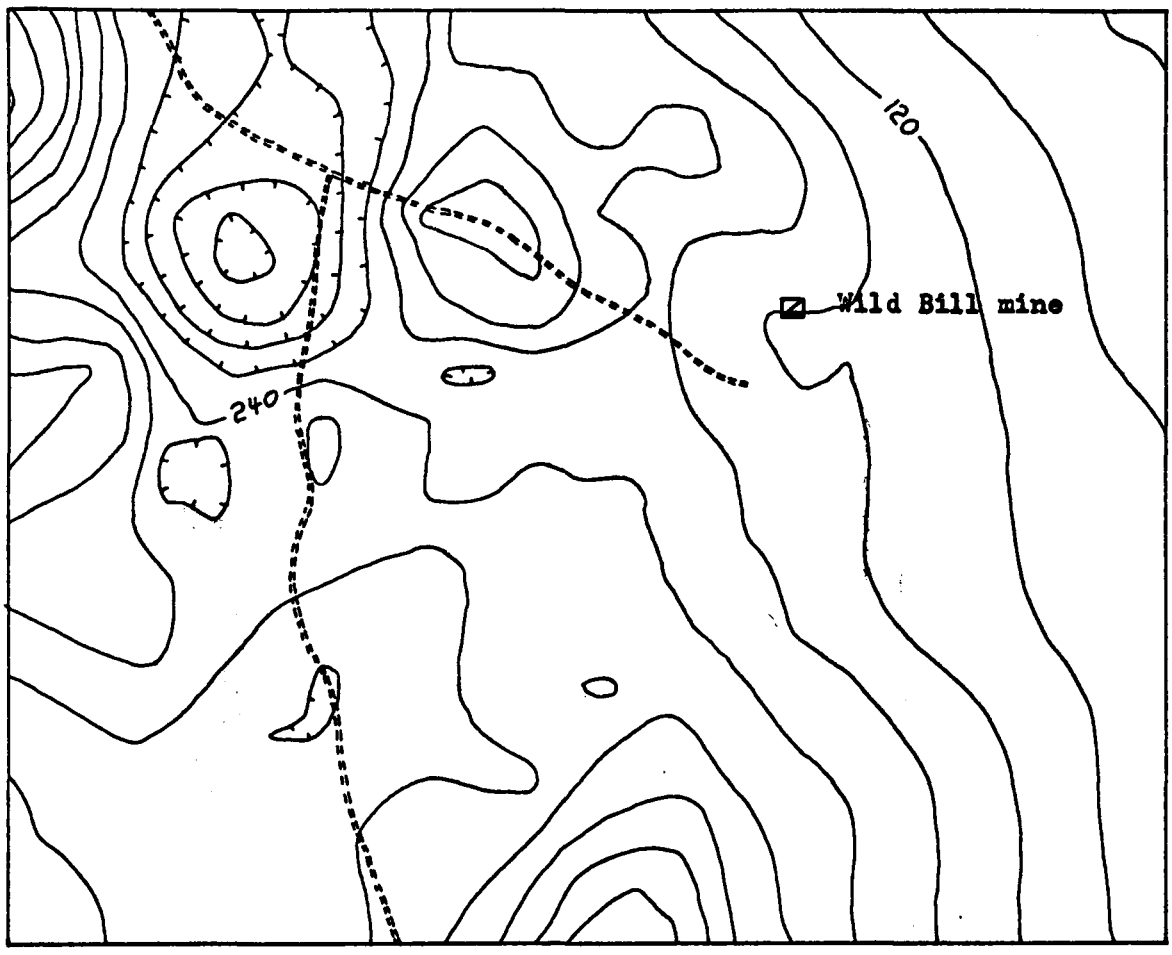

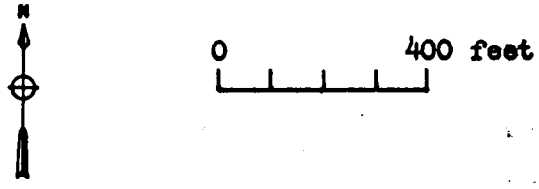

Figure 10-9. 3*3 running average regional map of the Wild Bill magnetic grid. Contour interval = 40 gammas. Area of coverage is the same as Figure 10-6.

correlate with the outcrop pattern of intrusive rock, but continues from north to south across the map area. This gradient indicates that the local intrusive body extends southward across the map area, with its surface dipping to the east. The strike of the local intrusive structure thus parallels the magnetic gradient, the strike of the limestone bedding (which dips 50° east), and a zone of altered limestone, which has no magnetic expression. Butler's map of the Wild Bill mine indicates that near the mine location shown on Figure 10-6 the average dip of the intrusive surface to the east is about 50 degrees.

The original magnetic map shows minor noses in the eastern gradient which appear in the eastern portion of the residual map (Figure 10-8) as alternating bands of positive and negative, east-west magnetic lineaments. Since they parallel the lines along which the data were taken, and have no consistent relationship to topography, it is thought that these lineations are spurious anomalies reflecting primarily small errors in the adjustment of each profile to the regional base. Similar anomalies sometimes parallel the flight lines of aeromagnetic maps. Although their actual amplitudes are less than 10 gammas, they are very apparent on the residual map because they happen to straddle a contour level and are not distorted by other magnetic anomalies.

Two narrow, aplitic dikes were mapped in the eastern part of the area (Figure 10-6). Their measured susceptibility was about .0025 cgs units, but they apparently were too small to exert a noticeable magnetic effect at a station spacing of 100 feet.

The single zone of contact alteration that was exposed and continuous enough to be mapped had a susceptibility of only .0002 cgs

units and no magnetic expression.

The northwest part of the original map (Figure 10-7), in the area of the exposed intrusive rock, shows a number of areally-small, high and low closures with amplitudes ranging up to several hundred gammas. Figure 10-3, over the Milford Flat intrusive body, showed a one-dimensional example of a similar pattern. These anomalies are not interrupted by the limestone outcrop which nearly divides the intrusive exposure into northern and southern portions (Figure 10-6). This limestone exposure thus appears to be thin and lying on the intrusive body.

There is a positive magnetic anomaly of greater than average amplitude over this limestone tongue, which probably results from the magnetite content of a small contact-replacement mineralized zone in the limestone. A sample from a prospect in this area had a high magnetite content, and its susceptibility exceeded the range of the susceptibility bridge.

Near the western edge of the area, acidic Tertiary volcanic rocks are present, and just beyond the map area completely cover the surface. There are magnetic highs over each of the two main volcanic exposures. The measured susceptibilities of two volcanic samples were less than .001 cgs units, but local remanent effects and zones of higher susceptibility are possible and could produce the observed anomalies. A window in the volcanic rocks reveals limestone, over which the magnetic gradient is sharply decreased. If the two anomalies over the volcanics are attributed to the volcanic rock, there are no anomalies in the extreme western map area typical of the near-surface intrusive body.

To the south, the many small closures generated by the intrusive body tend to terminate, indicating a probable deepening of the intrusive surface. There is, however, a positive anomaly midway along the southern boundary. This anomaly can be reproduced by a three-dimensional model representing an upward extension of the intrusive body. Figure 10-10 shows such a model, and Figure 10-11 compares the magnetic anomaly computed over this model to the observed anomaly.

The vertical magnetic field of the model was computed using the three-dimensional magnetic computation program, and an assumed susceptibility of .003450 cgs units, the average measured susceptibility of quartz monzonite samples. The top of the dike-like plate was 50 feet below the ground surface, the top of the main block 60 feet, and the top of the small, upper plate was 30 feet below the surface. The base of the model was 200 feet deep, with the assumption that there the upward protrusion merged into the main intrusive body.

Magnetic Work in the Beacon Claims Area

South of the old site of Shauntie and west of the site of South Camp, quartz monzonite intrusive rock is exposed (Figure 10-1 and Plate 1). This intrusive - here called the Shauntie intrusive - is singular in that it has an average measured magnetic susceptibility of only .0004 cgs units (Section VI). Figure 10-12 is a topographic and generalized geologic map of the area southeast of the site of Shauntie, showing the southern part of the Shauntie intrusive body and the surrounding geology. The square drawn around a road junction in the upper-left corner of the figure is also drawn on Figure 10-1,

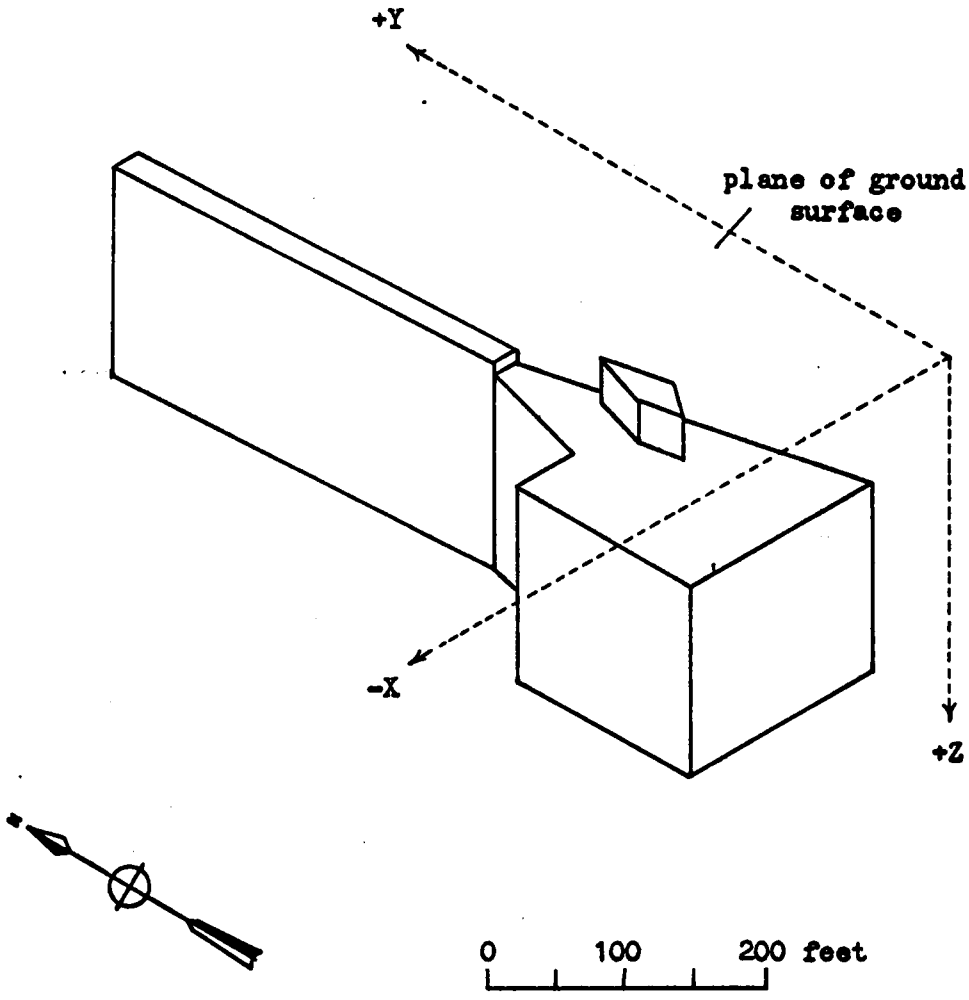

Figure 10-10. Perspective drawing of the intrusive body which generates a magnetic anomaly similar to the observed south-central anomaly of the Wild Bill magnetic grid.

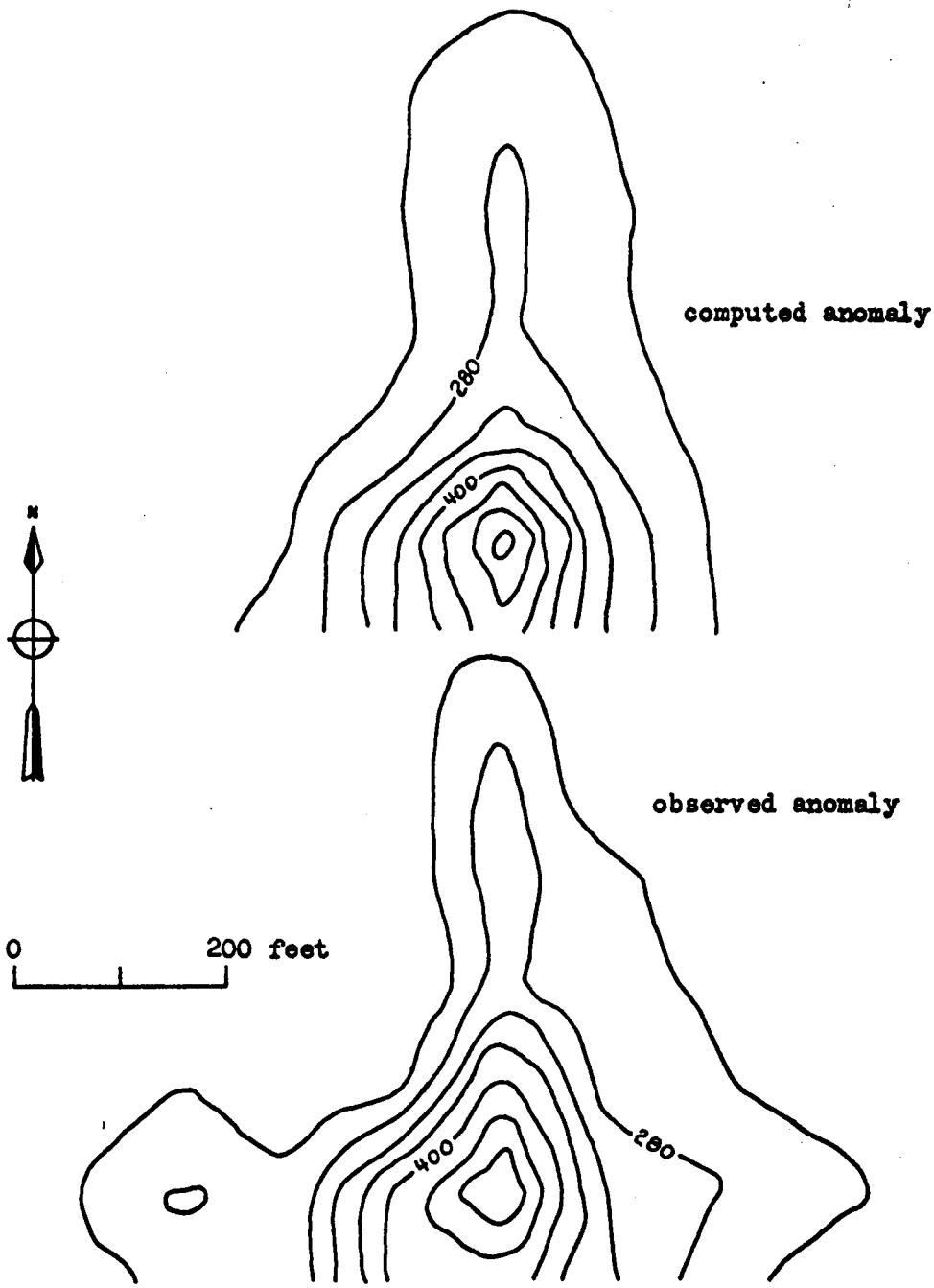

Figure 10-11. A comparison of the observed south-central magnetic anomaly to the anomaly computed over the intrusive model of Figure 10-10. Susceptibility = .003450 cgs units. Contour interval = 40 gammas.

the base map of the Star Range vicinity, to facilitate the regional orientation of Figure 10-12. The topographic base of Figure 10-12 is adapted from the U.S.G.S. 7½ minute preliminary sheet of the southwest quadrant of the 15 minute Milford quadrangle. The geology is based on the author's field observations.

Limestone contacts the southeastern border of the Shauntie intrusive. Where exposed, this contact zone is found to have magnetite mineralization in places, with copper minerals frequently present. In this respect the area is similar to commercial copper deposits in the southern Rocky Range, where copper ore occurs as contact-replacement mineralization along with magnetite.

The nature and extent of mineralization along the contact was not apparent in many places because of surface weathering and a cover of slope wash. Vertical magnetic field intensity measurements were taken along the southeastern contact zone of the Shauntie intrusive to define areas of magnetite mineralization. The measured values are here referred to as the Beacon Claims data.

The Beacon Claims base line extends generally northeast from station 1 for 4100 feet along the limestone-intrusive contact (Figure 10-12). Base line stations are spaced at 100 foot intervals, and profiles more or less perpendicular to the base line cross the contact zone at 100 foot intervals or less. Data spacing on these transverse profiles is 25 feet or less.

Terrain was rugged, and topographic slopes ranging up to 30 degrees made surveying by Brunton compass and tape difficult. Distances were measured on the ground surface and no attempt was made

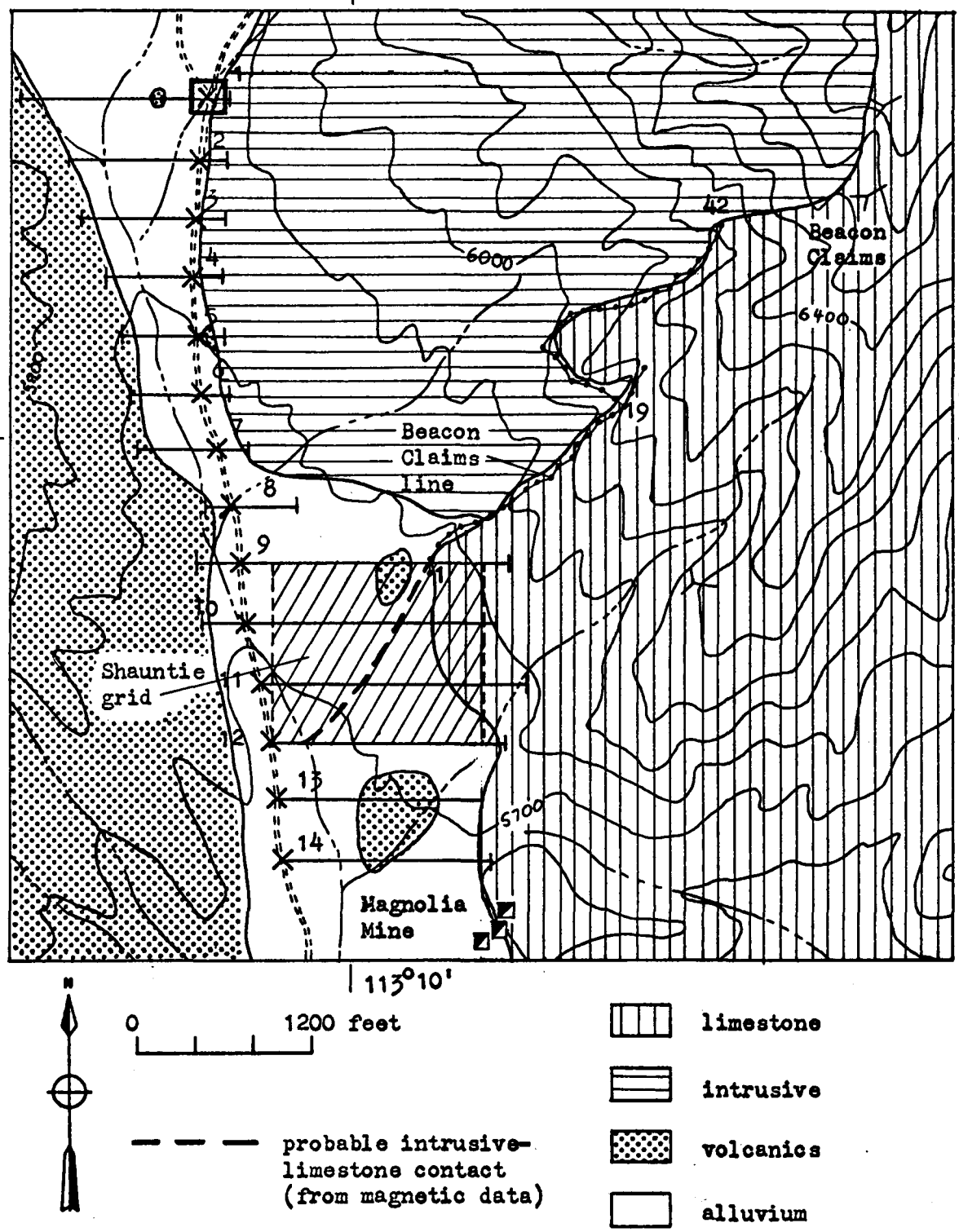

Figure 10-12. Topographic and generalized geologic map of the area around the southern exposure of the Shauntie intrusive body. The location of magnetic work in this area is also shown. Contour interval = 100 feet.

to project them unto a horizontal plane.

Plate 2 in the map pocket is a contoured magnetic map of the Beacon Claims data. Plate 2 also shows the base line and profile locations, and local surface geology. Because of the extreme local variations in magnetic field intensity, the magnetic data were contoured at 1000 gamma intervals. Areas where magnetic values were higher than 2000 gammas or lower than -2000 gammas were denoted by hatchures and not contoured. Anomaly amplitudes ranged from near zero to 10,000 gammas, with high to low differences of 3000 gammas common. The Shauntie intrusive body, with its low susceptibility, could not be reliably distinguished from the limestone on the basis of the magnetic data.

The anomalies of Plate 2 represent the magnetite distribution along the intrusive-limestone contact zone. The mineralized zones parallel the contact, and occur in the limestone within 100 feet of the intrusive body. The magnetite mineralization is very irregular. Measured susceptibilities of samples from prospects in the zone of contact alteration ranged from near zero to the high value of .140 cgs units.

The magnetic anomalies fall into four general groupings, as designated on Plate 2. The anomalies within each group are similar in character and alignment. Table 10-2 lists the location and physical parameters of each group, as well as two descriptive parameters of each group's average magnetic anomaly. Anomaly amplitude was not listed as a basic magnetic parameter in this case. Only anomaly shape terms were considered, in order to solve for the geometrical parameters

Table 10-2. Summary of the physical and magnetic characteristics of the four anomaly groups - Beacon Claims data.

Group	Station Numbers	Strike of Contact	Slope of Topography	Ave. Ratio of High to Low Magnetic Closure	Average Magnetic Anomaly Width*
1	9-19b	N45°E	20°NW	1.4	2.7
2	19b-22	N78°E	25°N	6.9	3.2
3	24-29	N35°E	17°NW	1.6	3.9
4	30-41	N65°E	30°N	∞	1.2

*Anomaly widths have been normalized relative to a "standard width," and so are dimensionless.

of the causative structures. The direction of magnetization was assumed to parallel the earth's main field vector. Although remanent magnetization is a possibility, no consideration was given to anomalous vector directions since related experimental data were not available.

The magnetic anomalies over each group were assumed to have two shape parameters - the amplitude ratio of positive to negative anomaly maxima and the total anomaly width (measured between the points where the magnetic values had decreased to 10% of the maxima's amplitude). Representative magnetic profiles were determined for each group of anomalies (Plate 2), and the average ratio of high to low closure and anomaly width were determined for each group (Table 10-2).

The causative zones of magnetite mineralization were assumed to be reasonably represented by simple tabular bodies, outcropping at the surface, whose dip and thickness are important but unknown physical parameters. To determine the dip angle and thickness of the mineralized contact zones, families of magnetic profiles were computed over representative two-dimensional dike models. The anomaly width and ratio of high to low closure of each of the computed profiles were determined and plotted as a single point on a graph having as axes the ratio of high to low closure and anomaly width. Figure 10-13 is such a graph, computed for dike models using a bearing and slope of surface topography similar to the contact zones of anomaly groups 1 and 3, and showing the individual points determined for these groups. Similar charts were constructed for anomaly groups 2 and 4.

Using these charts and the average anomaly parameters listed in Table 10-2, the dip angle and thickness of the four zones of magnetite

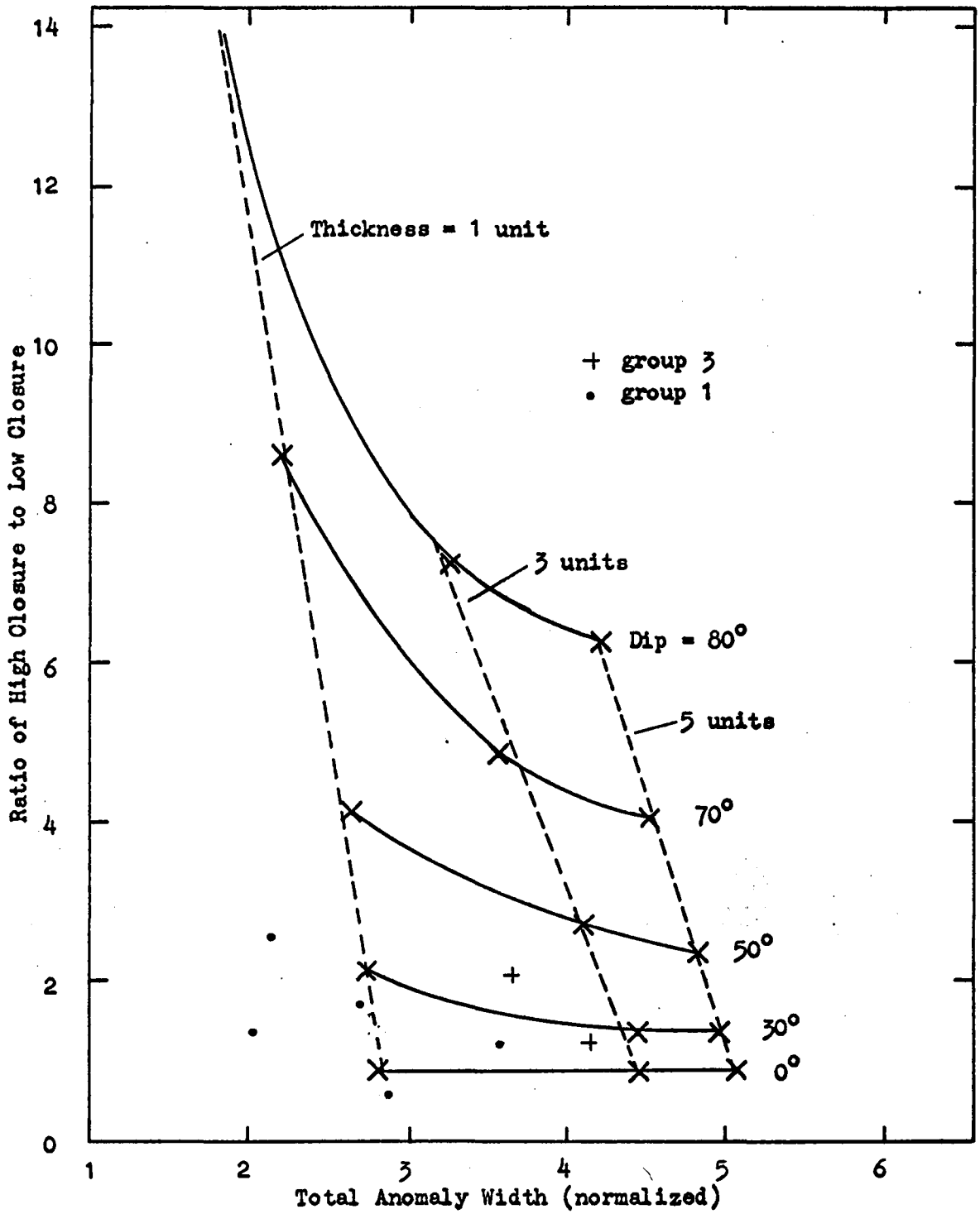

Figure 10-13. Chart used to determine the dip and thickness of contact zone mineralization - anomaly groups 1 and 3, Beacon Claims data. Dip angles are relative to the horizontal. A thickness of 1 unit = 50/6 feet, and is measured perpendicular to dip.

Table 10-3. Summary of the physical parameters of the contact zone - Beacon Claims data.

Anomaly Group	Dip of Contact	Thickness of Mineralization, feet
1	15°SE	8
2	30°N	25
3	30°SE	16
4	110°S*	25

* contact is overturned

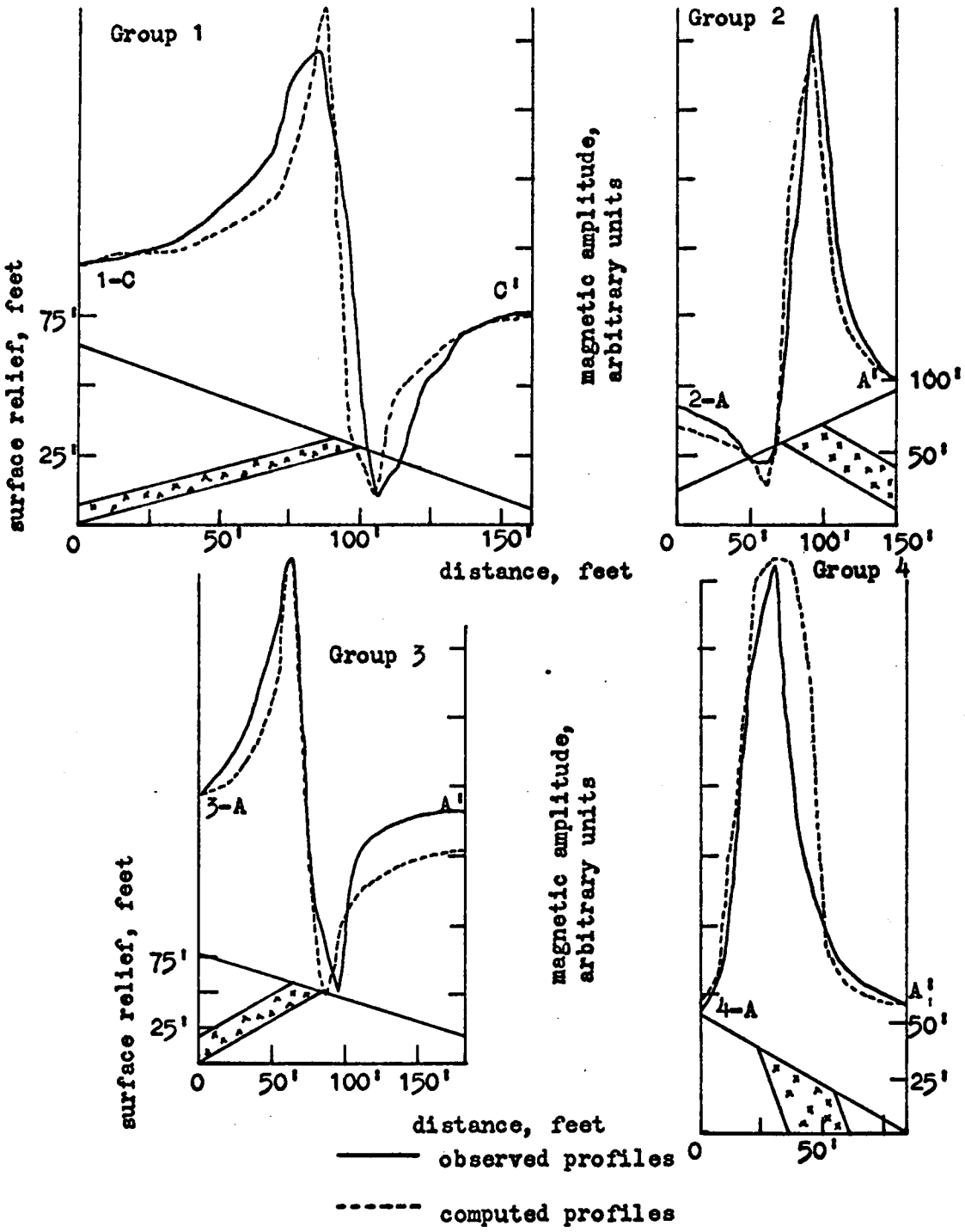

Vertical scale is in arbitrary units.

Figure 10-14. Comparison of observed magnetic anomalies to anomalies computed over the tabular dike models of Table 10-3. The observed profile designations refer to Plate 2. Also shown are the ground surface and the causative dike model for each profile.

mineralization were determined, and are shown in Table 10-3. The angle of dip for the contact zone of group 4 was given as 110 degrees, measured from the south, rather than 70 degrees north, to emphasize that the intrusive side of the contact forms the hanging wall.

Figure 10-14 compares the computed magnetic anomalies over two-dimensional tabular models, having parameters of dip and thickness as listed in Table 10-3 and orientation and surface topography as listed in Table 10-2, to an observed profile from each anomaly group. The general agreement is sufficient to confirm the validity of the method of interpretation.

Between stations 1 and 9 (Plate 2), anomalies associated with the contact zone were of only a few hundred gammas amplitude. The contact zone itself was poorly exposed southwest of station 6. The typical width of the lower amplitude anomalies between stations 1 and 9 was not greater than the average width of the large anomalies, however, which implies that the decreased anomaly amplitude is due to lack of magnetite rather than depth of burial.

Magnetic Exploration South and West of the Shauntie Intrusive

To the south and west the Shauntie intrusive body appears covered by alluvium and could extend under the volcanics exposed in the western map area of Figure 10-12. From surface evidence, the southern and western extent of the intrusive body cannot be determined. Vertical-intensity magnetic field measurements were carried out in this area in an attempt to detect and map the southern and western contact zones of the intrusive body.

To conduct a general magnetic reconnaissance of the area, a base line of 14 stations, 400 feet apart, was placed along the Shauntie road, beginning at the junction of Shauntie road and the road leading to the Old Moscow mine, and continuing southward (Figure 10-12). East-west magnetic profiles, with data spacing of 25 feet, were run from each base station. From stations 1 through 7 the east-west profiles extended from intrusive outcrop on the east to volcanics on the west. Profile 8 was a transition profile, while the profiles extending from stations 9 through 14 started on or near volcanics to the west and continued east until limestone outcrop was reached.

On the basis of these reconnaissance profiles, the remaining time available for field work in 1967 was used to obtain magnetic data on a grid in the area south of the Shauntie intrusive exposure (Figure 10-12). The resulting Shauntie magnetic survey extends 1400 feet in an east-west direction and 1200 feet north and south, with data taken at 50 foot intervals on a grid.

The magnetic data of reconnaissance profiles 1 through 8 showed no anomalies which could be attributed to a mineralized contact zone. Either the contact zone was farther to the west than the survey extended, or it was buried too deeply or contained too little magnetite to be detected. Study of the southeastern edge of the intrusive (Beacon Claims data and following discussion) indicated an alluvial cover of stream wash not more than 50 feet thick (note in Figure 10-12 the volcanic remnants projecting through the alluvium), and a sufficient magnetite content in the contact zone to produce detectable anomalies. It is thus probable that the quartz monzonite intrusive

extends to the west under the volcanic rocks and beyond the coverage of the magnetic data.

Profiles 9 through 14 contained many local anomalies having amplitudes from 50 to 200 gammas, which were defined in greater detail by the Shauntie magnetic grid. Figure 10-15 shows the contoured magnetic data of the Shauntie grid. The data contain numerous areally-small, low-amplitude anomalies. Many of these anomalies are too small, both in amplitude and areal extent, to have individual significance. Taken as a group, however, the anomalies have a well defined range of occurrence, suggesting that as a group they are indicators of geologic structure.

To emphasize the distinct zone of anomaly occurrence, Figure 10-16 was prepared showing the center point of each magnetic closure on the Shauntie magnetic grid. Dashed lines on this figure isolate a region of the map - called the "trend zone" - comprising about 35% of the total map area but containing 78% of the magnetic closures. Comparison of the anomalies within the trend zone to those without confirms that the many small anomalies are not randomly generated but represent a geologic source.

There are 24 closures containing two or more data points ("large" anomalies) on Figure 10-15, of which 19, or 79%, occur in the trend zone of Figure 10-16. There are 30 one-point ("small") closures, of which 23, or 77%, occur in the trend zone. The "large" anomalies presumably have more individual significance, but equal percentages of both "large" and "small" anomalies fall within the trend zone, indicating that the "small" anomalies are not randomly generated

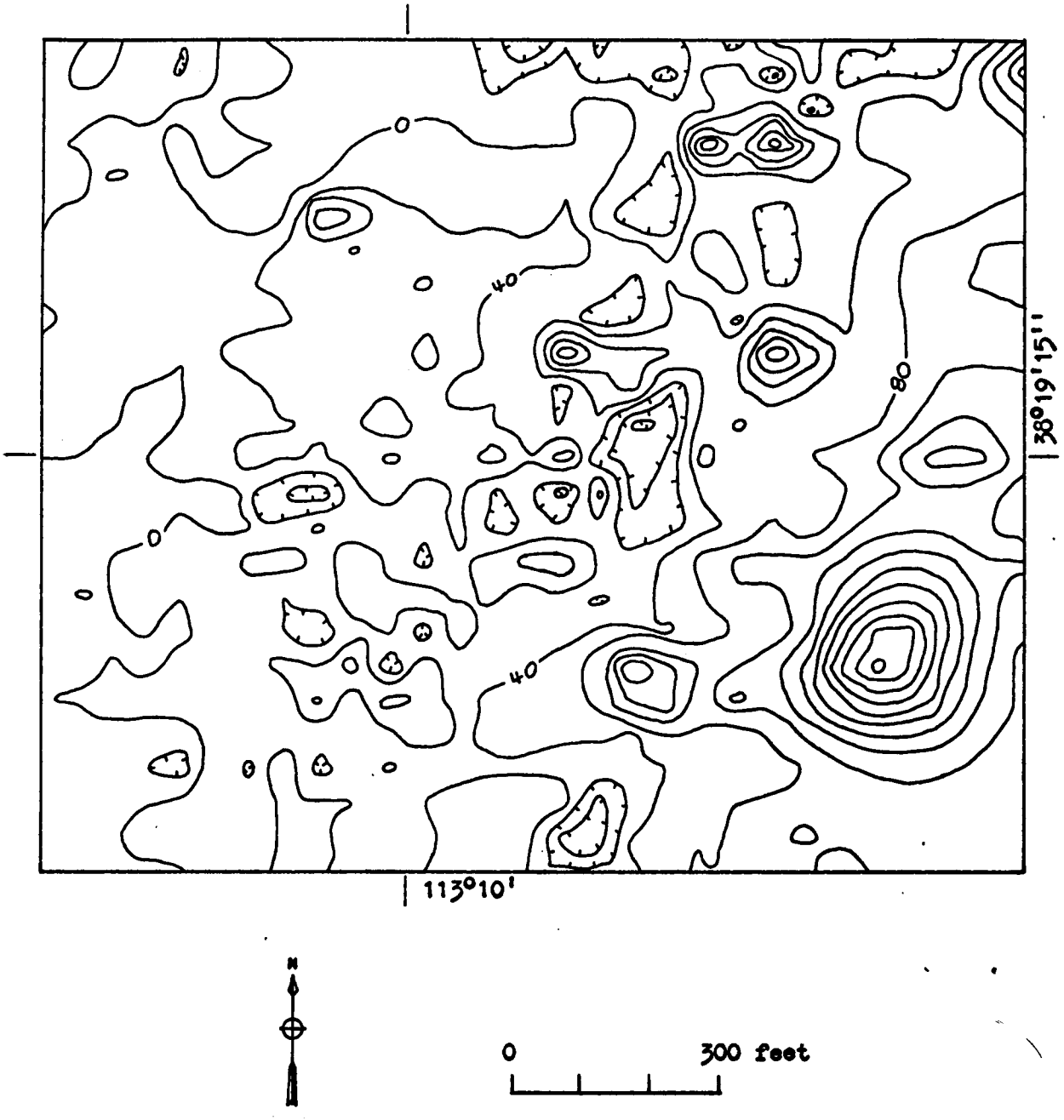

Figure 10-15. The Shauntie magnetic grid. Data have been corrected for instrument and diurnal drift and adjusted to an arbitrary datum. Contour interval = 40 gammas. The area covered by this map is shown on Figure 10-12.

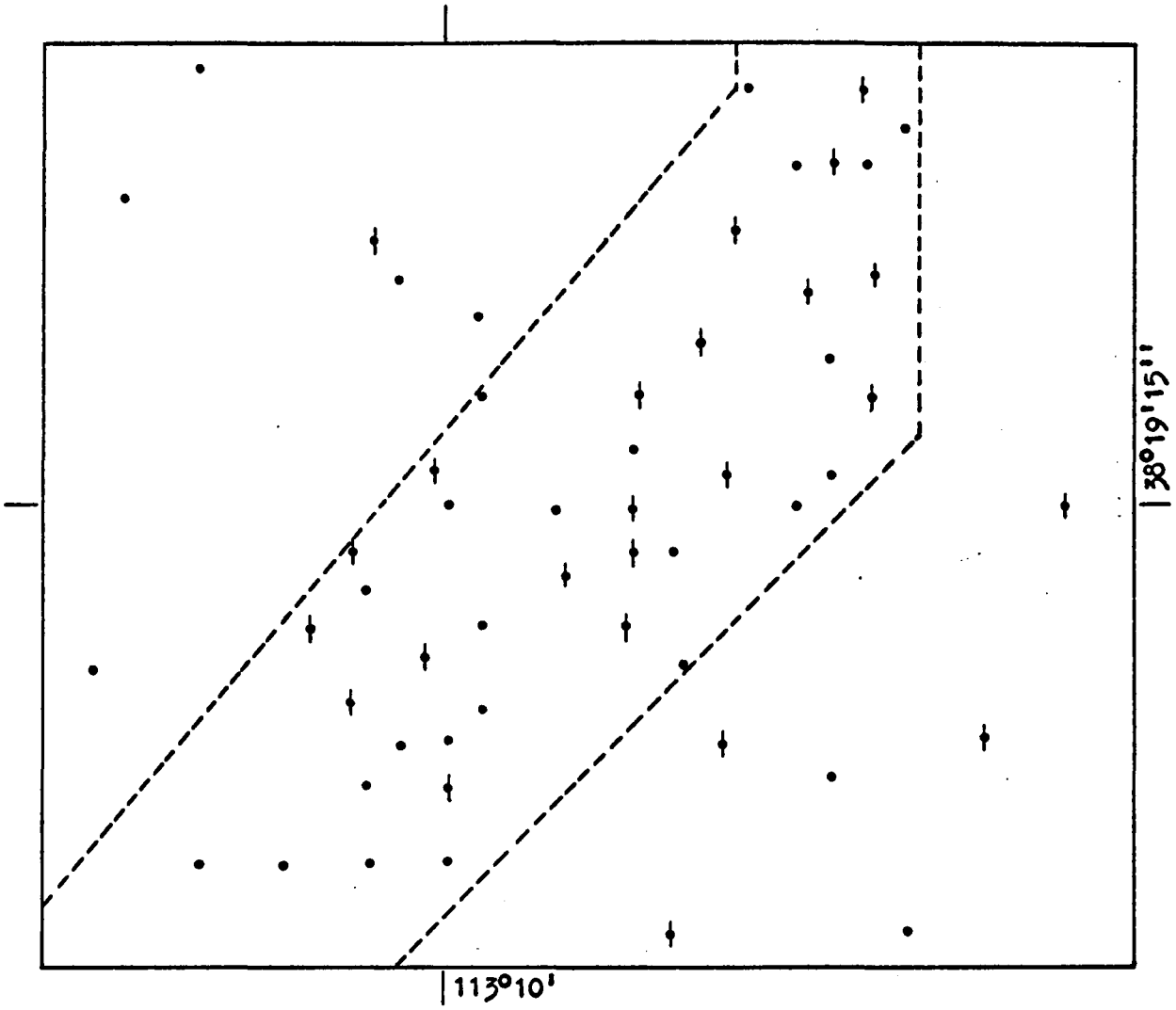

centers of magnetic closures containing two or more data points

• centers of magnetic closures containing one data point

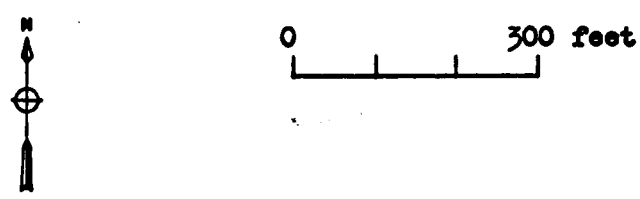

Figure 10-16. Map of the Shauntie magnetic grid area showing only the center point of each magnetic closure.

and can probably be considered geologically significant. 50% of the "large" closures within the trend zone are positive, 50% are negative, while outside the trend zone, 80% are positive. 55% of the "small" anomalies in the trend zone are positive, but outside the trend zone, 86% are positive. Within the trend zone there are thus approximately equal numbers of positive and negative anomalies of both sizes, while outside the trend zone most of the anomalies are positive. This is interpreted as further evidence that anomalies within the trend zone represent a particular type of causative structure, and in particular a structure which would generate equal numbers of positive and negative closures.

The trend of magnetic anomalies is interpreted as representing magnetite mineralization in the southeastern contact zone of the Shauntie intrusive body. The intrusive-limestone contact shown on Figure 10-12 in the area of the Shauntie grid is drawn accordingly. Note that the northern part of the anomaly trend coincides with the probable extension of the contact into the area of the Shauntie grid.

The zone of magnetite mineralization is up to 400 feet wide, which could indicate a nearly horizontal contact zone. The many scattered anomalies indicate a very irregular magnetite distribution, which could reflect the initial distribution of magnetite, as well as erosional dissection of the nearly horizontal mineralized zone.

The contact is presently covered by alluvium. Two parameters of the magnetic anomalies of the contact zone are sensitive to depth of burial. They are the total amplitude of the anomaly, and the horizontal separation of the positive and negative closures (a measure of

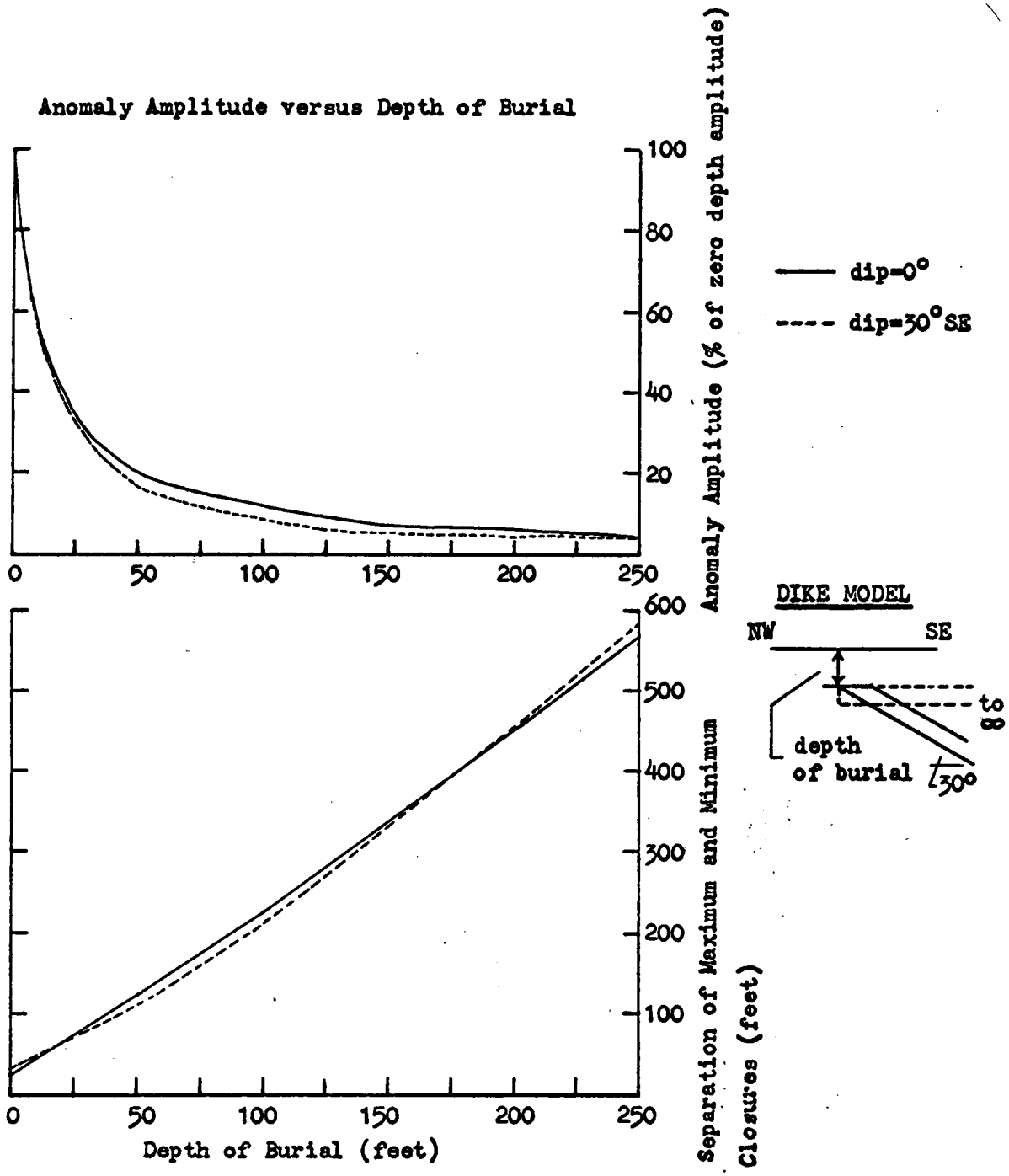

Figure 10-17. Magnetic anomaly variations as a function of depth of burial for a dike. Dike had a strike of N40°E and was 16 feet thick.

the anomaly width). Figure 10-17 shows the dependence of these two parameters upon depth of burial, as computed for a buried, two-dimensional, infinite dike representing a uniform contact zone.

The decrease of anomaly amplitude with depth of burial is not a useful parameter for determining the thickness of alluvial cover in the area of the Shauntie grid, because the magnetization of the contact zone (and thus the zero depth anomaly amplitude) is unknown. The Beacon Claims data, where the contact zone was exposed at the surface, demonstrates the variability of the magnetite content of the contact zone.

The distance between positive and negative closures is the more promising parameter for depth estimation. Error is involved in the assumption of a uniform dike model, for the source distribution appears irregular, and is difficult to model realistically. Another serious problem, in this instance, is to determine matched pairs of closures. The average separation of closures thought to be from the same source and to represent the contact zone is 80 feet, which indicates a depth of burial, from Figure 10-17, of about 35 feet. It must be emphasized that this is only an estimate of the depth of burial, and is open to question. Another model form, such as a dipole or horizontal bar, could have been used for depth estimation, and would probably have indicated a lesser depth of burial.

If one accepts 35 feet as the approximate thickness of alluvial cover over the nearly horizontal contact zone, Figure 10-17 shows that the amplitude of the anomalies has been attenuated by about a factor of four. Observed anomaly amplitudes in the contact zone, measured from maximum to minimum, attain values of about 240 gammas (Figure 10-15), which would imply anomalies of up to 1000 gammas if the contact were

exposed.

The area to the north and west of the contact zone, Figure 10-15, is largely devoid of magnetic relief. Southeast of the contact there is a trend toward higher magnetic values, and a symmetrical, positive anomaly which has an amplitude of 360 gammas and a diameter of about 350 feet. The symmetry of this anomaly is not consistent with tabular, contact mineralization, although it is felt that a source related to the contact zone is most likely. The known chimney-type ore bodies in the Star Range have no magnetic expression. The Shauntie intrusive body appears to have very low magnetization, and no evidence of volcanics was found in the area of the anomaly. The approximate depth of burial of the anomaly source, based on a vertical-prism model half the width of the anomaly, is 40 feet.

Summary of Section X - Ground Magnetic Data

Vertical magnetic field intensity surveys were carried out in four areas of the Star Range, Beaver County, Utah:

1) Milford Flat. Eight magnetic profiles were obtained over the Milford Flat intrusive body, in an effort to define the intrusive structure under the alluvium. Two-dimensional models whose computed magnetic fields resemble the observed data are developed, and a structural contour map on the surface of the intrusive is presented (Figure 10-5). The abrupt termination of the structure to the northwest is interpreted as resulting from post-intrusive faulting, while the gradually increasing depth of burial to the east could represent either

an erosional surface, now covered by alluvium, or the original intrusive configuration.

2) Wild Bill Mine Vicinity. Magnetic data on a grid were obtained in the vicinity of the Wild Bill mine. No extensive zones of contact mineralization are represented by the magnetic data. The intrusive body exposed west of the Wild Bill mine strikes generally north-south across the survey area. Its surface dips sharply to the east. An anomaly in the south-central portion of the magnetic grid is attributed to an upward protrusion of the local quartz monzonite body.

3) Beacon Claims Area. Magnetic data were obtained along the southeastern contact zone of the Shauntie intrusive body. The portion of the contact zone covered by the magnetic data has four areas of appreciable magnetite content, with thickness of magnetite mineralization ranging from eight to twenty-five feet.

4) Exploration South and West of the Shauntie Intrusive. Gridded magnetic data south of the exposed Shauntie intrusive are interpreted as reflecting the southeastern contact zone of the intrusive, extending in a southwesterly direction across the survey area. The contact zone is nearly horizontal, and buried under about 35 feet of alluvium. An anomaly in the southeastern portion of the magnetic grid is of uncertain origin, but is most likely associated with the contact zone.

XI. GENERAL SUMMARY

Sections VI through IX of the thesis are concerned with the interpretation of regional potential field data, while Section X deals with local magnetic data scaled in tens of feet rather than miles. The general scheme of interpretation is the same in both cases, however, for the quantitative treatment of the data is carried out using the grid or data interval as the basic unit of length.

To present the potential field data in a form more readily associated with geologic causative structures, the observed data are separated into regional and residual components by the method of running averaging. Such a separation, by any method, must be based on subjective judgement, but by interpreting both the regional and residual maps to obtain a complete geologic model, the problems of non-uniqueness inherent in the regional-residual separation are avoided.

Interpretation of the potential field data in terms of causative geologic structures is aided and substantiated by machine computation of the gravity and magnetic fields generated by models of the proposed causative structures. Modeling of complex two and three-dimensional structures, subject to the controls of the measured potential field data, known geological data, and assumptions imposed by the interpreter, is shown to be both feasible and useful. Such modeling demonstrates the validity of a proposed model and establishes in a quantitative manner limits for the models' physical parameters.

Intrusive rocks exert a major influence on the potential field

data of the thesis area. The aeromagnetic data are explained entirely in terms of magnetic intrusive structures, and a model is developed for the configuration of the pluton underlying the area. The computed gravity effect of the pluton model, assuming a positive density contrast with the rocks in which the pluton is intruded, is shown to be present in the observed gravity data. The ground-magnetic data, in the Star Range, are explained in terms of the near-surface configuration of the regional pluton and by magnetite mineralization in the zone of contact between the intruded and intrusive rocks.

Local data over magnetic intrusive structures are irregular and demonstrate the heterogeneity of magnetite distribution in intrusive rocks as measured over distances of 500 feet or less. The aeromagnetic data, in which higher frequency magnetic components are not present because of the distance between sources and sensor, show that regionally the magnetization of the intrusive rock can be assumed homogeneous. This is one characteristic difference between the regional and local magnetic data from this area. Another is that on a regional scale plutons are magnetically detectable only on the basis of the susceptibility contrast of the intrusive rock, while on a local scale the mineralization of the contact zone can also serve to magnetically define the intrusive configuration.

The regional gravity and magnetic data are explained using models of very simple geometry, which provide insight into the regional geology but which could differ significantly from the actual configuration of the causative structures. The gravity or magnetic expression of mineralization or related processes are not recognized on the regional

data, and such effects, if present, are presumably within the error limits of model reproduction of observed data. The local data permit the resolution of causative structures to an accuracy measurable in tens of feet, and can provide specific information on geologic features such as faults, depth of alluvium, and magnetite mineralization, which are of importance to detailed geologic studies.

The computer operations employed in this thesis saved hundreds of hours of tedious (and error-prone) manual computations. Of course, interpretation of geophysical data is and must be done by the mind of the geophysicist, not a computer. Economic trends in the United States, however, seem to point to a continued increase in the cost of labor with respect to capital investment, and together with an apparently chronic shortage of trained personnel, and a proliferation of data, would appear to justify continued and increased application of the computer to geophysical problems.

APPENDIX I -- PSEUDO-GRAVITY ANOMALIES

If U represents the gravitational potential of a body, and V the magnetic potential, the two quantities can be related through Poisson's relationship (Grant and West, 1965):

$$V = (m/\gamma\sigma)\,\frac{\partial U}{\partial \vec{a}} \qquad \text{(A-1)}$$

where m is the magnitude of the magnetization vector of the body and $\vec{a}$ its direction, σ its density, and γ the gravitational constant. With the assumption

$$(m/\gamma\sigma) = \text{constant} = 1 \qquad \text{(A-2)}$$

Baranov (1957) obtains from Poisson's relationship the expression

$$g(o) = -\frac{1}{2\pi}\int_{\theta=0}^{2\pi}\int_{r=0}^{\infty} T(r,\theta)\Omega(\theta)\,dr\,d\theta \qquad \text{(A-3)}$$

where g(o) is the vertical gravitational attraction at the origin, T the total magnetic field at the point defined by the polar coordinates r and θ, and

$$\Omega(\theta) = ((\lambda^2 - \mu^2) + \lambda^3\cos\theta)/(1 + \lambda\cos\theta)^2 \qquad \text{(A-4)}$$

where $\mu = \sin I$, $\lambda = \cos I$ and I is the inclination of the earth's magnetic field.

Equation A-3 relates the total magnetic field induced in a body by the earth's field to the vertical gravitational acceleration of that body. Knowing the magnetic field, the corresponding

gravitational field can be computed.

Equation A-3 can be regarded as a convolution integral, with $\Omega(\theta)$ corresponding to the filter operator in the space domain. In cartesion coordinates $\Omega(\theta)$ is given by the expression

$$\Omega(x,y) = \frac{\sqrt{x^2+y^2}\,(\lambda^2-\mu^2) + \lambda^3 x}{(\sqrt{x^2+y^2} + \lambda x)^2} \qquad \text{(A-5)}$$

where +x is in the direction of magnetic north. Using the computer and gridded magnetic data, g(o) is evaluated using the expression

$$g(o) = \sum_{i=-N}^{N} \sum_{j=-M}^{M} T(x_i,y_j)\Omega(x_i,y_j) \qquad \text{(A-6)}$$

where N and M represent the size of the pseudo-gravity grid operator $\Omega(x_i,y_j)$.

The pseudo-gravity grid operator must be large enough so that its edge coefficients are small, and at the same time must be considerably smaller than the data set if the method is to be of practical value. A pseudo-gravity coefficient set of 20 by 20 points was found to be the smallest which gave acceptable results.

The 20 by 20 pseudo-gravity coefficient set is shown in Table A-1. Magnetic north is toward the top of the page. The coefficient set is not normalized in any way. Note that in an east-west direction the 20 columns of coefficients are symmetric about the line y = 0, but in a north-south direction, the asymmetry of the coefficient set was such that only four rows of coefficients were used north of the line x = 0 and 16 rows were retained south of this line. The grid

	1	2	3	4	5	6	7	8	9	10	11	12	13	14	15	16	17	18	19	20
1	0.04	0.05	0.05	0.05	0.06	0.06	0.07	0.07	0.07	0.07	0.07	0.07	0.07	0.07	0.06	0.06	0.05	0.05	0.05	0.04
2	0.05	0.05	0.06	0.06	0.07	0.08	0.08	0.09	0.10	0.10	0.10	0.10	0.09	0.08	0.08	0.07	0.06	0.06	0.05	0.05
3	0.05	0.06	0.07	0.07	0.08	0.10	0.11	0.13	0.15	0.17	0.17	0.15	0.13	0.11	0.10	0.08	0.07	0.07	0.06	0.05
4	0.06	0.07	0.08	0.09	0.10	0.12	0.15	0.20	0.29	0.46	0.46	0.29	0.20	0.15	0.12	0.10	0.09	0.08	0.07	0.06
5	0.07	0.08	0.09	0.10	0.12	0.15	0.20	0.30	0.55	2.01	2.01	0.55	0.30	0.20	0.15	0.12	0.10	0.09	0.08	0.07
6	0.08	0.09	0.10	0.12	0.14	0.18	0.25	0.38	0.67	1.29	1.29	0.67	0.38	0.25	0.18	0.14	0.12	0.10	0.09	0.08
7	0.08	0.09	0.11	0.13	0.16	0.21	0.28	0.40	0.61	0.84	0.84	0.61	0.40	0.28	0.21	0.16	0.13	0.11	0.09	0.08
8	0.09	0.10	0.12	0.14	0.17	0.22	0.29	0.38	0.51	0.62	0.62	0.51	0.38	0.29	0.22	0.17	0.14	0.12	0.10	0.09
9	0.09	0.11	0.13	0.15	0.18	0.22	0.28	0.35	0.43	0.49	0.49	0.43	0.35	0.28	0.22	0.18	0.15	0.13	0.11	0.09
10	0.10	0.11	0.13	0.15	0.18	0.22	0.27	0.32	0.37	0.40	0.40	0.37	0.32	0.27	0.22	0.18	0.15	0.13	0.11	0.10
11	0.10	0.12	0.13	0.15	0.18	0.21	0.25	0.29	0.32	0.34	0.34	0.32	0.29	0.25	0.21	0.18	0.15	0.13	0.12	0.10
12	0.10	0.12	0.13	0.15	0.18	0.20	0.23	0.26	0.28	0.29	0.29	0.28	0.26	0.23	0.20	0.18	0.15	0.13	0.12	0.10
13	0.11	0.12	0.13	0.15	0.17	0.19	0.21	0.23	0.25	0.26	0.26	0.25	0.23	0.21	0.19	0.17	0.15	0.13	0.12	0.11
14	0.11	0.12	0.13	0.15	0.16	0.18	0.20	0.21	0.23	0.23	0.23	0.23	0.21	0.20	0.18	0.16	0.15	0.13	0.12	0.11
15	0.11	0.12	0.13	0.14	0.16	0.17	0.18	0.20	0.21	0.21	0.21	0.21	0.20	0.18	0.17	0.16	0.14	0.13	0.12	0.11
16	0.10	0.11	0.12	0.14	0.15	0.16	0.17	0.18	0.19	0.19	0.19	0.19	0.18	0.17	0.16	0.15	0.14	0.12	0.11	0.10
17	0.10	0.11	0.12	0.13	0.14	0.15	0.16	0.17	0.17	0.18	0.18	0.17	0.17	0.16	0.15	0.14	0.13	0.12	0.11	0.10
18	0.10	0.11	0.12	0.13	0.13	0.14	0.15	0.16	0.16	0.16	0.16	0.16	0.16	0.15	0.14	0.13	0.13	0.12	0.11	0.10
19	0.10	0.11	0.11	0.12	0.13	0.14	0.14	0.15	0.15	0.15	0.15	0.15	0.15	0.14	0.14	0.13	0.12	0.11	0.11	0.10
20	0.10	0.10	0.11	0.12	0.12	0.13	0.13	0.14	0.14	0.14	0.14	0.14	0.14	0.13	0.13	0.12	0.12	0.11	0.10	0.10

TABLE A-1. COEFFICIENTS FOR PSEUDO-GRAVITY GRID OPERATOR.

operator is intended to produce symmetric gravity anomalies from asymmetric magnetic anomalies, and so must itself be asymmetric along a north-south line.

Baranov's stated purpose was to eliminate magnetic anomaly distortion due to the earth's oblique inducing field by locating anomalies on the vertical of the causitive bodies, and by presenting magnetic anomalies in the simpler shapes of gravity anomalies. The generation of absolute gravity data from observed magnetic data, however, is valid only if two conditions are satisfied:

1) The direction of magnetization parallels the present earth's field.
2) The magnetic susceptibility of the rocks is linearly proportional to the rock density throughout the entire map area.

Assumption (1) was made in solving the differential equation A-1. Assumption (2) results from setting the quantity $(m/\gamma\sigma)$ equal to a constant, for the magnitude of the magnetization vector $\vec{m}$ is directly proportional to the magnetic susceptibility of the rock. Since the quantity $(m/\gamma\sigma)$ is arbitrarily set equal to one, the gravity values given by equation A-6 will not be of the correct amplitude and must be normalized by a multiplying factor which is dependent upon the physical parameters of rock density and susceptibility. In addition, the observed magnetic data $T(x_i,y_j)$ is in practice usually arbitrarily adjusted relative to some base value, so the computed pseudo-gravity values will in general have to be adjusted to the proper regional base value also.

To summarize, the method serves Baranov's original purposes well, if a sufficiently large coefficient set is used, but the computation of absolute gravity data using the method of pseudo-gravity must be undertaken with caution, for the necessary constraints are severe.

APPENDIX II. COMPUTATION OF GRAVITY FIELD OF A THREE-DIMENSIONAL BODY

Reference: Talwani and Ewing, 1960.

Consider (in plan view) a horizontal, polygonal lamina with vertical sides, thickness Δz, and depth to midpoint z:

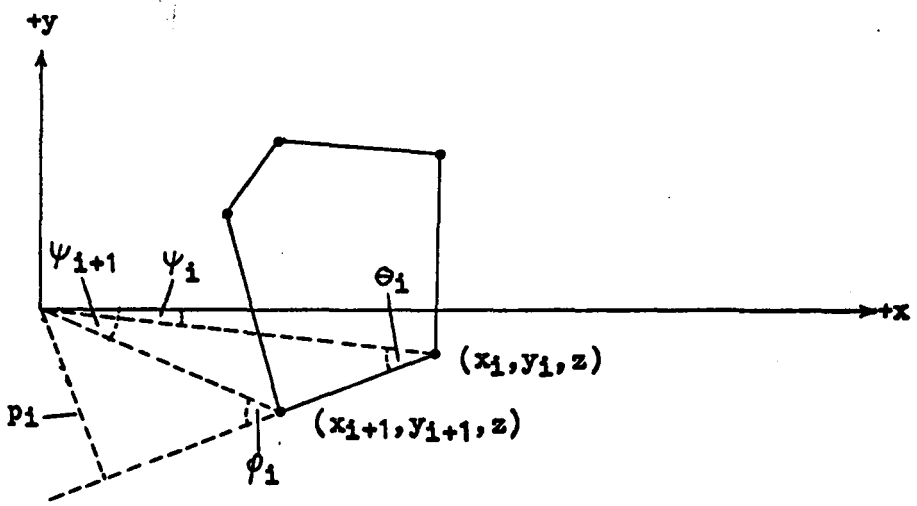

The vertical component of gravitational attraction, at the origin, due to the lamina is given by

$$V = \Delta z G \rho \sum_i (\psi_{i+1} - \psi_i - \arcsin (z\cos\theta_i/(p_i^2 + z^2)^{\frac{1}{2}}) + \arcsin (z\cos\phi_i/(p_i^2 + z^2)^{\frac{1}{2}})) \qquad \text{(II-1)}$$

where G is the universal constant of gravitation and ρ the volume density of the body.

The following computer program computes V on a grid using this formula. The complete three-dimensional model consists of an arbitrary number of horizontal laminas, whose vertical gravity effects are added linearly to obtain the gravitational field of the total structure.

```
C       MAIN TO COMPUTE GRAVITY OVER A 3-D MODEL
C       BODIES MUST BE VERTICALLY SIDED
C       BODY DIMENSIONS ARE IN UNITS LIKE THE MAGNETIC MODELS
C       IMAX, JMAX=MAXIMUM VALUES OF THE COMPUTED GRID
C       GZ=SET OF ANSWERS---VERTICAL GRAVITY IN MILLIGALS
C       NP=NO. OF PLATES IN MODEL
C       SCLE=NO. OF FEET IN 1 GRID UNIT
C       RO=DENSITY OF MODEL
C       Z1,Z2=UPPER AND LOWER DEPTHS OF BURIAL, IN GRID UNITS
C       NC=NO. OF CORNERS FOR A GIVEN PLATE
C       XC,YC=COORDINATES OF EACH CORNER, READ IN CLOCKWISE,
C       MEASURED IN UNITS, WITH ORIGIN IN LOWER LEFT CORNER,
C       (IMAX,0), AND +X EXTENDING TO THE RIGHT, +Y GOING UP
C       X,Y=COORDINATES OF CORNERS RELATIVE TO POINT OF
C       COMPUTATION.
C       ZPNT=SET OF SURFACE ELEVATIONS
        DIMENSION ITLE(60),ISYMB(60),P(50),W(50),F(50),AM(50),
       1R(50),RIII(50),X(50),Y(50),XC(50),YC(50)
        DIMENSION GZ(36,28)
      1 FORMAT(60A1)
      2 FORMAT(3I10,F10.1)
      3 FORMAT(F5.2,2F10.2,I5)
      4 FORMAT(2F7.2)
      5 FORMAT(/// 20X,60A1)
      6 FORMAT(49HO       IMAX       JMAX      NO. OF PLATES
       1  SCALE              )
      7 FORMAT(3I10,F15.2)
      8 FORMAT(//// 10X,27H DATA FOLLOWS FOR PLATE NO. ,I2)
      9 FORMAT(51HO  DENSITY    Z1    Z2    NO. OF CORNERS )
     10 FORMAT(3F10.2,I15)
     11 FORMAT(45HO CORNER COORDINATES      X       Y    )
     12 FORMAT(F29.2,F10.2)
   9999 CONTINUE
C*****
C       INSERT TO READ ELEVATIONS OF COMPUTATION POINTS
C       THIS INSERT PERMITS COMPUTATION OF GRAVITY VALUES ON
C       THE GROUND SURFACE, RATHER THAN ON A PLANE
     20 FORMAT(13F6.0)
        DIMENSION ZPNT(18,14),SS(18,14)
        DO600 I=1,18
    600 READ20,(ZPNT(I,J), J=1,14)
        DO601 I=1,18
        DO601 J=1,14
    601 ZPNT(I,J)=(9000.-ZPNT(I,J))/5280.
C       END OF INSERT
C*****
        GMA=6.67*.00000001
        READ1,ITLE
        READ1,ISYMB
        READ2,IMAX,JMAX,NP,SCLE
```

```
      PRINT5,ITLE
      PRINT6
      PRINT7,IMAX,JMAX,NP,SCLE
      DO100 I=1,IMAX
      DO100 J=1,JMAX
  100 GZ(I,J)=0.
      DO1001 IPLT=1,NP
      READ3,RO,Z1,Z2,NC
      READ4,(XO(I),YO(I), I=1,NC)
      XO(NC+1)=XO(1)
      YO(NC+1)=YO(1)
      DZ=(Z2-Z1)*SCLE*12.*2.54001
      Z=(Z1+Z2)/2.
      ZZZ=Z
      DO2001 II=1,IMAX
      DO2001 JJ=1,JMAX
C*****
C     INSERT TO USE WHEN COMPUTING ON SURFACE
C     WORKS AS LONG AS POINT IS STILL ABOVE ALL MODELS
      Z=ZZZ-ZPNT(II,JJ)
C     END OF INSERT
C*****
      XGRID=JJ-1
      YGRID=IMAX-II
      GTEMP=0.
      DO3001 I=1,NC
      X(I)=XO(I)-XGRID
      Y(I)=YO(I)-YGRID
      X(I+1)=XO(I+1)-XGRID
      Y(I+1)=YO(I+1)-YGRID
      R(I)=SQRT(X(I)*X(I)+Y(I)*Y(I))
      R(I+1)=SQRT(X(I+1)*X(I+1)+Y(I+1)*Y(I+1))
      T1=(X(I)-X(I+1))*(X(I)-X(I+1))
      T2=(Y(I)-Y(I+1))*(Y(I)-Y(I+1))
      RIII(I)=SQRT(T1+T2)
      A1=(Y(I)-Y(I+1))*X(I)/RIII(I)
      A2=(X(I)-X(I+1))*Y(I)/RIII(I)
      P(I)=A1-A2
      S=1.
      IF((P(I)) .LT.0.) S=-1.
      IF((R(I)) .EQ. 0.) GO TO 200
      RATXR=X(I)/R(I)
      RATYR=Y(I)/R(I)
      GO TO 300
  200 RATXR=0.
      RATYR=0.
      Q(I)=RATXR*(X(I)-X(I+1))/RIII(I)+RATYR*Y(I)-Y(I+1))/
 3001RIII(I)
      IF((R(I+1)) .EQ. 0.) GO TO 201
      RATXR1=X(I+1)/R(I+1)
```

```
      RATYR1=Y(I+1)/R(I+1)
      GO TO 301
  201 RATXR1=0.
      RATYR1=0.
      F(I)=RATXR1*(X(I)-X(I+1))/RIII(I)+RATYR1*(Y(I)-Y(I+1))/
  301 RIII(I)
      AM(I)=RATYR*RATXR1-RATYR1*RATXR
      W=1.
      IF((AM(I)) .LT. 0.) W=-1.
      AS1=ARSIN((Z*Q(I)*S)/(SQRT(P(I)*P(I)+Z*Z)))
      AS2=ARSIN((Z*F(I)*S)/(SQRT(P(I)*P(I)+Z*Z)))
      AC1=W*ARCOS(RATXR*RATXR1+RATYR*RATYR1)
 3001 GTEMP=GTEMP+GMA*RO*(AC1-AS1+AS2)*DZ*1000.
 2001 GZ(II,JJ)=GZ(II,JJ)+GTEMP
      PRINT8,IPLT
      PRINT9
      PRINT10, RO,Z1,Z2,NC
      PRINT11
      PRINT12,(XO(I),YO(I), I=1,NC)
 1001 CONTINUE
C***** PUT OUTPUT STATEMENTS HERE
C*****
      GO TO 9999
C     DATA CARDS NEEDED
C     WITH INSERT, NEED SURFACE ELEVATIONS AT POINTS OF
C     COMPUTATION.  IN FEET ABOVE SEA LEVEL
C     1--ITLE
C     2--ISYMB
C     3--IMAX,JMAX,NP,SCLE  (3I10,F10.1)
C     4--RO,Z1,Z2,NC  (F5.2,2F10.2,I5)
C     5--XO(I),YO(I)  (2F7.2)  ( A CARD FOR EACH CORNER)
C     REPEAT 4 AND 5 FOR EACH PLATE
C     REPEAT THE WHOLE THING FOR EACH COMPLETE CASE
C
 9998 STOP
      END
```

APPENDIX III. COMPUTATION OF GRAVITY FIELD OF A TWO-DIMENSIONAL BODY

Reference: Talwani, 1959.

Consider a two-dimensional body which is polygonal in section:

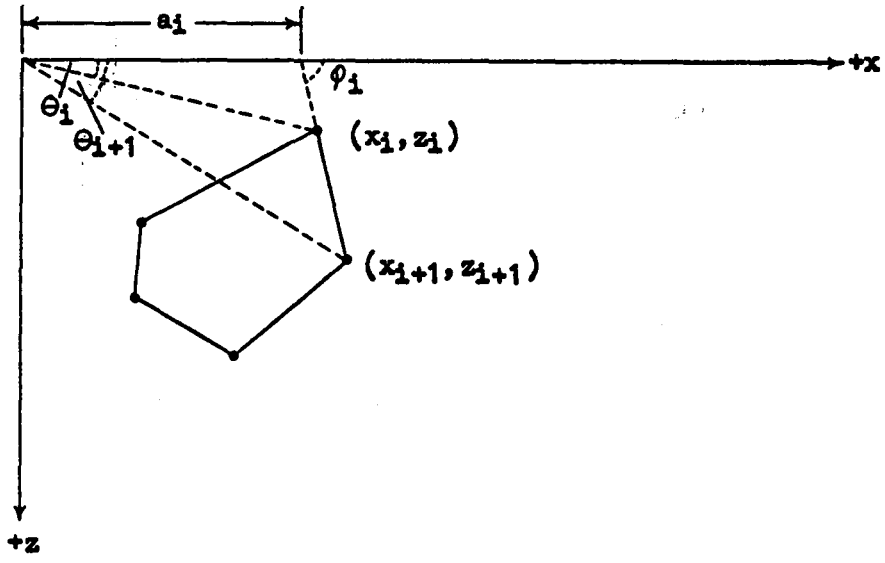

The vertical component of gravitational attraction, at the origin, due to the polygon is given by

$$V = 2G\rho \sum_i z_i \qquad \text{(III-1)}$$

where G is the universal constant of gravitation, ρ the volume density of the body, and

$$z_i = a_i \sin\phi_i \cos\phi_i \,(\theta_i - \theta_{i+1} + \tan\phi_i \ln((\cos\theta_i (\tan\theta_i - \tan\phi_i))/((\cos\theta_{i+1} (\tan\theta_{i+1} - \tan\phi_i))) \qquad \text{(III-2)}$$

The following computer program computes V (VGRAV) at specified intervals along a profile using these formulas. The complete two-dimensional model consists of an arbitrary number of polygonal bodies, whose vertical gravity effects are added linearly to obtain the gravitational field of the total structure. The program is written so that the point Z=0 can be made to coincide with the topographic surface, giving one the option of computing the gravity effect of a model on the ground surface, rather than a straight line.

```
C      MAIN TO COMPUTE VERTICAL GRAVITY OVER 2-D MODEL.
C      GRAVITY IS COMPUTED ALONG A PROFILE PERPENDICULAR TO
C      MODEL.
C      COMPLETE MODEL CONTAINS NBDYS INDIVIDUAL 2-D MODELS.
C      ITLE=TITLE OF THE PROBLEM
C      NBPTS=NO. OF CORNERS FOR A GIVEN 2-D MODEL.
C      RO=DENSITY OR DENSITY CONTRAST OF BODY
C      TBASE=VALUE TO BE ASSIGNED TO STATION(1), MILLIGALS
C      ISMIN, ISMAX=LIMITS OF PROFILE TO BE COMPUTED, IN LINES
C      INTR=INTERVAL,IN LINES, BETWEEN COMPUTED POINTS.
C      GRAVITY CAN BE COMPUTED ON GROUND SURFACE OR ON A PLANE
C      IF IOPTN=1, DATA LINE IS STRAIGHT AND BODY COORDINATES
C      ARE IN LINES OF COMPUTER PRINTOUT.
C      IF IOPTN=2, DATA LINE IS ALONG ACTUAL GROUND SURFACE,
C      AND ELEVATIONS OF THE POINTS OF COMPUTATION MUST BE READ
C      IN.  IN THIS CASE, ELEVATIONS AND BODY POINTS ARE IN
C      CARRIAGE LINES.
C      6 LINES=1 MILE
C      XX,ZZ=COORDINATES OF BODY, READ IN CLOCKWISE
C      BODY POINTS AND STATION LOCATIONS ARE BOTH MEASURED
C      FROM SAME ORIGIN.
C      X POSITIVE TOWARDS THE RIGHT      Z POSITIVE DOWNWARD
       DIMENSION VGRAV(999),ITLE(60),SPCES(130),DTAPNT(1),
      1FINANS(999),ELEV(999),XX(99),ZZ(99)(DIST(999),XREL(99),
      2ZREL(99)
     1 FORMAT(80A1)
     2 FORMAT(A1)
     3 FORMAT(5I3,F5.1)
     4 FORMAT(2F10.2)
     5 FORMAT(F4.2,I6)
     6 FORMAT(10F8.2)
     7 FORMAT(60A1)
     8 FORMAT(////30X,60A1)
     9 FORMAT(70HO  INTERVAL   OPTION   ISMIN   ISMAX   NO.
      1OF STATIONS          )
    10 FORMAT(5I10)
    11 FORMAT(30HO OPTION=1--FLAT DATA PLANE              )
    12 FORMAT(45HO OPTION=2--DATA PLANE FOLLOWS TOPOGRAPHY  )
    13 FORMAT(35HO STATION NO.   ELEVATION (LINES)     )
    14 FORMAT(I10,F10.2)
    15 FORMAT(40HO ASSUMED DENSITY   NO. OF BODY POINTS  )
    16 FORMAT(F12.2,I16)
    17 FORMAT(52HO VALUE OF BODY POINTS---NO.     X     Z    )
    18 FORMAT(I29,2F10.2)
    19 FORMAT(44HO FINAL ANSWERS---STATION NO.   GRAVITY    )
    20 FORMAT(I25,F15.2)
    21 FORMAT(1H1,30X,60A1)
  9999 CONTINUE
       READ3,INTR,IOPTN,ISMIN,ISMAX,NBDYS,TBASE
       READ7, ITLE
```

```
      NSTAT=((ISMAX-ISMIN)/INTR)+1
      DO601 I=1,NSTAT
  601 FINANS(I)=0.
      IF(IOPTN.EQ.2) READ6,(ELEV(I), I=1,NSTAT)
      DO600 IJK=1,NBDYS
      IF(IOPTN .EQ. 2) GO TO 100
      DO101 I=1,NSTAT
  101 ELEV(I)=0.
      READ5,RO,NBPTS
      DO110 I=1,NBPTS
  110 READ4,XX(I),ZZ(I)
      GO TO 200
  100 READ5,RO,NBPTS
      DO121 I=1,NBPTS
  121 READ4,XX(I),ZZ(I)
C     ALL PARAMETERS ARE IN CARRIAGE LINES.
C     6 LINES=1 MILE.  1 LINE=880 FEET.
  200 XX(NBPTS+1)=XX(1)
      ZZ(NBPTS+1)=ZZ(1)
      PRINT8, ITLE
      PRINT9
      PRINT10,INTR,IOPTN,ISMIN,ISMAX,NSTAT
      PRINT11
      PRINT12
      IF(IOPTN .EQ. 1) GO TO 201
      PRINT13
      PRINT14,(I,ELEV(I), I=1,NSTAT)
  201 PRINT15
      PRINT16,RO,NBPTS
      PRINT17
      PRINT18,(I,XX(I),ZZ(I), I=1,NBPTS)
      DO202 I=1,NSTAT
  202 DIST(I)=ISMIN+(I-1)*INTR
      DO500 IS=1,NSTAT
      NNNN=NBPTS+1
      DO301 I=1,NNNN
      XREL(I)=XX(I)-DIST(IS)
      IF(IOPTN .EQ. 1) ZREL(I)=ZZ(I)-ELEV(IS)
      IF(IOPTN .EQ. 2) ZREL(I)=ELEV(IS)-ZZ(I)
      ZREL(I)=ABS(ZREL(I))
  301 CONTINUE
      ZEE=0.
      DO501 IB=1,NBPTS
C     VGRAV(I)=SET OF ANSWERS--VERTICAL GRAVITY AT EACH POINT
      IF((XREL(IB)) .EQ. (ZREL(IB))) GO TO 400
      IF((XREL(IB+1)) .EQ. (ZREL(IB+1))) GO TO 400
      IF((XREL(IB)) .EQ. 0. .AND. (XREL(IB+1)) .EQ. 0.)
     1GO TO 400
      IF((XREL(IB)) .EQ. 0.) GO TO 410
      IF((XREL(IB+1)) .EQ. 0.) GO TO 420
```

```
      THETA1=ATAN2(ZREL(IB),XREL(IB))
      THETA2=ATAN2(ZREL(IB+1),XREL(IB+1))
      IF(THETA1 .EQ. THETA2) GO TO 400
      IF((XREL(IB)) .EQ. (XREL(IB+1))) GO TO 430
      IF((ZREL(IB)) .EQ. (ZREL(IB+1))) GO TO 440
      A=XREL(IB+1)+ZREL(IB+1)*(XREL(IB+1)-XREL(IB))/(ZREL(IB)
     1-ZREL(IB+1))
      ST1=SIN(THETA1)
      CT1=COS(THETA1)
      ST2=SIN(THETA2)
      CT2=COS(THETA2)
      PSII=ATAN2((ZREL(IB+1)-ZREL(IB)),(XREL(IB+1)-XREL(IB)))
      SP=SIN(PSII)
      CP=COS(PSII)
      TP=SP/CP
      TT1=ST1/CT1
      TT2=ST2/CT2
      TRMA=A*SP*CP
      TRMB1=CT1*(TT1-TP)
      TRMB2=CT2*(TT2-TP)
      TRMB=TP*ALOG(TRMB1/TRMB2)
      ZEE=ZEE+TRMA*(THETA1-THETA2+TRMB)
      GO TO 501
  400 GO TO 501
  410 PS=ATAN2((ZREL(IB+1)-ZREL(IB)),(XREL(IB+1)-XREL(IB)))
      THETA2=ATAN2(ZREL(IB+1),XREL(IB+1))
      IF((ZREL(IB)) .EQ. (ZREL(IB+1))) GO TO 450
      A=XREL(IB+1)+ZREL(IB+1)*(XREL(IB+1)-XREL(IB))/(ZREL(IB)
     1-ZREL(IB+1))
      SPS=SIN(PS)
      CPS=COS(PS)
      TPS=SPS/CPS
      ST2=SIN(THETA2)
      CT2=COS(THETA2)
      TT2=ST2/CT2
      TRMA=A*SPS*CPS
      DUM=CT2*(TT2-TPS)
      TRMB=TPS*ALOG(DUM)
      ZEE=ZEE-TRMA*(THETA2-(3.141593/2.)+TRMB)
      GO TO 501
  450 ZEE=ZEE+ZREL(IB)*(THETA2-(3.141593/2.))
      GO TO 501
  420 PS=ATAN2((ZREL(IB+1)-ZREL(IB)),(XREL(IB+1)-XREL(IB)))
      THETA1=ATAN2(ZREL(IB),XREL(IB))
      IF((ZREL(IB)) .EQ. (ZREL(IB+1))) GO TO 460
      A=XREL(IB+1)+ZREL(IB+1)*(XREL(IB+1)-XREL(IB))/(ZREL(IB)
     1-ZREL(IB+1))
      SPS=SIN(PS)
      CPS=COS(PS)
      TPS=SPS/CPS
```

```
      CT1=COS(THETA1)
      ST1=SIN(THETA1)
      TT1=ST1/CT1
      TRMA=A*SPS*CPS
      DUMM=CT1*(TT1-TPS)
      TRMB=TPS*ALOG(DUMM)
      ZEE=ZEE+TRMA*(THETA1-(3.141593/2.)+TRMB)
      GO TO 501
  460 ZEE=ZEE+ZREL(IB)*((3.141593/2.)-THETA1)
      GO TO 501
  430 CT1=COS(THETA1)
      CT2=COS(THETA2)
      ZEE=ZEE+XREL(IB)*ALOG(CT1/CT2)
      GO TO 501
  440 ZEE=ZEE+ZREL(IB)*(THETA2-THETA1)
      GO TO 501
  501 CONTINUE
  500 VGRAV(IS)=2.*RO*ZEE*6.67*.00000001*5280.*12.*2.54001
     1*1000./6.
C     THIS GIVES GRAVITY IN MILLIGALS.
      DO602 I=1,NSTAT
  602 FINANS(I)=FINANS(I)+VGRAV(I)
  600 CONTINUE
      CNSTNT=FINANS(1)-TBASE
      DO550 I=1,NSTAT
  550 FINANS(I)=FINANS(I)-CNSTNT
C****
C     PUT OUTPUT STATEMENTS HERE
C****
C     VGRAV=ANSWER FOR INDIVIDUAL BODY.
C     FINANS=ANSWER FOR COMPLETE MODEL.
      GO TO 9999
C**** DATA CARDS NEEDED
C     1--INT,IOPTN,ISMIN,ISMAX,NBDYS,TBASE   (5I3,F5.1)
C     2--ITLE   (60A1)
C     3--ELEV, IF IOPTN=2   (10F8.2)
C     4--RO,NBPTS     (F4.2,I6)
C     5--XX,ZZ     (2F10.2)
C     CONTINUE 5 FOR ALL BODY POINTS, READ IN CLOCKWISE.
C     REPEAT 4 AND 5 FOR EACH BODY IN THE TOTAL MODEL
C     REPEAT 1 TO 5 FOR EACH COMPLETE MODEL
C*****
  700 STOP
      END
```

APPENDIX IV. COMPUTATION OF MAGNETIC FIELD OF A THREE-DIMENSIONAL BODY

Reference: Talwani, 1965.

Consider (in plan view) a horizontal, polygonal lamina with vertical sides, thickness Δz, and depth to midpoint z:

magnetic north

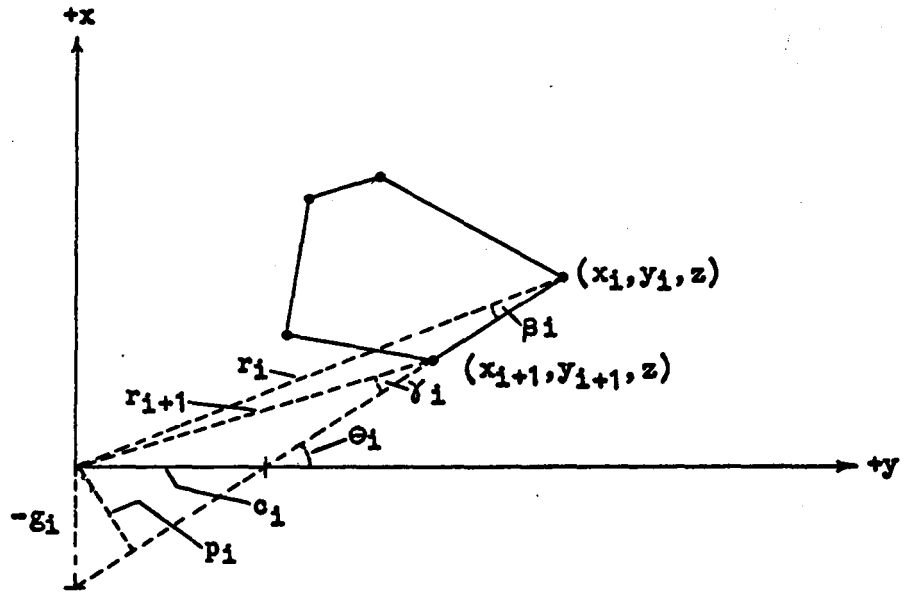

The vertical magnetic field of the lamina at the origin is given by

$$Z = J_x V_3 + J_z V_6 \qquad \text{(IV-1)}$$

and the total magnetic field by

$$T = J_x(V_1 \cos I + V_3 \sin I) + J_z(V_3 \cos I + V_6 \sin I) \qquad \text{(IV-2)}$$

where J_x and J_z are the induced pole strengths in the +x and +z directions, I is the inclination of the earth's main field, and

$$V_1 = -\Delta z \sum_i (\cos^2\theta_i/(z^2 + p_i^2))(((g_i y_{i+1} - z^2\tan\theta_i)/ R_{i+1}) - ((g_i y_i - z^2\tan\theta_i)/R_i)) \qquad \text{(IV-3)}$$

$$V_3 = -\Delta z \sum_i (z\cos^2\theta_i/(z^2 + p_i^2))(((y_{i+1}\sec^2\theta_i + g_i\tan\theta_i)/R_{i+1}) - ((y_i\sec^2\theta_i + g_i\tan\theta_i)/R_i)) \qquad \text{(IV-4)}$$

$$V_6 = -\Delta z \sum_i (p_i/z^2 + p_i^2))((r_{i+1}\cos\gamma_i/R_{i+1}) - (r_i\cos\beta_i/R_i)) \qquad \text{(IV-5)}$$

where $R_i = \sqrt{x_i^2 + y_i^2 + z^2}$ (IV-6)

and $R_{i+1} = \sqrt{x_{i+1}^2 + y_{i+1}^2 + z^2}$

The following computer program computes Z (DELZ) and T (DELT) on a grid using these formulas. The complete three-dimensional model consists of an arbitrary number of horizontal lamina, whose magnetic field components are added linearly to obtain the magnetic field of the total structure. The coordinates of the grid and laminas, read by the computer, are with respect to geographic north, and are converted to a magnetic-north coordinate system by the computer.

```
C      MAIN TO COMPUTE 3-D MAGNETIC ANOMALY.
C      PROGRAM COMPUTES TOTAL AND VERTICAL FIELD ANOMALIES--
C      DELT AND DELZ.
C      NP=NO. OF PLATES IN MODEL
C      SUSC=SUSCEPTIBILITY, K
C      REMANENT MAGNETIZATION NOT INCLUDED
C      IMAX, JMAX=MAXIMUM VALUES OF FIELD POINTS WHERE
C      VALUES ARE TO BE COMPUTED.
C      INTERVAL=1 UNIT
C      +X=MAGNETIC NORTH.
C      FOR STATION LABELING (1,1) IS IN UPPER LEFT CORNER.
C      FJX AND FJZ=INDUCED POLE STRENGTHS
C      X(I),Y(I)=COORDINATES OF CORNERS, READIN CLOCKWISE--
C      ONE PAIR OF COORD. PER CARD.
C      INCLINATION=64 DEGREES.  DECLINATION=16 DEGREES.
C      ITLE=TITLE ASSIGNED TO THE PROBLEM.
C      Z1=DEPTH TO TOP OF PLATE, GRID UNITS.
C      Z2=DEPTH TO BOTTOM OF PLATE, GRID UNITS.
C      NC=NO. OF CORNERS OF THE PLATE.
C      X(I), Y(I) IN GRID UNITS ALSO.
       DIMENSION X(30),Y(30),THETA(30),P(30),G(30),R(30),
      1CSBETA(30),CSGAMA(30),XM(30),YM(30),SR(30),ITLE(60),
      2DELT(26,28),DELZ(26,28),SRI(30)
     1 FORMAT(F10.9,3I3)
     2 FORMAT(60A1)
     3 FORMAT(52H0    SUSC    NP    IMAX    JMAX    )
     4 FORMAT(F10.9,F10.0,3I10)
     5 FORMAT(55H0 PLATE NO.  NC    Z1    Z2    CORNER COORD.  )
     6 FORMAT(2F5.1,I2)
     7 FORMAT(I5,I10,2F10.1)
     8 FORMAT(2F6.1)
     9 FORMAT(I40,2F6.1)
    10 FORMAT(90H0
      1              FINISHED THIS PLATE          )
       READ1,SUSC,NP,IMAX,JMAX
       READ2,ITLE
       PRINT2,ITLE
       PRINT3
       PRINT4,SUSC,TBASE,NP,IMAX,JMAX
       FTOT=54000.
       RINC=64./57.296
       COSINC=COS(RINC)
       SININC=SIN(RINC)
       FJX=SUSC*FTOT*COSINC
       FJZ=SUSC*FTOT*SININC
       PRINT5
       DO101 I=1,IMAX
       DO101 J=1,JMAX
       DELT(I,J)=0.
   101 DELZ(I,J)=0.
```

```
      ANGL=-16./57.296
      COSA=COS(ANGL)
      SINA=SIN(ANGL)
C     NOW START A DO LOOP WHICH HANDLES AN ENTIRE PLATE
      DO201 IP=1,NP
      READ6,Z1,Z2,NC
      PRINT7, IP,NC,Z1,Z2
      DO102 I=1,NC
      READ8,X(I),Y(I)
      XDUM=X(I)
      YDUM=Y(I)
      X(I)=XDUM*COSA-YDUM*SINA
      Y(I)=YDUM*COSA+XDUM*SINA
  102 PRINT9,I,XDUM,YDUM
C     EVERYTHING IS NOW IN FOR THIS PLATE
      DZ=Z2-Z1
      Z=(Z2+Z1)/2.
      X(NC+1)=X(1)
      Y(NC+1)=Y(1)
C     X(I),Y(I)=ORIGINAL, ABSOLUTE CORNER POINTS.
C     XM(I),YM(I)=COORD. RELATIVE TO THE FIELD POINT.
C     ABSOLUTE ORIGIN IS IN LOWER LEFT CORNER OF
C     COMPUTED FIELD--(IMAX,1).
C     XF,YF=COORD. OF FIELD POINT IN THIS ABSOLUTE SYSTEM
C     YF=J-1     XF=IMAX-I
C     THEN   XM(I)=X(I)-XF      YM(I)=Y(I)-YF
C     NOW START DO LOOP WHICH RUNS OVER ALL FIELD POINTS.
      DO250 II=1,IMAX
      DO250 JJ=1,JMAX
      S1=0.
      S3=0.
      S6=0.
      YFDUM=JJ-1
      XFDUM=IMAX-II
      XF=XFDUM*COSA-YFDUM*SINA
      YF=YFDUM*COSA+XFDUM*SINA
C     THIS LOOP RUNS OVER EACH CORNER OF PLATE.
      DO103 I=1,NC
      XM(I)=X(I)-XF
      YM(I)=Y(I)-YF
      XM(I+1)=X(I+1)-XF
      YM(I+1)=Y(I+1)-YF
      SR(I)=SQRT(XM(I)*XM(I)+YM(I)*YM(I))
      SR(I+1)=SQRT(XM(I+1)*XM(I+1)+YM(I+1)*YM(I+1))
      R(I)=SQRT(SR(I)*SR(I)+Z*Z)
      R(I+1)=SQRT(SR(I+1)*SR(I+1)+Z*Z)
      SRI(I)=SQRT((XM(I)-XM(I+1))*(XM(I)-XM(I+1))+(YM(I)-
     1YM(I+1))*(YM(I)-YM(I+1)))
      XX1=(XM(I)-XM(I+1))/SRI(I)
      YY1=(YM(I)-YM(I+1))/SRI(I)
```

```
      P(I)=XX1*YM(I)-YY1*XM(I)
      CSBETA(I)=XX1*XM(I)/SR(I)+YY1*YM(I)/SR(I)
      CSGAMA(I)=XX1*XM(I+1)/SR(I+1)+YY1*YM(I+1)/SR(I+1)
      PRT1=P(I)/(Z*Z+P(I)*P(I))
      PRT2=SR(I+1)*CSGAMA(I)/R(I+1)
      PRT3=SR(I)*CSBETA(I)/R(I)
      S6=S6-PRT1*(PRT2-PRT3)
C     NOW START IN ON S3 AND S1
      IF(YM(I).EQ.YM(I+1)) GO TO 606
      DISX=XM(I+1)-XM(I)
      DISY=YM(I+1)-YM(I)
      THETA(I)=ATAN2(DISX,DISY)
      SNTETA=SIN(THETA(I))
      CSTETA=COS(THETA(I))
      TTETA=SNTETA/CSTETA
      SCTETA=1./CSTETA
      G(I)=XM(I)-YM(I)*TTETA
      AA=CSTETA*CSTETA/(Z*Z+P(I)*P(I))
      BB1=(G(I)*YM(I+1)-Z*Z*TTETA)/R(I+1)
      CC1=(G(I)*YM(I)-Z*Z*TTETA)/R(I)
      S1=S1-AA*(BB1-CC1)
      BB3=(YM(I+1)*SCTETA*SCTETA+G(I)*TTETA)/R(I+1)
      CC3=(YM(I)*SCTETA*SCTETA+G(I)*TTETA)/R(I)
      S3=S3-Z*AA*(BB3-CC3)
      GO TO 608
  606 S1=S1
      S3=S3
  608 CONTINUE
  103 CONTINUE
      V1=S1*DZ
      V3=S3*DZ
      V6=S6*DZ
      DELZ(II,JJ)=DELZ(II,JJ)+(FJX*V3+FJZ*V6)
      TRM1=V1*COSINC+V3*SININC
      TRM2=V3*COSINC+V6*SININC
  250 DELT(II,JJ)=DELT(II,JJ)+FJX*TRM1+FJZ*TRM2
C     NOW HAVE COMPUTED ANOMALY OF FIRST PLATE.  GO TO
C     THE NEXT PLATE.
      PRINT 10
  201 CONTINUE
C     AT THIS POINT HAVE THE TOTAL ANOMALY.
C***** PUT OUTPUT STATEMENTS HERE
C*****
C     DATA CARDS NEEDED
C     1--SUSC,TBASE,NP,IMAX,JMAX  (F10.9,F10.0,3I3)
C     2--ITLE   (60A1)
C     3--Z1,Z2,NC  (2F5.1,I2)
C     4--X(I),Y(I)  (2F6.1)
C     CONTINUE FOR EACH CORNER OF THE PLATE, READING
C     IN CLOCKWISE.
```

```
C     REPEAT CARDS 3 AND 4 FOR EACH PLATE.
C*****
      STOP
      END
```

APPENDIX V. COMPUTATION OF MAGNETIC FIELD OF A TWO-DIMENSIONAL BODY

Reference: Heirtzler, 1962.

Consider a horizontal plate of finite thickness, which extends to $+\infty$ in the X direction:

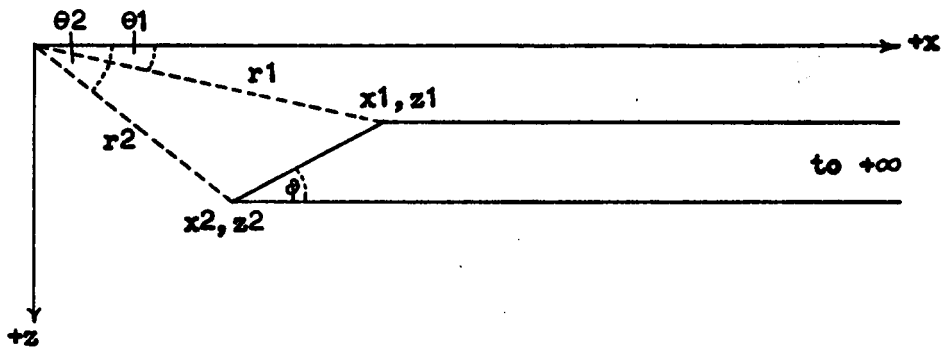

The vertical magnetic field of the plate at the origin is given by

$$V = 2\sin\phi\,(Ix\,((\theta 2-\theta 1)\cos\phi + \sin\phi \ln(r2/r1)) - Iz\,((\theta 2-\theta 1)\sin\phi - \cos\phi \ln(r2/r1))) \qquad (V\text{-}1)$$

and the horizontal magnetic field by

$$H = 2\sin\phi\,(Ix\,((\theta 2-\theta 1)\sin\phi - \cos\phi \ln(r2/r1)) + Iz\,((\theta 2-\theta 1)\cos\phi + \sin\phi \ln(r2/r1))) \qquad (V\text{-}2)$$

where Ix and Iz are the induced pole strengths in the +x and +z directions.

The following computer program computes V, H, and the total magnetic field, F, at specified intervals along a profile, using

these formulas. The complete two-dimensional model consists of an arbitrary number of horizontal plates, whose magnetic field components are added linearly to obtain the magnetic field of the total structure.

```
C      MAIN TO COMPUTE MAGNETIC FIELD OF A 2-D BODY.
C      ANOMALY IS COMPUTED ON A STRAIGHT LINE PERPENDICULAR
C      TO MODEL.   LINE MAY BE INCLINED.
C      NP=NUMBER OF PLATES IN MODEL.
C      SUSC=MAGNETIC SUSCEPTIBILITY, CGS UNITS.
C      TBASE=VALUE TO BE ASSIGNED TO STATION(1), IN GAMMAS.
C      ISMIN, ISMAX=LIMITS OF PROFILE TO BE COMPUTED, IN UNITS
C      OF CARRIAGE LINES.
C      INT=INTERVAL, IN LINES, BETWEEN STATION POINTS.
C      PSTRZ=VERTICAL INDUCED POLE STRENGTH.
C      PSTRX=HORIZONTAL INDUCED POLE STRENGTH.
C      INCLINATION=64 DEGREES, DECLINATION=16 DEGREES.
C      BEARNG=BEARING OF PROFILE W.R.T. MAGNETIC NORTH (DEG)
C      BEARING RANGES FROM 0 TO 90 DEGREES
C      ITLE=TITLE OF THE PROBLEM.
C      H=HORIZONTAL FIELD STRENGTH, GAMMAS.
C      V=VERTICAL FIELD STRENGTH
C      F=TOTAL FIELD STRENGTH.
C      ANGL=DIP OF GROUND SURFACE--DEGREES
C      IF PLATE IS ADDITIVE, SGN=+1.
C      IF PLATE IS NEGATIVE, SGN=-1.
C      +X RUNS TO THE NORTH.
C      PLATES EXTEND TO +INFINITY (NORTH).
C      IF PLATES EXTEND TO -INFINITY, CONVENTION FOR SGN
C      MUST BE REVERSED.
C      SEE SKETCH FOR PSI,Z1,X1,Z2,X2.  X,Z IN UNITS OF LINES.
C****
C      DATA CARDS NEEDED
C      1--TBASE,SUSC,NP,ISMIN,ISMAX,INT,BEARNG
C      FORMAT IS (F10.0,E10.0,4I3,F4.0)
C      2--ANGL (F5.0)
C      3--PSI,Z1,X1,Z2,X2,SGN (6F5.1)
C      REPEAT 3 FOR EACH PLATE IN MODEL.
C      4--ITLE (60A1)
C*****
    1 FORMAT(F10.0,E10.0,4I3,F4.0)
    2 FORMAT(19HO POLE STRENGTH(Z)= ,F10.5,19HO POLE
     1STRENGTH(X)= ,F10.5)
    3 FORMAT(6F5.1)
    4 FORMAT(22HO NUMBER OF STATIONS=  ,I3)
    5 FORMAT(34HOPERTINENT DATA FOR PLATE NUMBER= ,I3)
    6 FORMAT(68HO   PSI    Z1    X1    Z2    X2    SIGN    )
    7 FORMAT(6F10.1)
    8 FORMAT(21HOBEARING OF PROFILE= ,F4.0,10HO DEGREES  )
    9 FORMAT(39HO      ISMIN       ISMAX      INTERVAL          )
   10 FORMAT(3I10)
   11 FORMAT(18HO SUSCEPTIBILITY=  ,F10.6)
   12 FORMAT(35HO STATION NO. 1 ADJUSTED TO EQUAL, F10.0,
     110HO GAMMAS      )
   13 FORMAT(54HO SUMMSRY OF VALUES AT INTERMEDIATE STAGE  )
```

```
   14 FORMAT(21H  HAVE FINISHED PLATE, I3)
   15 FORMAT(125HO STATION NO.  STATION LOC., LINES
     1CONT. OF THIS PLATE, GAMMAS   TOTAL ANOMALY  R1  R2  TH1
     2TH2   )
   16 FORMAT(I10,F20.0, F30.0,F35.0,F20.0,3F5.0)
   17 FORMAT(48HO VALUE SUBTRACTED FROM COMPUTED ANOMALY=
     1,F10.0   )
   18 FORMAT(69HO STATION LOCATION, X(I) VS. AMPLITUDE    )
   19 FORMAT(44HO STATION NUMBER   X   AMP.   )
   20 FORMAT(I10,2F15.0)
   21 FORMAT(60A1)
   22 FORMAT(15HOABOVE WAS FOR ,60A1)
      DIMENSION X(999), V(999), ITLE(60), H(999), F(999)
  202 CONTINUE
      READ1, TBASE, SUSC, NP, ISMIN, ISMAX, INTRVL, BEARNG
      FTOT=54000.
      PSTRZ=SUSC*FTOT*.90
      BRNG=BEARNG/57.296
      COSBRG=COS(BRNG)
      PSTRX=SUSC*FTOT*.44*COS(BRNG)
C**** INSERTION FOR COMPUTING ON DIPPING GROUND SURFACE.
C     INSERTION MODIFIES PSTRX AND PSTRZ, FOR DATA OBSERVED
C     ON A SLOPING SURFACE.
C     ROTATION OF OBSERVATION LINE COUNTER CLOCKWISE
C     REQUIRES A NEGATIVE VALUE OF ANGL.
C     Z POSITIVE DOWNWARD, X POSITIVE FROM LEFT TO RIGHT
   24 FORMAT(F5.0)
      READ24,ANGL
      PRINT2,PSTRZ,PSTRX
      ANGL=ANGL/57.296
      PSTRZ1=PSTRZ
      PSTRX1=PSTRX
      PSTRZ=PSTRZ1*COS(ANGL)-PSTRX1*SIN(ANGL)
      PSTRX=PSTRX1*COS(ANGL)+PSTRZ1*SIN(ANGL)
      PRINT2,PSTRZ,PSTRX
C*****END OF INSERTION
      NSTAT=((ISMAX-ISMIN)/INTRVL)+1
      PRINT4, NSTAT
      PRINT 8, BEARNG
      PRINT 9
      PRINT10, ISMIN, ISMAX, INTRVL
      PRINT11, SUSC
      PRINT12, TBASE
      PRINT 2, PSTRZ, PSTRX
      DO88 I=1,NSTAT
      H(I)=0.
      F(I)=0.
   88 V(I)=0.
C     NOW START A BIG DO LOOP WHICH DOES ONE PLATE COMPLETELY.
C     IP DESIGNATES THE PLATE NUMBER
```

```
C       READ IN ALL DATA PERTINENT TO THE GIVEN PLATE.
        DO99 IP=1,NP
        READ3, PSI, Z1, X1, Z2, X2, SGN
        FAC=-2.
        IF(SGN .EQ. 1.) FAC=2.
        PRINT5, IP
        PRINT6
        PRINT7, PSI, Z1, X1, Z2, X2, SGN
        PSI=PSI/57.296
        COSPSI=COS(PSI)
        SINPSI=SIN(PSI)
        PRINT 13
        PRINT14, IP
        PRINT15
C       NOW RUN THROUGH ALL STATIONS FOR THE GIVEN PLATE.
        DO 89 I=1,NSTAT
        X(I)=ISMIN+(I-1)*INTRVL
        RD1=(X(I)-X1)*(X(I)-X1)+Z1*Z1
        R1=SQRT(RD1)
        RD2=(X(I)-X2)*(X(I)-X2)+Z2*Z2
        R2=SQRT(RD2)
        TD1=(X1-X(I))/R1
        THETA1=ARCOS(TD1)
        TD2=(X2-X(I))/R2
        THETA2=ARCOS(TD2)
        THDEG1=THETA1*57.296
        THDEG2=THETA2*57.296
        RATO=R2/R1
        T1=PSTRX*((THETA2-THETA1)*COSPSI+SINPSI*ALOG(RATO))
        T2=PSTRZ*((THETA2-THETA1)*SINPSI-COSPSI*ALOG(RATO))
        CONTV=FAC*SINPSI*(T1-T2)
        V(I)=V(I)+CONTV
        T1H=PSTRX*((THETA2-THETA1)*SINPSI-COSPSI*ALOG(RATO))
        T2H=PSTRZ*((THETA2-THETA1)*COSPSI+SINPSI*ALOG(RATO))
        CONTH=FAC*SINPSI*(T1H-T2H)
        H(I)=H(I)+CONTH
        CONTF=CONTV*.90+CONTH*COSBRG*.44
        F(I)=F(I)+CONTF
        READ21,ITLE
   89 CONTINUE
   99 CONTINUE
C****
C       PUT OUTPUT STATEMENTS HERE
C       ALSO CAN PUT IN SECTION TO NORMALIZE VALUES TO TBASE.
C****
        GO TO 202
 6789 STOP
        END
```

BIBLIOGRAPHY

Affleck, J., 1963, Magnetic anomaly trend and spacing patterns: Geophysics, v. 28, p. 379.

Allingham, J.W., and Zietz, I., 1962, Geophysical data on the Climax stock, Nevada test site, Nye County, Nevada: Geophysics, v. 28, p. 599.

Armstrong, R.L., 1968, Sevier Orogenic Belt in Nevada and Utah: Geol. Soc. America Bull., v. 79, p. 429.

Baranov, V., 1957, A new method for interpretation of aeromagnetic maps: Pseudo-gravimetric anomalies: Geophysics, v. 22, p. 359.

Billings, M.P., 1954, Structural geology: Englewood Cliffs, Prentice-Hall, 514 p.

Blank, H.R., and Mackin, J.H., 1967, Geologic interpretation of an aeromagnetic survey of the Iron Springs district, Utah: U.S. Geol. Survey Prof. Paper 516-B.

Boardman, L., compiler, 1954, Geologic map index of Utah: U.S. Geol. Survey.

Butler, B.S., 1913, Geology and ore deposits of the San Francisco region, Utah: U.S. Geol. Survey Prof. Paper 80.

Butler, B.S., et.al, 1920, Ore deposits of Utah: U.S. Geol. Survey Prof. Paper 111.

Carlson, J.E., and Mabey, D.R., 1963, Gravity and aeromagnetic investigations of the Ely area, Nevada: U.S. Geol. Survey Geophysical Investigations Map GP-392.

Cohee, G.V., et.al., 1962, Tectonic map of the United States: U.S. Geol. Survey and the Am. Assoc. of Petroleum Geologists.

Cook, K.L., and Berg, J.W., 1961, Regional gravity survey along the central and southern Wasatch front, Utah: U.S. Geol. Survey Prof. Paper 316-E.

Cook, K.L., and Mudgett, P.M., 1966, Regional gravity survey of the Mineral, San Francisco, Beaver, and northern Wah Wah Mountains region, in Beaver and Millard Counties, Utah (abs): Utah Academy Proceedings, v. 43, part 2, p. 62.

Dampney, C.N.G., 1967, The equivalent source technique: 37th Annual International SEG meeting.

Davis, W.M., 1925, The Basin Range problem: Natl. Acad. Sci. Proc., v. 11, p. 387.

Doell, R.R., and Cox, A., 1962, Determination of the magnetic polarity of rock samples in the field: U.S. Geol. Survey Prof. Paper 450-D, p. 105.

Eardley, A.J., 1962, Structural geology of North America: 2nd edition, New York, Harper and Row, 743 p.

Fuller, M.D., 1964, Expression of E-W fractures in magnetic surveys in parts of the U.S.A.: Geophysics, v. 29, p. 602.

Gilbert, G.K., 1874, Progress report of U.S. Geological Surveys west of the 100th meridian for 1872: U.S. Geol. Survey, p. 50.

———1928, Studies of Basin Range structure: U.S. Geol. Survey Prof. Paper 153.

Grant, F.S., and West, G.F., 1965, Interpretation theory in applied geophysics: New York, McGraw-Hill, 583 p.

Haalck, F., 1956, A torsion magnetometer for measuring the vertical component of the earth's magnetic field: Geophysical Prospecting, v. 4, p. 424.

Hamilton, W., and Meyers, W.B., 1967, The nature of batholiths: U.S. Geol. Survey Prof. Paper 554-C.

Hammer, S., 1939, Terrain corrections for gravimeter stations: Geophysics, v. 4, p. 184.

Harris, H.D., 1959, A late Mesozoic positive area in western Utah: Am. Assoc. Petroleum Geologists Bull., v. 43, p. 2636.

Heirtzler, J., et.al., 1962, Magnetic anomalies caused by two-dimensional structures of arbitrary shape: Technical Report No. 6, CUG-62, Lamont Geological Observatory, Columbia University.

Heyl, A.V., 1963, Oxidized zinc deposits of the United States - part 2, Utah: U.S. Geol. Survey Bull. 1135-B.

Hilpert, L.S., and Roberts, R.J., 1964, Economic geology, in Mineral and water resources of Utah: Utah Geol. and Mineralog. Survey Bull. 73, p. 28.

Hobbs, S.W., 1944, Tungsten deposits in Beaver County, Utah: U.S. Geol. Survey Bull. 945-D.

Jaffe, H.W., et.al., 1959, Lead-alpha age determinations of accessory minerals of igneous rocks (1953-1957): U.S. Geol. Survey Bull. 1097-B.

Longwell, C.R., 1945, Low-angle normal faults in the Basin and Range Province: Trans. Amer. Geophy. Union, v. 26, part 1, p. 107.

Mabey, D.R., 1960, Regional gravity survey of part of the Basin and Range Province: U.S. Geol. Survey Prof. Paper 400-B, p. 283.

———1963, Complete Bouguer anomaly map of the Death Valley region, California: U.S. Geol. Survey Geophysical Investigations Map GP-305.

Mabey, D.R., et.al., 1964, Aeromagnetic and generalized geologic map of part of north-central Utah: U.S. Geol. Survey Geophysical Investigations Map GP-422.

Mabey, D.R., and Morris, H.T., 1967, Geologic interpretation of gravity and aeromagnetic maps of Tintic Valley and adjacent areas, Tooele and Juab Counties, Utah: U.S. Geol. Survey Prof. Paper 516-D.

Mack, J.W., 1963, A least-square method of gravity analysis and its applications in the study of sub-surface geology: Ph.D. Thesis, University of Wisconsin.

Mackin, J.H., 1960, Structural significance of Tertiary volcanic rocks in southwestern Utah: Am. Jour. Sci., v. 258, p. 81-131.

———1960a, Eruptive tectonic hypothesis for origin of Basin-Range structure (abs): Geol. Soc. America Bull., v. 71, p. 1921.

Moore, J.G., 1960, Curvature of normal faults in the Basin and Range Province of the western United States: U.S. Geol. Survey Prof. Paper 400B, p. 409.

Nettleton, L.L., 1954, Regionals, residuals, and structures: Geophysics, v. 19, p. 1.

Nolan, T.B., 1943, The Basin and Range Province in Utah, Nevada, and California: U.S. Geol. Survey Prof. Paper 197-D, p. 141.

Roberts, R.J., et.al., 1958, Paleozoic rocks of north-central Nevada: Am. Assoc. Petroleum Geologists Bull., v. 42, p. 2813.

Roberts, R.J., 1960, Paleozoic structure in the Great Basin (abs): Geol. Soc. America Bull., v. 71, p. 1955.

Skeels, D.C., 1947, Ambiguity in gravity interpretation: Geophysics, v. 12, p. 43.

Talwani, M., et.al., 1959, Rapid gravity computations for two-dimensional bodies with application to the Mendocino submarine fracture zone: Jour. Geophys. Research, v. 64, p. 49.

Talwani, M., and Ewing, M., 1960, Rapid computation of gravitational attraction of three-dimensional bodies of arbitrary shape: Geophysics, v. 25, p. 203.

Talwani, M., 1965, Computation with the help of a digital computer of magnetic anomalies caused by bodies of arbitrary shape: Geophysics, v. 30, p. 797.

Townsend, J.W., 1950, Investigation of the Vicksburg lead-zinc mine, Beaver County, Utah: U.S. Bureau of Mines Report of Investigation No. 4642.

———1953, Investigation of lead-zinc deposits at the Harrington-Hickory mine, Beaver County, Utah: U.S. Bureau of Mines Report of Investigation No. 4953.

U.S. Coast and Geodetic Survey, 1955, Total intensity chart of the United States: U.S. Coast and Geodetic Survey Chart 3077f.

U.S. Geological Survey, 1966, Aeromagnetic map of the San Francisco Mountains and vicinity, southwestern Utah: U.S. Geol. Survey Geophysical Investigations Map GP-598.

———1966a, Complete Bouguer gravity anomaly map of the San Francisco Mountains vicinity, Beaver and Millard Counties, Utah: U.S. Geol. Survey, File No. 482G, open file map.

Utah Geol. and Mineralog. Survey, 1963, Geologic map of southwestern Utah (L.F. Hintze, compiler): Utah Geol. and Mineralog. Survey.

———1968, Publications: Utah Geol. and Mineralog. Survey.

Vacquier, V., and Affleck, J., 1941, A computation of the average depth to the bottom of the earth's magnetic crust, based on a statistical study of local magnetic anomalies: Trans. Amer. Geoph. Union, v. 22, Am. Mtg. Pt. 2, p. 446.

Vestine, E.H., et.al., 1947, Description of the earth's main magnetic field and its secular change, 1905-1945: Carnegie Inst. Washington Pub. 578, 532 p.

Wendell, L., 1966, Subroutine CONTUR: University of Utah Computer Center Program Library, Program Library No. 0135.

Zietz, I., and Kirby, J.R., 1968, Transcontinental geophysical survey (35°-39°N) - magnetic map from 112°W longitude to the coast of California: U.S. Geol. Survey Misc. Geologic Investigations Map I-532-A.

Zurflueh, E.G., 1967, Applications of two-dimensional linear wavelength filtering: Geophysics, v. 32, p. 1015.

The vita has been removed from the scanned document

James William Schmoker
"Interpretation of aeromagnetics)..."

COMPLETE BOUGUER GRAVITY ANOMALY MAP OF THE SAN FRANCISCO MOUNTAINS VICINITY, BEAVER AND MILLARD COUNTIES, UTAH

BY

DONALD L. PETERSON

Base from U.S. Geological Survey topographic quadrangles.

EXPLANATION

-190

GRAVITY CONTOURS

CONTOUR INTERVAL 2 MILLIGALS. HACHURED CONTOURS INDICATE AREAS OF LOW GRAVITY CLOSURE.

-190.3

GRAVITY STATION

VALUE IS COMPLETE BOUGUER ANOMALY IN MILLIGALS FOR ASSUMED DENSITY OF 2.67 G PER CC.

SCALE 1:62,500

1 0 1 2 3 4 5 MILES

1966

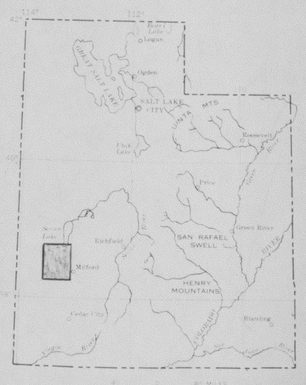

INDEX MAP OF UTAH SHOWING LOCATION OF THIS OPEN FILE MAP.

NOTE: GP-598 IS AN AEROMAGNETIC MAP OF THE SAME AREA AS THIS GRAVITY MAP.

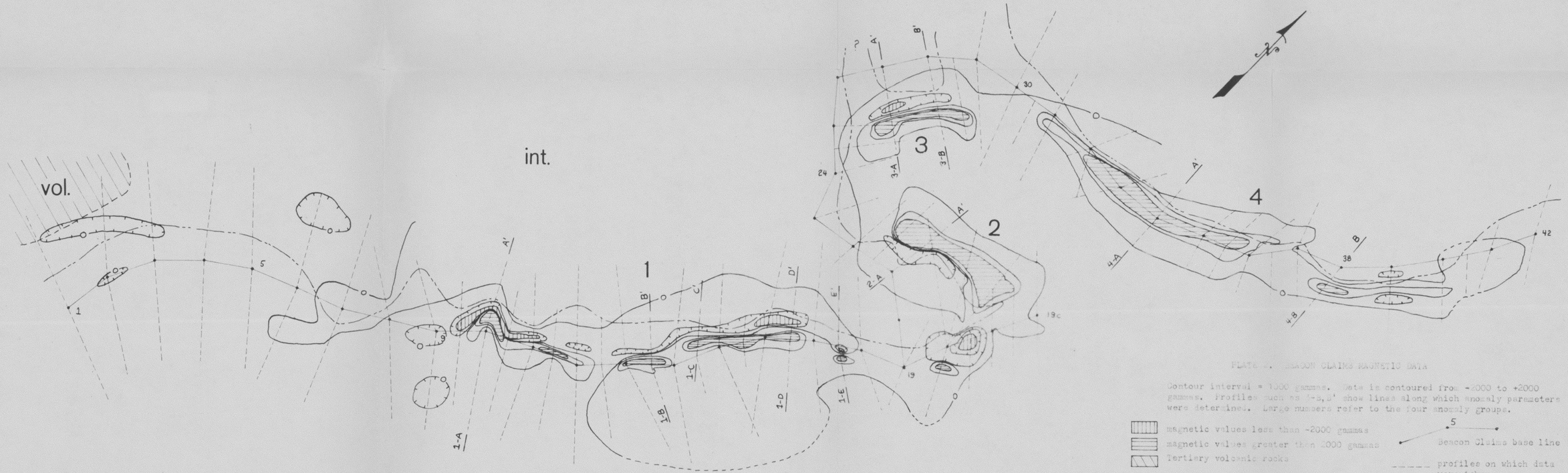

PLATE V. BEACON CLAIMS MAGNETIC DATA

Contour interval = 1000 gammas. Data is contoured from -2000 to +2000 gammas. Profiles such as 'A-A,' show lines along which anomaly parameters were determined. Large numbers refer to the four anomaly groups.

magnetic values less than -2000 gammas

magnetic values greater than 2000 gammas

Tertiary volcanic rocks

5 Beacon Claims base line

profiles on which data were taken

contact between limestone and the Shauntie intrusive body. The intrusive body lies on the northwest side of the contact.

0 100 200 feet

James Stillman Schmoker
Interpretation of aeromagnetic...

UNITED STATES
DEPARTMENT OF THE INTERIOR
GEOLOGICAL SURVEY

FRISCO PEAK QUADRANGLE
UTAH
15 MINUTE SERIES (TOPOGRAPHIC)

UNITED STATES
DEPARTMENT OF THE INTERIOR
GEOLOGICAL SURVEY

BEAVER LAKE MTS. QUADRANGLE
UTAH
15 MINUTE SERIES (TOPOGRAPHIC)

PLATE 1A. TOPOGRAPHIC MAP OF THE SAN FRANCISCO MOUNTAINS VICINITY.

Mapped, edited, and published by the Geological Survey
Control by USGS and USC&GS
Topography from aerial photographs by photogrammetric methods and by planetable surveys 1959. Aerial photographs taken 1953
Polyconic projection. 1927 North American datum
10,000-foot grid based on Utah coordinate system, south zone
1000-meter Universal Transverse Mercator grid ticks, zone 12, shown in blue
Dashed land lines indicate approximate locations

FRISCO, UTAH
N3815—W11315/15
1959

Mapped, edited, and published by the Geological Survey
Control by USGS and USC&GS
Topography from aerial photographs by photogrammetric methods
Aerial photographs taken 1951, 1953, and 1955. Field check 1958
Polyconic projection. 1927 North American datum
10,000-foot grid based on Utah coordinate system, south zone
1000-meter Universal Transverse Mercator grid ticks, zone 12, shown in blue
Red tint indicates area in which only landmark buildings are shown
Dashed land lines indicate approximate locations
Unchecked elevations are shown in brown

ROAD CLASSIFICATION
Medium-duty — Light-duty
Unimproved dirt
State Route

SCALE 1:62500
CONTOUR INTERVAL 40 FEET
DOTTED LINES REPRESENT 10-FOOT CONTOURS
DATUM IS MEAN SEA LEVEL

APPROXIMATE MEAN DECLINATION, 1958

THIS MAP COMPLIES WITH NATIONAL MAP ACCURACY STANDARDS
FOR SALE BY U. S. GEOLOGICAL SURVEY, DENVER 25, COLORADO OR WASHINGTON 25, D. C.
A FOLDER DESCRIBING TOPOGRAPHIC MAPS AND SYMBOLS IS AVAILABLE ON REQUEST

ROAD CLASSIFICATION
Medium-duty — Light-duty
Unimproved dirt
State Route

The east half of this area also covered by 1:24 000-scale maps of Milford, 1958, and Milford Flat, 1953, 7.5 minute quadrangles

MILFORD, UTAH
N3815—W11300/15
1958

PLATE 1. GENERALIZED GEOLOGIC MAP OF THE SAN FRANCISCO MOUNTAINS VICINITY, SOUTHWESTERN UTAH.

2 0 2 4 6 8 miles

Geology from "Geologic map of southwestern Utah" (Utah Geol. Survey, 1963).

240 Contour Interval = 40 gammas

Aeromagnetic contours, with a plane regional gradient corresponding to the gradient of the earth's main field removed, from the "Aeromagnetic map of the San Francisco Mountains and vicinity, southwestern Utah" (U.S. Geol. Survey, 1966).

AA', BB', and CC' are profiles along which gravity data (U.S. Geol. Survey, 1966a) were interpreted.

N

Qal Quaternary alluvium, undifferentiated

Ti Tertiary intrusive rocks

Tv Tertiary extrusive rocks

Pu Cambrian to Jurassic sedimentary rocks

PEm Precambrian metasedimentary rocks

Fault (dashed where probable, dotted where concealed)

CAROL M. NEWMAN
VIRGINIA POLYTECHNIC
BLACKSBURG, VIRG

DEPARTMENT OF THE INTERIOR
UNITED STATES GEOLOGICAL SURVEY

GEOPHYSICAL INVESTIGATIONS
MAP GP-598

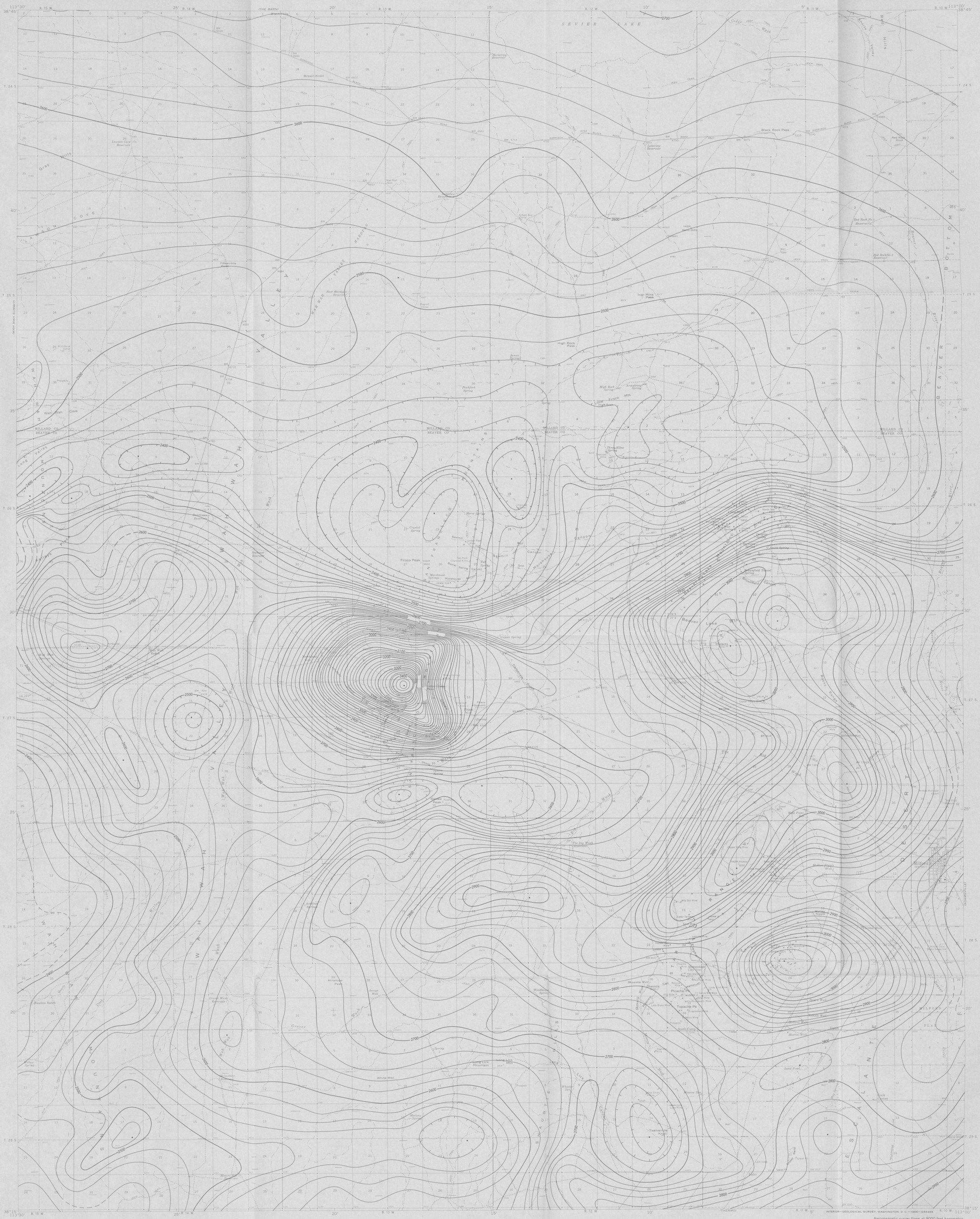

EXPLANATION

2500

Magnetic contours
Showing total intensity magnetic field of the earth in gammas relative to arbitrary datum. Hachured to indicate closed areas of lower magnetic intensity, dashed where data are incomplete. Contour interval is 20 gammas

Location of measured maximum or minimum intensity within closed high or closed low

Flight path
Showing location and spacing of data

NOTE

Aeromagnetic data are obtained and compiled along a continuous line, whereas ground magnetic surveys are made at separate points. Errors within the normal limits of any magnetic measurement may cause slight discrepancies between flight lines in an aeromagnetic map, which would be more obvious than similar discrepancies between points in a ground magnetic map. For this reason as much care should be exercised in evaluating magnetic features that appear as elongations along a single aeromagnetic traverse as in interpreting an anomaly indicated by a single ground station

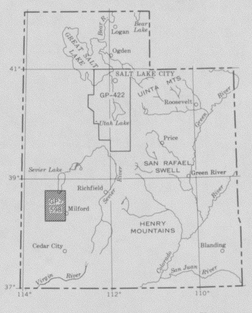

INDEX MAP OF UTAH SHOWING AEROMAGNETIC MAPS PUBLISHED BY THE U. S. GEOLOGICAL SURVEY, IN THE GP SERIES. GP-598 SHADED

Base from U.S. Geological Survey topographic quadrangles: Frisco Peak, 1960; Beaver Lake Mts., 1960; Frisco, 1959, and Milford, 1958

Aeromagnetic survey flown at 9000 feet barometric elevation by C. M. Mitchell, 1963. Compiled by C. L. Kruger and F. C. Moore

AEROMAGNETIC MAP OF THE SAN FRANCISCO MOUNTAINS AND VICINITY SOUTHWESTERN UTAH

SCALE 1:62 500

1 ½ 0 1 2 3 4 5 MILES

1 .5 0 1 2 3 4 5 KILOMETERS

1966

INTERIOR—GEOLOGICAL SURVEY, WASHINGTON, D. C.—1966—G66466

For sale by U.S. Geological Survey, price 50 cents